LBL-16422
c.2

Lawrence Berkeley Laboratory

UNIVERSITY OF CALIFORNIA

RECEIVED
LAWRENCE
BERKELEY LABORATORY

OCT 19 1983

LIBRARY AND
DOCUMENTS SECTION

Materials & Molecular Research Division

EFFECTS OF SMALL FLOW OBSTACLES ON THE LIMITING CURRENT AND PRESSURE DROP IN A SQUARE DUCT

D.S. Fischl*, R.H. Muller, and C.W. Tobias
(*M.S. Thesis)

August 1983

TWO-WEEK LOAN COPY

This is a Library Circulating Copy which may be borrowed for two weeks. For a personal retention copy, call Tech. Info. Division, Ext. 6782.

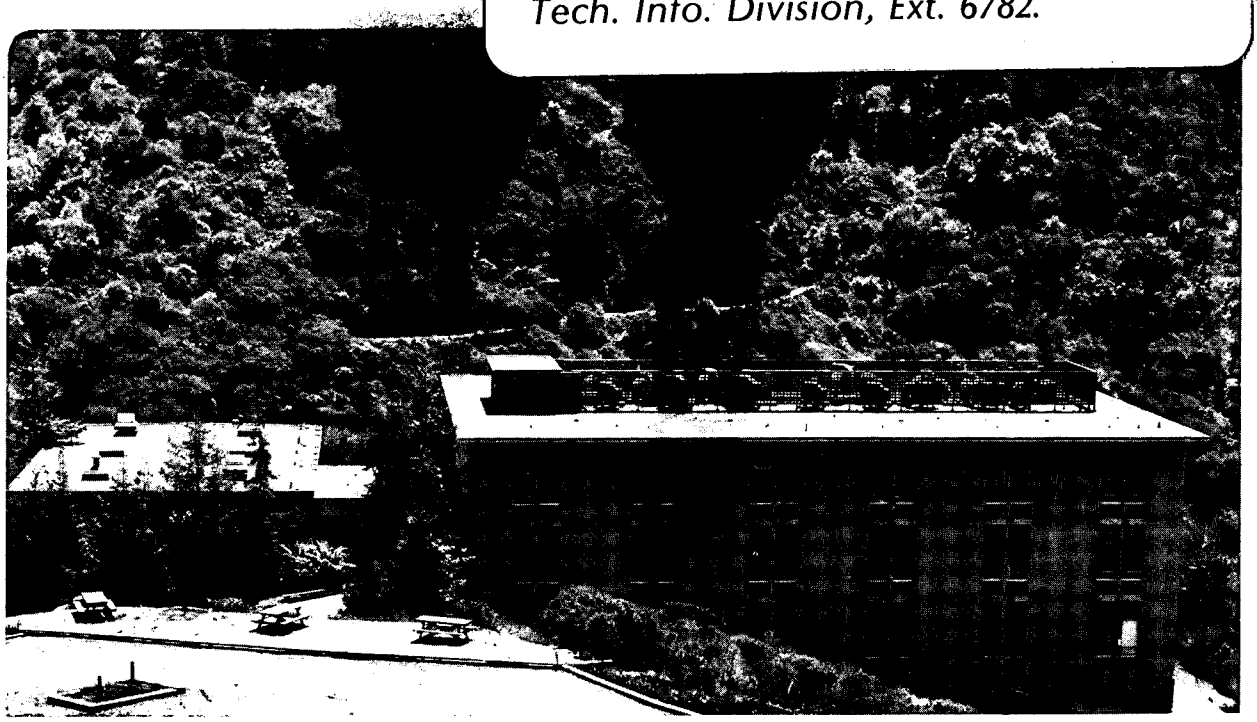

Prepared for the U.S. Department of Energy under Contract DE-AC03-76SF00098

LBL-16422
c.2

DISCLAIMER

This document was prepared as an account of work sponsored by the United States Government. While this document is believed to contain correct information, neither the United States Government nor any agency thereof, nor the Regents of the University of California, nor any of their employees, makes any warranty, express or implied, or assumes any legal responsibility for the accuracy, completeness, or usefulness of any information, apparatus, product, or process disclosed, or represents that its use would not infringe privately owned rights. Reference herein to any specific commercial product, process, or service by its trade name, trademark, manufacturer, or otherwise, does not necessarily constitute or imply its endorsement, recommendation, or favoring by the United States Government or any agency thereof, or the Regents of the University of California. The views and opinions of authors expressed herein do not necessarily state or reflect those of the United States Government or any agency thereof or the Regents of the University of California.

LBL-16422

EFFECTS OF SMALL FLOW OBSTACLES ON THE LIMITING CURRENT AND PRESSURE DROP IN A SQUARE DUCT

Daniel Seth Fischl

(M.S. Thesis)

with Rolf H. Muller and Charles W. Tobias

Materials and Molecular Research Division
Lawrence Berkeley Laboratory
and Department of Chemical Engineering
University of California
Berkeley, CA 94720

August 1983

This work was supported by the Director, Office of Energy Research, Office of Basic Energy Sciences, Materials Sciences Division of the U.S. Department of Energy under Contract No. DE-AC03-76SF00098.

TABLE OF CONTENTS

	Page
ABSTRACT	v
SYMBOLS	vii
INTRODUCTION	1
SYSTEM FUNDAMENTALS	3
Hydrodynamics	3
Electrochemical Mass Transfer	8
LITERATURE REVIEW - INCREASE TRANSFER RATES	21
Heat Transfer - Flow Obstacles	21
Mass Transfer - Flow Obstacles	27
Other Methods	53
EXPERIMENTAL APPARATUS	56
Electrolyte Flow System	56
Flow Channel	58
Electrical System	60
Pressure Monitoring System	66
Electrode Preparation	70
Electrolyte Preparation	72
Electrolyte Physical Properties	73
Obstacle Fabrication and Electrode Attachment	75
EXPERIMENTAL TECHNIQUES, PROCEDURES, AND CALCULATIONS	82
Pumping Power - Pressure Drop Measurement	82
Mass Transfer Rates - Limiting Current Technique	85

Page

Operation. 94

Errors 95

Flow Visualization 96

RESULTS. 98

Limiting Current Curves. 101

Quantitative Mass Transfer Results -
Limiting Current Measurements. 111

Pressure Drop Measurement. 123

Pressure Drop Versus Limiting Current -
Introduction to Obstacle Benefit 131

Flow Visualization 138

Micro Obstacles. 146

QUANTITATIVE DISCUSSION OF OBSTACLE BENEFIT. 154

CONCLUSIONS AND SUMMARY OF FINDINGS. 166

ACKNOWLEDGEMENTS 167

APPENDIX A - Limiting Current Curve Transient "Maxima" 168

APPENDIX B - Titration Techniques. 173

APPENDIX C - Comparison with Interferometric Results 174

REFERENCES 177

EFFECTS OF SMALL FLOW OBSTACLES ON THE LIMITING CURRENT AND PRESSURE DROP IN A SQUARE DUCT

Daniel Seth Fischl

Materials and Molecular Research Division
Lawrence Berkeley Laboratory
and Department of Chemical Engineering
University of California
Berkeley, CA 94720

ABSTRACT

The effectiveness of mass transfer enhancement by small obstacles attached to the cathode in a 0.5 by 0.5 cm square cross section 50.8 cm long electrochemical flow cell was investigated. Pressure drops, and limiting currents for the reduction of ferricyanide were measured in the range of $80 \leq Re \leq 3200$. Using rectangular obstacles extending 0.0254 to 0.160 cm from the surface, the spacing to height ratio ranged from 9 to 170. Flow patterns around obstacles were visualized using suspensions of inert materials and recorded by means of dark field photography.

Depending on the flow rate, addition of the obstacles can increase mass transfer rates by as much as five times over those in the unobstructed system. The degree of enhancement increases with decreasing obstacle spacing until an optimal spacing is reached. The maximum enhancement occurs when the spacing is approximately 15 times the obstacle size corresponding to the largest elongation of the recirculation zone observed downstream from an obstacle.

At $Re \approx 100$, the mass transfer rate is approximately doubled upon addition of the optimal number of obstacles without appreciably

affecting the pressure drop. The largest enhancement (5-fold) occurs at the upper laminar flow regime with a 2.7-fold increase in the pressure drop. These comparisons are made at the same flow rate.

In the unobstructed system, improved mass transfer rates (limiting currents) are achieved by increasing the flow rate to produce turbulent flow. This approach involves large pressure drops and consequently large pumping power requirements. An increase in the limiting current by the addition of obstacles, on the other hand, requires only a very small fraction (2-5 percent) of the pumping power required to obtain the same limiting current achieved by increasing the flow rate in the unobstructed system. Obstacles therefore produce efficient mixing near the electrode surface and correspondingly high mass transfer rates without causing large energy dissipation in the bulk fluid.

SYMBOLS

a	- Width of channel (cm)
A	- Active electrode area (cm^2)
b	- Height of channel (cm)
c_i	- Concentration of species i, ($mole/cm^3$)
C_o	- Concentration at electrode surface ($mole/cm^3$)
C_b	- Bulk concentration ($mole/cm^3$)
D_e	- Equivalent hydraulic diameter (cm)
D_i	- Diffusion coefficient of species i (cm^2/sec)
F	- Faraday's constant 96487 (coulomb/equiv)
g	- Acceleration due to gravity 976.77 (cm/sec^2)
h	- Parallel plate channel gap (cm)
Δh	- Manometer height difference (cm)
i	- Current density ($Amps/cm^2$)
i_{avg}	- Average current density (A/cm^2)
i_L	- Limiting current density (A/cm^2)
I_L	- Total limiting current (Amps)
I_{SS}	- "Steady state" current (Amps)
k	- Mass transfer coefficient (cm/sec)
L	- Active electrode length (cm)
n	- Number of electrons transferred in electrode reaction
N_i	- Flux of species i ($mole/cm^2$-sec)
p	- Pressure (N/m^2)
ΔP	- Pressure drop (N/m^2)
$\Delta P/L$	- Pressure drop per length (N/m^2-m)
P_p	- Pumping power (W/m^2)

Q	– Volumetric flow rate (cm^3/sec)
r	– Radial coordinate parameter ($r = 0$ at tube center)
R	– Tube radius (cm)
R_i	– Bulk chemical reaction rate (mole/cm^3–sec)
s_i	– Stoichiometric coefficient of species i
t	– Time (sec)
t_+	– Cation transference number
T	– Temperature (°K)
u	– Mobility of species i (cm^2–mole/J–sec)
v	– Mass average velocity (cm/sec)
V_{avg}	– Average velocity (cm/sec)
V_b	– Bulk velocity (cm/sec)
V_z	– Velocity in z direction (cm/sec)
$\bar{V}$	– Potential ramp sweep rate (volts/sec)
x,y,z	– Rectangular coordinate parameters ($x = y = 0$ at duct center)
z_i	– Charge number of species i
δ	– Boundary layer thickness (cm)
δ_N	– Nernst boundary layer thickness (cm)
δ_{99}	– Ninety-nine percent boundary layer thickness (cm)
μ	– Viscosity (cp)
ν	– Kinematic viscosity (cm^2/sec)
ρ	– Density (g/cm^3)
Φ	– Electric potential (volts)
σ	– Parameter for maxima analysis [162]
Γ	– Ionic strength (moles/liter)

Dimensionless Numbers

f - Friction factor $f = \frac{1}{4} \frac{D_e \Delta P}{\frac{1}{2}\rho V_b^2 L}$

Nu - Nusselt number for heat transfer

Pr - Prandtl number for heat transfer

Re - Reynolds number $Re = \frac{V_b D_e}{\nu}$

Sc - Schmidt number $Sc = \frac{\nu}{D_i}$

Sh - Sherwood number (average value) $Sh = \frac{k D_e}{D_i} = \frac{s_i D_e i}{D_i \Delta c_i nF}$

St - Stanton number $St = \frac{Sh}{(Re\ Sc)}$

INTRODUCTION

Mass and heat transfer in forced convection systems are important in many engineering disciplines. In a flow channel containing electrodes embedded in opposite walls, reacting substances (mass) must travel from the bulk electrolyte to the electrode and then undergo an electrochemical transformation. If the rate of the overall reaction is determined only by the rate at which material arrives at the reacting surface, the process is "mass transfer limited." The concentration of the reacting species varies in the channel creating a concentration profile. Away from the walls, where the convective motion is high, the concentration is at its bulk value. However, the fluid near the wall moves relatively slowly, convection is reduced, and consequently mass transfer is due mainly to diffusion and migration. This thin region next to the wall, which produces the major resistance to transfer, is called the "diffusion" or "mass transfer" boundary layer. The mass transfer boundary layer thickness (δ) can be decreased (producing higher rates of mass transfer) by pumping the electrolyte fluid faster. However, increased flow rates require a large input of pumping energy.

Previous studies using optical interferometry [1,2] have shown that small obstacles placed in the flow path near the electrode significantly decreased the mass transfer boundary layer thickness over extended distances in the flow direction. It was expected that the resulting increase in mass transfer rates was associated with only a small increase to the required pumping power because the obstacles disturbed the flow only in the small region close to the electrode surface.

The goal of the present work was to quantify the observed effects of these small obstacles (.762 mm) under laminar flow conditions in the square cross section (5 mm x 5 mm) flow cell used for the interferometric study [2]. Mass transfer rates were determined by measuring the limiting currents for the electrochemical reduction of ferricyanide ion to ferrocyanide ion. The required electrolyte pumping energy input was determined by measuring the additional pressure drop caused by the presence of the small obstacles.

Furthermore, because of similarities between mass, momentum, and heat transfer, the results of this study may be extended to evaluate the effects of small flow obstacles in many analogous heat or mass-transfer systems.

SYSTEM FUNDAMENTALS

Hydrodynamics

Viscous fluid flow through a tube, duct, or channel is characterized by two distinct regimes. These were described quantitatively by Osborne Reynolds in 1883 and are termed laminar and turbulent. Laminar flow is well ordered with fluid layers sliding smoothly over one another and mixing between layers occurring on a molecular level. Conversely, turbulent flow is chaotic with macroscopic packets of fluid transferring between layers creating random fluctuating phenomena.

The dimensionless quantity commonly used to describe flow regimes is the Reynolds number (Re). It is a ratio of inertial forces to viscous forces; for flow through a duct it is defined as:

$$Re = \frac{V_b \, D_e}{\nu}$$

The bulk fluid velocity (V_b) is non-dimensionalized by the duct equivalent diameter (D_e) and the fluid kinematic viscosity (ν). For a constant property system the Reynolds number is proportional to velocity. Ordinarily, a tube, duct, or channel flow system with a Reynolds number below 2100 usually is operating in the laminar regime; above 2100 the flow becomes turbulent. The kinematic viscosity is a physical property of the fluid whereas the hydraulic or equivalent diameter (D_e) is a characteristic length of the system geometry, and it is given by:

$$D_e = \frac{4\ (\text{cross section area to flow})}{\text{wetted perimeter}} \tag{1}$$

The specific flow system under investigation formed a square cross section duct. Fluid flow through a square duct (shown in Fig. 1) will be affected by the four walls. As one might expect, the velocity profile is symmetric in both the x and y-direction, with the velocity maximum in the center. Unlike flow through a circular pipe or between two infinite plates (channel flow), the equations describing fully developed laminar hydrodynamics in a square duct are not a function of only one spatial variable. For the simpler (one dimensional) case of channel flow, the side walls are assumed to be far apart when compared to the gap separation and the velocity distribution profile is only a function of vertical distance between the plates. However, in the square duct the motion of the fluid near the side walls is reduced and this has a pronounced effect on the velocity profile. The effect of the side walls on the velocity profile is shown in Fig. 2, (from Beach [3]). This figure shows the small effect of the side walls in a channel (curve A) as compared to the large effect in the square duct (curve B).

The exact analytic solution to laminar flow of a Newtonian fluid (Navier-Stokes equation) through a rectangular channel with width (a) and height (b) in the x-direction and y-direction respectively is given by Happel and Brenner [4] as:

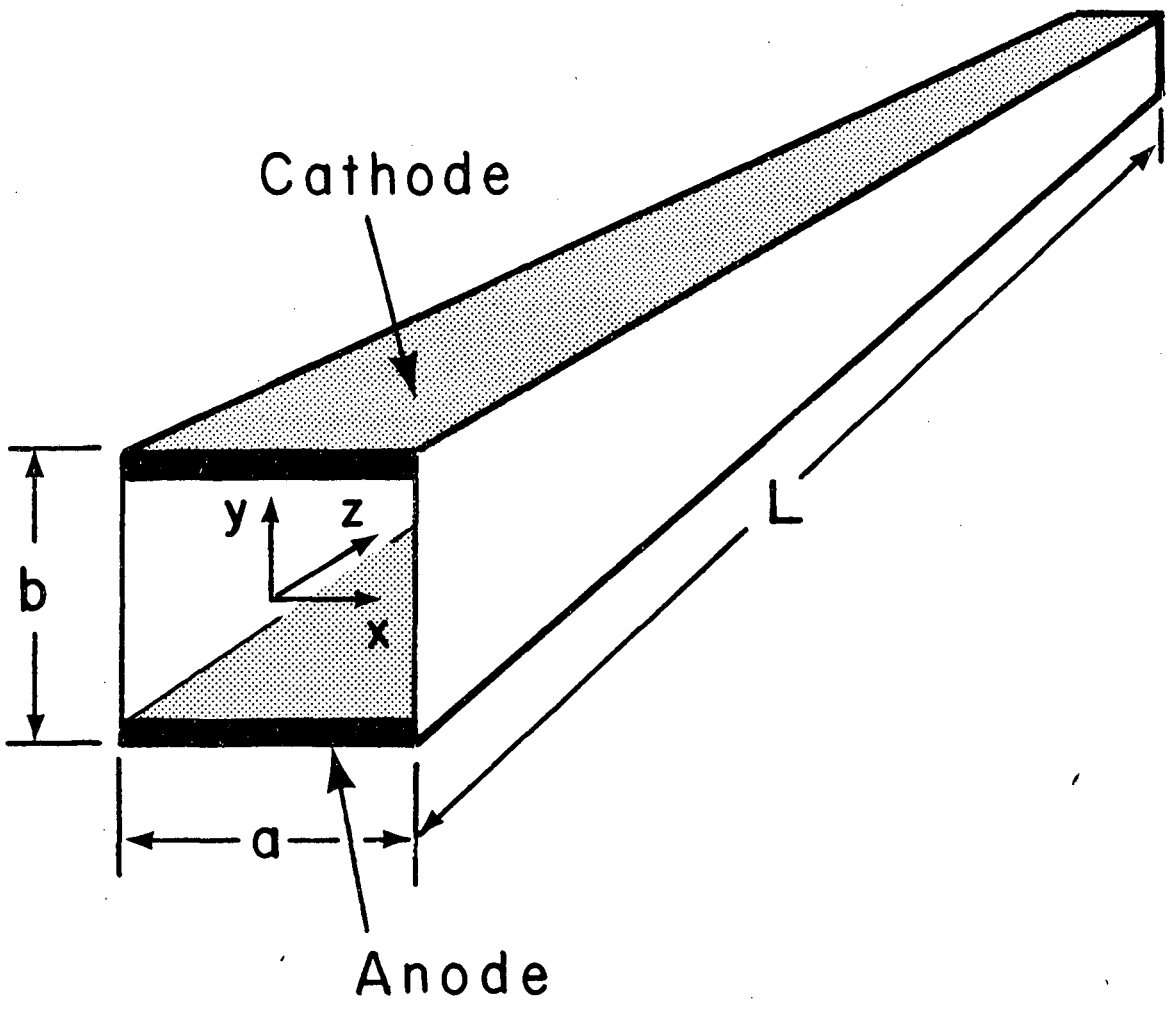

XBL 838-513

Fig. 1. Square duct geometry.

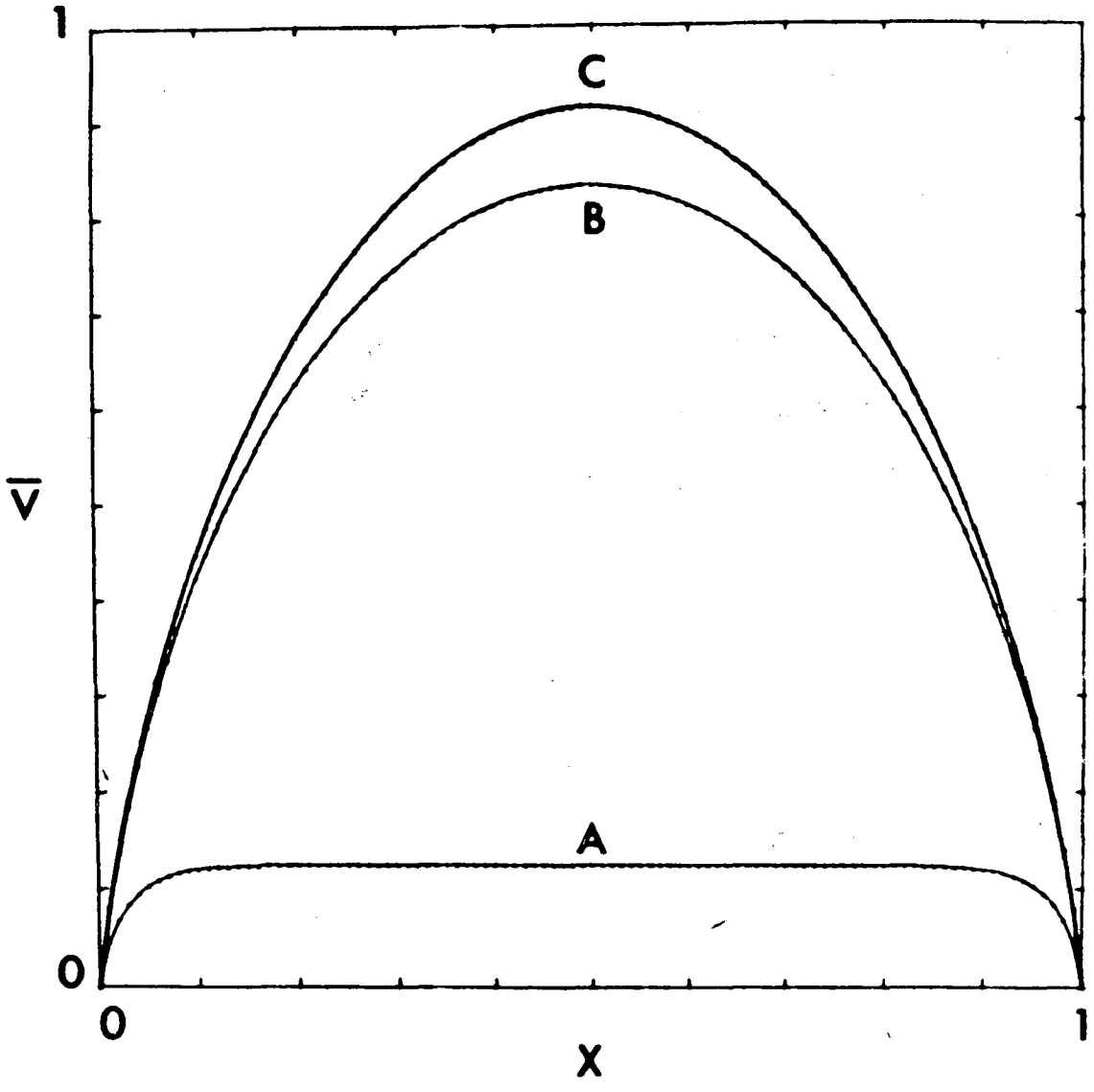

XBL 7011-7034

Fig. 2. Normalized velocity profile across the electrode at various aspect ratios (from Beach [3]).

Curve: A, $\frac{b}{a} = 0.1$ B, $\frac{b}{a} = 1$ C, $\frac{b}{a}$ = infinity

a = channel width
b = channel height

$$V_Z(x,y) = \frac{-dp}{dz}\frac{x(x-a)}{2\mu} + \sum_{m=1}^{\infty} \sin\left(\frac{m\pi x}{a}\right)\left[A_m \cosh\left(\frac{m\pi y}{a}\right) + B_m \sinh\left(\frac{m\pi y}{a}\right)\right] \quad (2)$$

where

$$A_m = 2\,\frac{dp}{dz}\,\frac{a^2}{\mu m^3 \pi^3}\left[\cos\,(m\pi) - 1.0\right]$$

and

$$B_m = \frac{-Am\,[\cosh\,(m\pi\ b/a) - 1]}{\sinh\,(m\pi\ b/a)}$$

The pressure (p), fluid viscosity (μ) and length of the side walls (a and b) are variables. For the case of a square duct a = b. This solution is well known and is described in a number of texts [5]. Evaluating the series for the square duct geometry gives the following expression for the volumetric flow rate (Q) in terms of the pressure drop (ΔP) and duct length (L):

$$Q = \frac{0.035144\Delta P a^4}{\mu L} \quad (3)$$

Purday [6] also gives the pressure drop equation as:

$$\frac{dp}{dz} = -28.6\,\frac{\mu(V_{avg})}{a^2} \quad (4)$$

$$V_{avg} = \frac{Q}{a^2}$$

This problem of laminar flow by a Newtonian fluid through a square duct has also been solved by R. S. Schechter using the Ritz method [7]. Here the velocity distribution is given by the following very accurate approximation in terms of the average velocity (V_{avg}).

$$\frac{V_{z(x,y)}}{V_{avg}} = \left[\left(\frac{x}{c}\right)^2 - 1\right]\left[\left(\frac{y}{c}\right)^2 - 1\right]\left\{2.09825 + 0.29180\left[\left(\frac{x}{c}\right)^2 + \left(\frac{y}{c}\right)^2\right] + 0.87545\left(\frac{x}{c}\right)^2\left(\frac{y}{c}\right)^2\right\} \tag{5}$$

In this case 2c is the length of one side of the square duct. Using a collocation technique Bird, Steward, Lightfoot, and Chapman have also solved this problem numerically [8].

For completeness, the one dimensional laminar channel flow velocity profile is given below.

$$\frac{V_z(y)}{V_{avg}} = 3\,\frac{y}{h}\left(1 - \frac{y}{2h}\right) \tag{6}$$

Here (y) is the vertical direction between the two infinite parallel plates and (h) is the plate separation (gap width).

The velocity profile for laminar flow through a circular tube (Poiseuille flow) is:

$$\frac{V_z(r)}{V_{avg}} = 2\left(1 - \frac{r^2}{R^2}\right) \tag{7}$$

where the radius of the tube is given by (R).

Electrochemical Mass Transfer

In the specific system under investigation electrolyte flows through a flow channel of square cross section that has electrodes forming the top and bottom walls (Fig. 1). The electrochemical reduction of the ferricyanide ion occurs on the upper electrode

(cathode) and the ferrocyanide ion is oxidized on the anode. According to Newman [9] in this redox system, using dilute-solution theory, the flux (N_i) of a solute species can be expressed as:

$$N_i = -z_i u_i F c_i \nabla \Phi - D_i \nabla c_i + v c_i \tag{8}$$

where Φ is the electric field potential and D_i is diffusivity of the ion. The terms on the right are the contribution to flux by migration in an electric field, diffusion in a concentration gradient, and convection by fluid motion respectively. A material balance for the electrolyte yields:

$$\frac{\partial c_i}{\partial t} = - \nabla N_i + R_i \tag{9}$$

In this case the bulk reaction term (R_i) is zero because the reaction occurs only on the electrode surface.

For an electrically neutral solution,

$$\sum_i z_i c_i = 0 \tag{10}$$

Finally, the current density (i) is due to the motion of the charged species:

$$i = F \sum_i z_i N_i \tag{11}$$

In the system under investigation, ions that do not participate in a reaction are added to the solution (NaOH). These ions are the

"supporting electrolyte" and have the effect of reducing the migration of the reacting species (in this case the ferricyanide ion). The addition of supporting electrolyte allows the migration term in Eq. (8) to be neglected. When Eq. (8) is substituted into Eq. (9) the equation of convective diffusion is obtained:

$$\frac{\partial c_i}{\partial t} + v\,\nabla c_i = D_i \nabla^2 c_i \tag{12}$$

(excess supporting electrolyte)

It is important to note that this equation also applies to convective mass transfer and convective heat transfer in non-electrochemical systems. This allows the results of this experimental study to be applied to analogous heat and mass transfer situations.

In rectangular coordinates and under steady state conditions the convective diffusion equation for the reacting species becomes:

$$V_x \frac{\partial c}{\partial x} + V_y \frac{\partial c}{\partial y} + V_z \frac{\partial c}{\partial z} = D_i \left[\frac{\partial^2 c}{\partial x^2} + \frac{\partial^2 c}{\partial y^2} + \frac{\partial^2 c}{\partial z^2} \right] \tag{13}$$

for flow in a rectangular channel velocity occurs only in the z-direction so we obtain:

$$V_z \frac{\partial c}{\partial z} = D_i \left[\frac{\partial^2 c}{\partial x^2} + \frac{\partial^2 c}{\partial y^2} + \frac{\partial^2 c}{\partial z^2} \right] \tag{14}$$

At this point an equation for the velocity (V_z) must be used to solve for the concentration profiles. For flow in a square duct the

velocity (V_z) was previously shown to be a function of both x and y (Eq. (2) or (5)). Due to the complicated nature of the equations, the convective diffusion equation was not solved in this investigation.

The simpler case of channel flow between two infinite parallel plates has already been solved [10]. Here the side wall effects on the hydrodynamics are eliminated (Eq. (6)) and the velocity (V_z) depends only on one variable (y). Furthermore, concentration variations in the x-direction (between the side walls) are eliminated ($\partial^2 c/\partial x^2$ in Eq. (14) is zero). The geometry for this problem is shown on Fig. 3. The solution yields concentration profiles similar to the one shown on Fig. 4. The concentration of the reacting species decreases from its bulk value (C_b) away from the electrode to the value on the electrode surface (C_o). The concept of the mass transfer diffusion layer is also shown. This diffusion layer is the thin region near the electrode surface where the major concentration variations occur. As stated earlier, fluid convection is slow close to the wall and the movement of material is mainly due to molecular diffusion (especially with supporting electrolyte). In forced convection systems, it is this thin diffusion layer that provides the major resistance to mass transfer (i.e., diffusion controlled). The thickness of the diffusion layer can be represented in a number of ways and these are shown on Fig. 4. The Nernst boundary layer thickness (δ_N) is a simple linear approximation. However, the ninety-nine percent diffusion layer thickness (δ_{99}) is the distance from the electrode surface to a point where the concentration is equal to ninety-nine

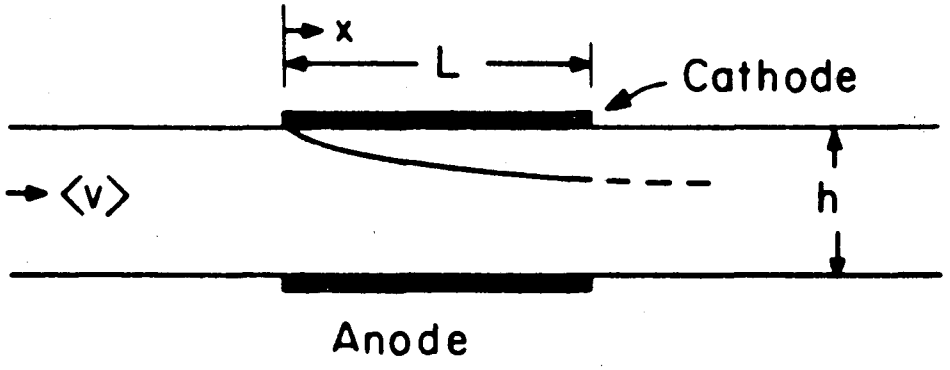

Plane electrodes in the walls of a flow channel

XBL673-2382A

Fig. 3. Plane electrodes in the walls of a parallel plate flow channel. The diffusion layer on the cathode is indicated schematically. [10]

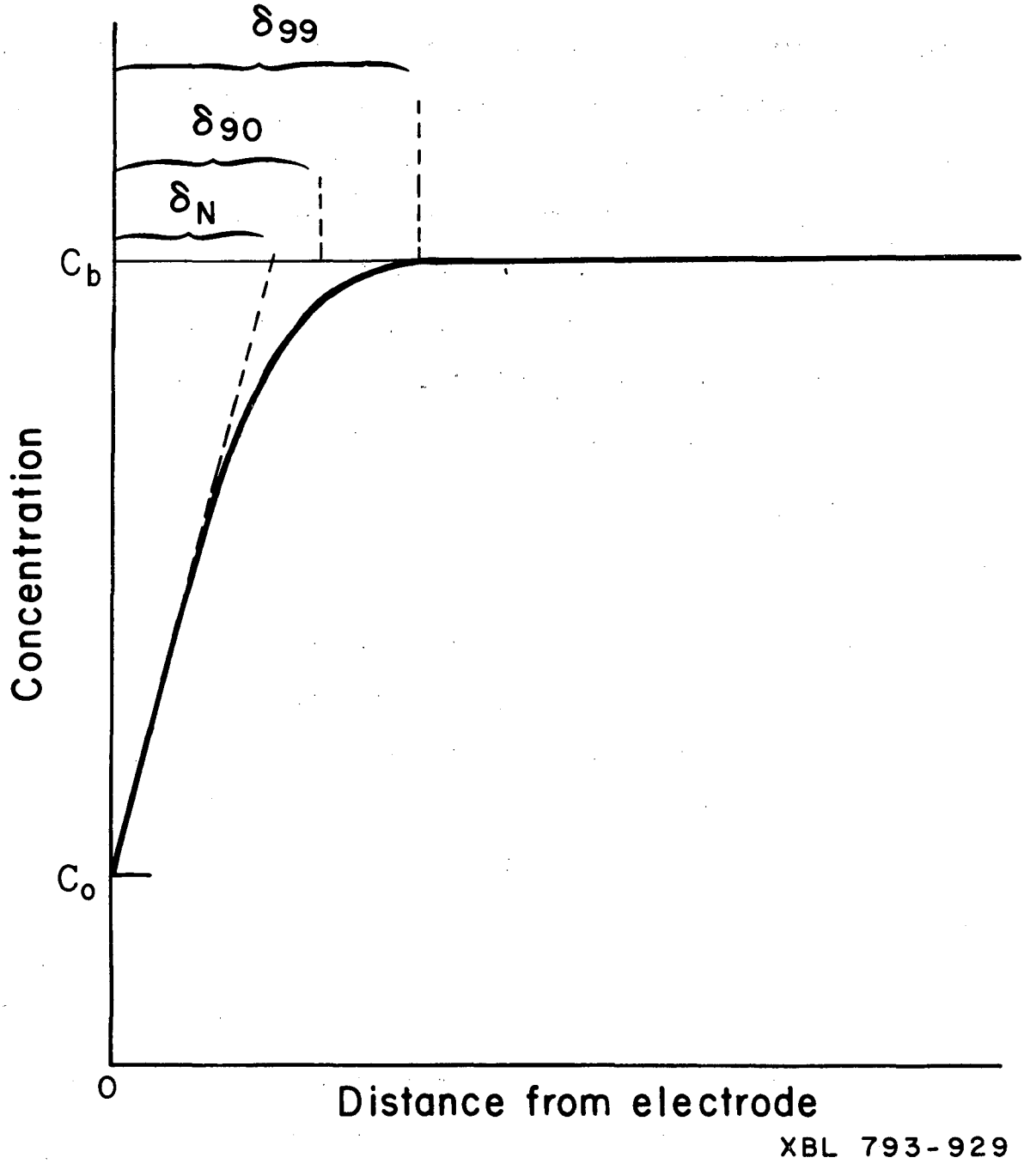

Fig. 4. The definition of the ninety-nine percent boundary layer thickness (δ_{99}), the ninety percent boundary layer thickness (δ_{90}), and the Nernst boundary layer thickness (δ_N). C_b and C_o refer to bulk concentration and surface concentration, respectively. [2]

percent of the bulk value. The flux of mass is related to the thickness of the diffusion boundary layer. A larger flux (greater mass transfer) is obtained with a thinner diffusion layer. One can see by Eq. (11) that the current is related to the flux of charged species. At the wall, where the fluid velocity is zero, and with excess supporting electrolyte, Eq. (8) relates the flux of species to the concentration gradient. Therefore, the current passed in an electrochemical reaction is related to the concentration gradient of the reacting species concentration profile evaluated at the wall and is given by:

$$i = \frac{nF\ D_i}{(1 - t_+)} \frac{\partial c}{\partial y} \bigg|_{y = o} \tag{15}$$

With a large excess of supporting electrolyte the transference number (t_+) becomes negligibly small. Through the use of the Nernst boundary layer thickness (δ_N) shown on Fig. 4, the current in the steady state can be related to the bulk concentration (C_b) and surface concentration (C_o) of reacting species:

$$i = \frac{nF\ D_i}{1 - t_+} \frac{C_b - C_o}{\delta_N} \tag{16}$$

From this expression it is apparent that the current can be increased by decreasing the mass transfer boundary layer thickness. During a limiting current sweep, which will be discussed in a later section, the surface concentration (C_o) of the reacting species decreases with increasing applied potential and the current passed is increased.

However, when the surface concentration drops to zero ($C_o = 0$), the current can no longer be increased. The reaction is now mass transfer limited and the "limiting current" (i_L) is:

$$i_L = \frac{nF\ D_i}{1 - t_+} \left.\frac{\partial c}{\partial y}\right|_{\substack{y = 0 \\ C_o = 0}} \approx \frac{nF\ D_i}{1 - t_+} \frac{C_b}{\delta_N} \tag{17}$$

With constant electrolyte properties, the limiting current can only be changed by changing the nature of the flow. Solving for the concentration profiles, and evaluating the concentration gradients along the surface of a reacting electrode yields (by Eq. (17)) the distribution of current to that electrode. The limiting current distribution is shown on Fig. 5 for the infinitely wide parallel plane cathode shown in Fig. 3 and is described by the following equations:

$$i_L = 0.9783\left[\frac{nFD_iC_b}{s_i} \frac{V_{avg}}{h\ xD_i}\right]^{1/3} \tag{18}$$

$$\frac{i_L}{i_{avg}} = \frac{2}{3}\left(\frac{x}{L}\right)^{-1/3} \tag{19}$$

where (s_i) is the stoichiometric coefficient of species in the electrode reaction and (x) is the distance in the flow direction measured from the leading edge of the electrode. The distribution is highly nonuniform and the majority of the reaction occurs at the upstream portion of the electrode. Under limiting conditions, these local values of current are proportional to mass transfer rates. One

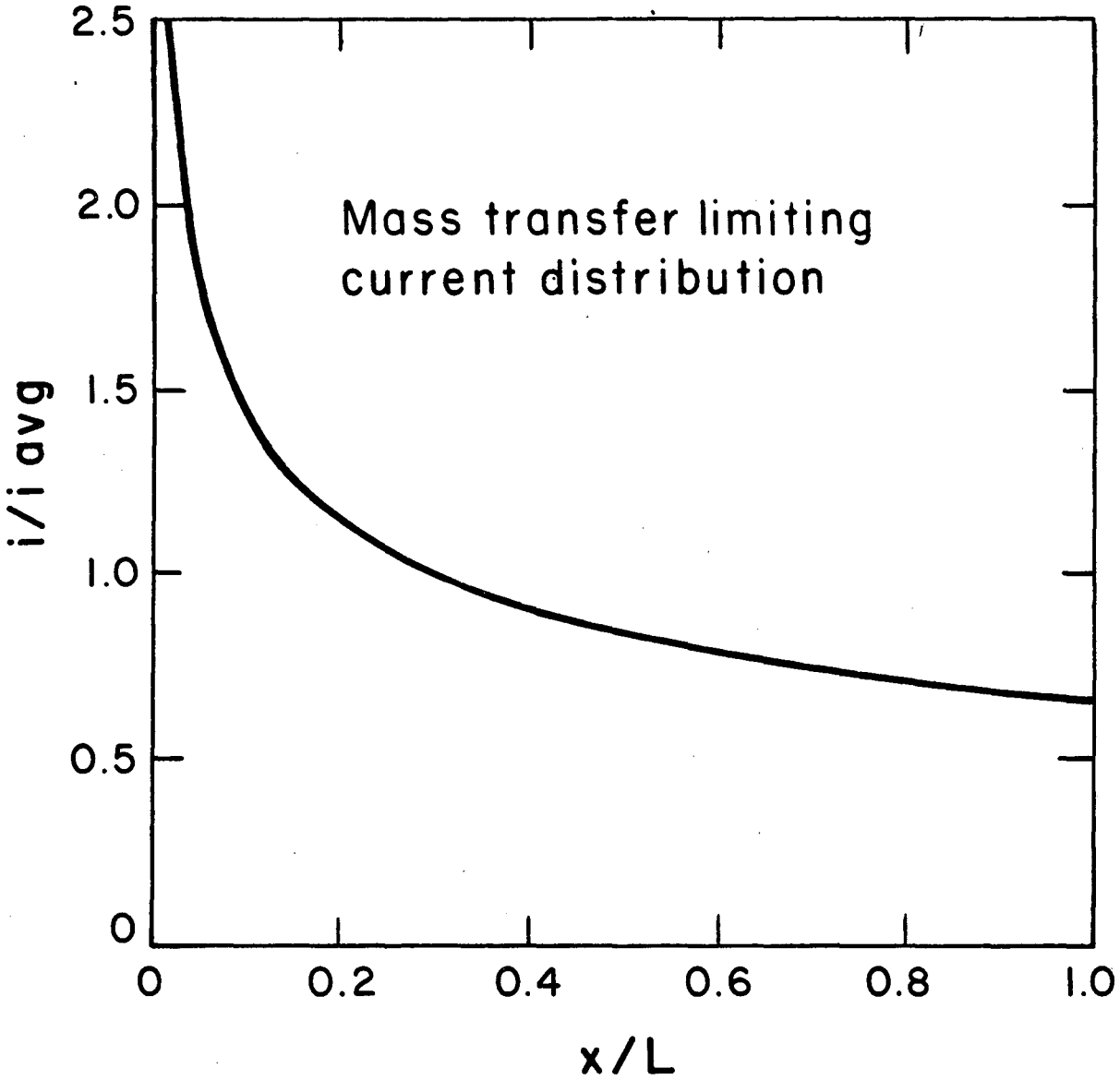

XBL 693-2183A

Fig. 5. Mass transfer limiting current distribution to an electrode of length (L) in a parallel plate flow channel. Note infinite current at leading edge. (From [10])

observes an extremely high rate of mass transfer at the leading edge where fresh solution is brought in contact with the electrode. This rate decreases in the flow direction because the solution in the diffusion layer is being depleted by the reaction upstream. The thickness of the diffusion layer (shown in Fig. 3) grows along the length of the electrode. Mass transfer rates can be conveniently correlated by the dimensionless Sherwood number (Sh).

$$Sh = \frac{-N_i D_e}{D_i \Delta c_i} = \frac{s_i D_e \; i}{D_i \Delta c_i \; nF} \tag{20}$$

$$\Delta c = C_b - C_o$$

In terms of a mass transfer coefficient the Sherwood number is:

$$Sh = \frac{k \; D_e}{D_i} \tag{21}$$

where k is defined by the flux (N) and concentration difference $(C_b - C_o)$:

$$N = k \; (C_b - C_o)$$

The hydraulic or equivalent diameter (D_e) was previously defined by Eq. (1). Using dimensionless quantities, the average mass transfer to a parallel plane electrode of length (L) under laminar channel flow hydrodynamics is given by the following correlation:

$$Sh = 1.8488 \left[\frac{ReScD_e}{L} \right]^{1/3} \tag{22}$$

The dimensionless Reynolds number (Re) and Schmidt number (Sc) are given by:

$$Re = \frac{V_{avg} D_e}{\nu} \tag{23}$$

$$Sc = \frac{\nu}{D_i} \tag{24}$$

where the kinematic viscosity ($\nu = \frac{\mu}{\rho}$) is used. Equation 22 was developed using the laminar channel flow hydrodynamics given by Eq. (6). The side walls do not enter into the equations and Eq. (22) can be used for a channel whose walls are sufficiently far apart so they do not affect the flow significantly. Excellent experimental validation of Eq. (22) has been achieved [11-13].

Figure 2 has shown that the fluid velocity is decreased near side walls. The two dimensional velocity profile in a channel which shows side wall effects (i.e., the square duct) gives rise to a three dimensional concentration profile. Therefore a square duct electrochemical flow cell produces a current distribution that varies both in the flow direction, and across the channel. Figure 6 shows the effect of the side wall on the velocity and concentration profiles. Near the wall these profiles become steeper and the associated diffusion layers become thicker. It can be concluded that the highest mass transfer rates to the electrode under investigation occur along the centerline of the electrode. Specifically, the rate is highest at the center of

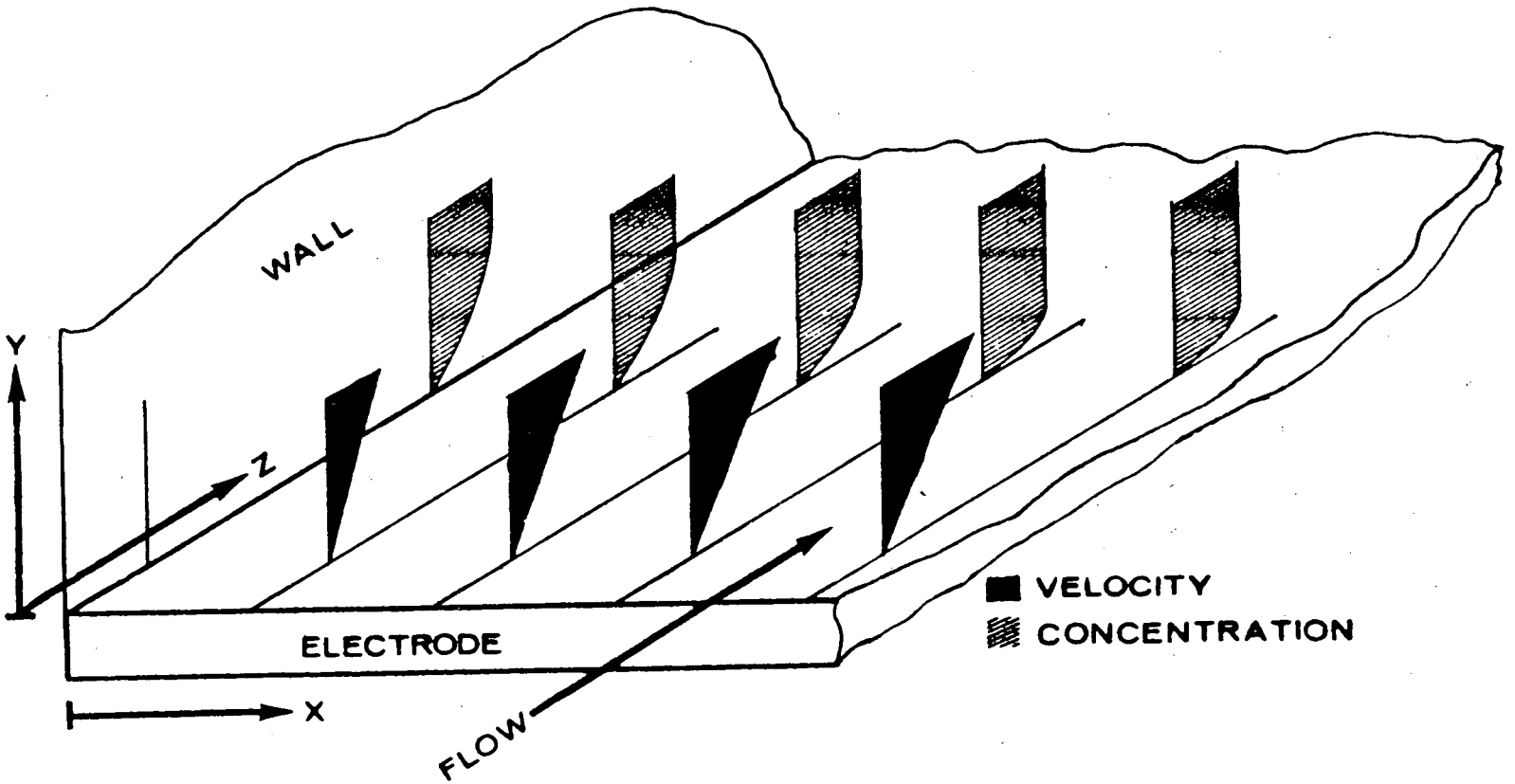

XBL 7012-7376

Fig. 6. Velocity and concentration profiles. The approximately linear velocity profile (near the electrode) is shown to have a zero velocity gradient at the side wall and it increases away from the wall. The concentration boundary layer is diffusion controlled and decreases in thickness as the velocity increases away from the wall. [3]

the leading edge and decreases not only in the flow direction but also as the side walls are approached. The overall effect of the square duct geometry is to decrease the overall rate of mass transfer to the electrode as compared to an electrode of the same length which is embedded in a channel with no side wall effects. This decrease to mass transfer has been calculated for a number of geometries by I. Rousar, J. Hostomsky, and V. Cezner [14]. Their results are presented in terms of a correction factor (ϕ) to the channel flow equation:

$$Sh = 1.85\phi\ (ReScD_e/L)^{1/3} \tag{25}$$

This equation is valid for the laminar flow regime. For the case of this study, where the electrodes form the top and bottom surfaces of a square duct, the laminar flow mass transfer equation becomes:

$$Sh = 1.56 \left[ReSc\ \frac{D_e}{L} \right]^{1/3} \tag{26}$$

$$\phi = .842$$

The side walls reduce the overall mass transfer by approximately 16 percent. This solution shows very good agreement with the data obtained in this study as will be shown in the Results section (Fig. 36).

LITERATURE REVIEW

The problem of increasing transfer rates through the use of flow obstructions has received considerable attention in the past. Most of the previous work involved investigations of forced convection systems in the turbulent flow regime.

Heat Transfer

Early studies were concerned with increasing heat transfer by flow through roughened tubes. D. F. Dipprey and R. H. Sabersky in 1963 [15] were among the first to study this effect using a liquid as the flowing fluid. Before them the only work they reference was Cope in 1941 [16], J. W. Smith and N. Epstein in 1957 [17], Nunner in 1958 [18] who used air, Grass in 1958 [19], Gambill in 1960 [20] who induced swirl flow by twisted tapes passing through the pipes, and J. Nikuradse in 1933 [21] who set the stage by measuring the effect of tube roughness on the velocity and overall pressure drop in a tube. Dipprey and Sabersky used distilled water in roughened tubes (nominal diameter 0.4 inch) manufactured by electroplating nickel over mandrels coated with sand grains (roughness ratio 0.0024–0.049). Results were obtained for Prandtl numbers (Pr) from 1.20 to 5.94 and Reynolds numbers (Re) from approximately 10^4 to 10^5. Heat transfer coefficients (C_H) and friction coefficients (C_F) were obtained. They observed an increase in C_H by as much as 270 percent. However, C_F increased even more. An exception occurred at the highest Prandtl number (5.94) and when the tubes were not fully rough. Under these conditions $2C_H/C_F$ exceeded that of a smooth tube.

In 1967, W. A. Sutherland [22] of the General Electric Company, conducted an experimental investigation on the effect of roughness elements on the performance of an array of heat exchanger rods (1 inch diameter). This heat exchanger geometry had possible use in nuclear reactors. Sutherland called these roughness elements "boundary-layer turbulence promoters" and produced them by winding fine wire around the rods (the thermal resistance of the wire was 500 times that of the rods). The heat transfer and friction measurements were made with air ($Pr = .7$) flowing past the electrically heated rods. When the spacing to promoter height ratio (s/e) was varied from 7.15 to 14.82 using 0.010 inch wire, the results were similar. However, when the effect of promoter heights was varied (e/D_H) from 0.00692 to 0.0349 with a constant s/e of 10.0, the largest promoter gave the largest increase in Nusselt number. The fact that these were turbulence promoters is inferred from the results that show the heat transfer rates of the smaller promoters eventually obtaining the heat transfer rates achieved by the largest promoters with increasing Reynolds number (5000 to 150,000). This suggests that the boundary layer is "tripped" and turbulent flow is eventually produced (fully rough condition) at lower Reynolds number. A larger rib or roughness element will promote turbulence at a lower Reynolds number; but once the fully rough condition is established, the performance is the same with respect to increased heat transfer. The maximum increase in heat transfer was 2.23 times the unpromoted case. Conversely, the friction factor was a function of promoter size, spacing (increasing with larger size and

closer spacing) and Reynolds number. However, once fully rough behavior was achieved, the friction factor (f) was independent of the Reynolds number. No experiments were done below Re = 5000.

The results of Sutherland were plotted using the transformation method proposed by Hall in 1962 [23]. These were then compared to the previous results for the turbulence promoted annular geometries of V. Walker and A. C. Rapier in 1963 [24], O. Wilkie in 1966 [25], N. Sheriff and P. Gumley in 1966 [26], J. Gargaud and G. Paumard in 1964 [27]; the promoted tubular geometry of E. W. Sams in 1952 [28] and in 1965 [29]; and the promoted rectangular geometry of F. J. Edwards and N. Sheriff in 1961 [30]. R. L. Webb in 1972 [31] also used the same dimensionless roughness parameter. Sutherland's paper describes the utility of transformation techniques when analyzing complex problems such as these.

The concept of promotion into turbulence was further studied by R. E. Hicks and W. G. B. Mandersloot in 1968 [32]. Their goal was to develop a correlation between transfer rates and viscous forces that would be general for any type of flow obstruction and process. They performed experiments studying both heat and mass transfer between liquids and a channel formed by placing turbulence promoters between narrowly spaced parallel plates. The heat transfer was promoted by using expanded aluminum and the mass transfer was promoted by using corrugated perforated hard PVC. Measurements of heat transfer rates were performed in a plate heat exchanger using countercurrent flow and a plate spacing of .187 cm. The void fraction was 0.746. The results

of McConnachie and Thodos in 1963 [33] for transfer in packed beds were also used. The heat and mass transfer data were correlated in terms of a j-factor and modified Reynolds number Re* (which contains the viscous energy constant).

The correlation valid for only non-laminar flow is:

$$j = .121(Re^*)^{-0.49}$$

Hicks and Mandersloot's goal, as with earlier work, was to operate in turbulent flow, but obtain this turbulence at lower flow rates (Reynolds numbers). The effect of obstacles on the laminar regime was not investigated apart from finding the transition to turbulence. They reference the work of Thomas [34] who in 1965 used small promoters (thin wires) to increase the transfer rates. However, they conclude large surface area promoters are unavoidable due to their function as membrane supports.

The advantages of increasing heat transfer by the use of turbulence promoters is utilized in plate heat exchangers. As described by J. Marriott in 1971 [35], plate heat exchangers consist of closely spaced plates (2 to 5 mm) with a hydraulic diameter of 4 to 10 mm. The plates are corrugated and produce a high degree of turbulence. From experiments, Marriott correlates heat transfer through the following equation:

$$Nu = .374\ Re^{.668} Pr^{.333} \left(\frac{\mu}{\mu_m}\right)^{.15}$$

Plate heat exchangers are shown to have an advantage over shell and tube exchangers from a pumping cost consideration. Compared to tubular exchangers, plate exchangers have the additional advantages of being small, having less hold up, effective cleaning, and lower fouling factors due to the high turbulence and minimal dead spaces.

In 1978 J. C. Han, L. R. Glicksman and W. M. Rohsenow [36] studied the effect of repeating small rectangular roughness elements (ribs) in a parallel plate channel. Additional work referenced by them on roughness elements not yet mentioned in this review include: Brouillette in 1957 [37]; Koch in 1960 [38]; Molloy in 1967 [39]; Kalinin in 1963 [40]; Webb, Eckert and Goldstein in 1971 [41]; and Dalle, Donne and Meyer in 1977 [42]. Dalle, Donne, and Meyer proposed modifications to the transformation method used by earlier workers with annular geometry.

Han, Glocksman, and Rohsenow attempted to eliminate the need for Hall type transformations and to present a general correlation for heat transfer coefficients and friction factors by using experimental results from a simple channel flow geometry with repeating rib roughness elements. Previous investigators looked at higher flow rates (Re ranging from 10^5 to 10^6) and smaller ribs (the ratio of rib height to hydraulic diameter varying from 10^{-2} to 10^{-3}) than Hans et al. They used air blown through the channel at Reynolds numbers from 3000 to 30,000. The rib height to channel hydraulic diameter was varied from .076 to .102 and the rib spacing to rib height varied from 5 to 20. Different angles of attack and shapes

were also investigated. These larger ribs were used to promote turbulence at lower flow rates. Ribs were placed on both surfaces of the channel. The staggered rib position produced results similar to those obtained with ribs placed symmetrically on both plates. The Nusselt number was increased from 1 to 3 times over that in a smooth channel. Larger ribs produced a continuing increase to the friction factor but yielded only a slight additional increase in heat transfer over the smaller ribs. Both the Stanton number and friction factor showed a maximum when the ratio of the rib spacing to rib height was approximately 10. Ribs with a 45° flow attack angle produced larger heat transfer rates for the same friction power than either a 90° flow attack angle or roughness by sand grains.

Additional work studying the idea of small ribs or roughness elements with high Reynolds number (turbulent) flow was done by J. A. C. Humphrey and J. H. Whitelaw in 1979 [43]. Here the emphasis was to measure the velocity and turbulent characteristics of water flowing through a rib roughened duct of square cross section 4.0 cm on each side and 190.5 cm long. The ribs were .395 cm x .395 cm x 4.0 cm and attached to the lower surface. They were spaced 3.95 cm apart to give a spacing to height ratio of 10. The flow properties were measured using a laser-Doppler velocimeter. The water flowed through the duct at a Reynolds number of 2.6×10^4. They showed a large increase in turbulent kinetic energy at the roughened wall and observed wall effects due to the square cross section of the flow channel.

Finally in 1980 S. E. Faas and D. M. McEligot [44] developed a preliminary computer model to analyze the effect or ribs on heat

transfer and momentum transfer at lower Reynolds numbers. As with previous simple geometries, channel flow is used to reduce side wall effects that cause variations in the flow pattern. In the development of the computer code, it was assumed that the fluid properties are independent of temperature and that a constant heat flux is applied to the outer edge of the plate. The program is designed to calculate local and average Nusselt numbers and friction factors. Unfortunately only one run was completed with this program which is called RUFF. This solution was for Re = 100, Pr = .7 (air), stainless steel plate and ribs, spacing to height ratio of rib = 6.25, width of rib in flow direction to height of rib = 3, and rib height to channel hydraulic diameter = 0.4. The results from the run show the presence of two flow recirculation zones. One upstream and one downstream from the rib with the leeward recirculation zone being larger. The calculated average Nusselt number and average friction factor were respectively 2.9 and 16.7 percent greater than that for laminar flow between two parallel plates without ribs or obstacles. They conclude that the large increase in friction factor might be due to a not fully converged solution.

Mass Transfer

One of the earliest studies using obstructions to fluid flow to increase mass transport was already described in the heat transfer section (Hicks and Mandersloot in 1968 [32]). Hicks et al. used corrugated perforated hard PVC placed between narrowly spaced (.085 cm) parallel plates to promote turbulence during the mass transfer

study. The void fraction was .870 and the mass transfer rates were measured using the limiting current technique. The electrolyte used was 0.1 N ferricyanide and 0.1 N ferrocyanide in 2.0 N sodium hydroxide. The average Schmidt number (Sc) was 2500. As stated earlier, the transfer data were correlated utilizing a parameter called the viscous energy constant. The correlation, which was also valid for packed bed data, relates transfer j-factors to a modified Reynolds number. It is important to note that this equation was limited to non-laminar flow; the promoters were used to produce bulk turbulence (at lower Reynolds numbers).

In 1971 Solan, Winograd, and Katz [45] proposed a "mesh step" model to represent the beneficial effects of using spacer nets (turbulizers) for electrodialysis operating in the laminar regime. Previous models by Sonin and Probstein [46] and Pneuli and Grossman [47] attacked the problem from only a hydrodynamic standpoint. Gregor [48] in 1965 made use of a very simplified model that assumed a decreased, but constant boundary layer thickness. No promoter or flow variables could be described. The model of Solan, Winograd, and Katz used fully developed channel flow hydrodynamics and two parameters: the mesh size and the mixing efficiency to describe a non-constant boundary layer thickness. The laminar mass transfer boundary layer thickness was assumed to grow until a distance of one mesh size was reached. At this point the concentration profile is decreased by a fraction related to the mixing efficiency. After this "partial mixing" the boundary layer again grows according to laminar behavior from its new value for

a distance of again one mesh size. The process and model is represented by a saw-tooth laminar concentration boundary layer.

Then in 1973 the model was revised and experimentally validated [49]. The model still utilized fully developed laminar channel flow hydrodynamics and the two velocity independent parameters: the mesh step and the mixing efficiency. However, in the revised model not only is the concentration boundary layer partially "mixed" after one mesh step, but so is the velocity boundary layer. The new thicknesses are a fraction of the values before "mixing" and they then grow according to laminar behavior until the next mesh step. Experimental studies of various mixing nets used for electrodialysis are described in a 1972 reference by Belfort and Guter [50]. The attempt by Solan, Winograd et al. was to model these mixing nets unfortunately referred to as "turbulence promoters." This revised mesh step model was experimentally validated using the electrochemical technique (the limiting current of the cathodic reduction of ferricyanide was measured). The electrolyte used was 0.01 M potassium ferrocyanide and 0.01 M potassium ferricyanide in 1.5 M sodium hydroxide. The channel produced a 2.3 x 100 mm cross section to flow. The "turbulence promoters" used were commercial plastic nets 1.3 to 1.7 mm thick and a mesh step of 2.5 to 5 mm. Also .9 mm diameter plastic wires at various mesh steps were used. Mass transfer results were presented as a function of Peclet number (Pe = ReSc). The Schmidt number (Sc) was approximately 2000 for the electrolyte used, though the Schmidt number for salt water is about 600. The investigation covered a range of Reynolds numbers from

approximately 4 to 250 (based on an unobstructed channel). Comparison with the mass transfer "mesh step" model was quite good. The predited 1/2 power dependence on Peclet number was observed. The model did not compare well with the experiments when the mesh step was less than 9 mm. Though the promoters were large and created an unmeasured increased resistance to flow, the importance of flow obstacles used to increase mass transfer was shown with a system operating far below bulk turbulence (laminar Reynolds numbers).

In 1975 E. Schlach and N. Ibl [51] presented a technique for increasing mass transfer in a stagnant bath-type electrochemical cell. The idea was to wipe the electrode surface with moving nets which produced local motion near the electrode without stirring the bulk. The mass transfer was measured using the limiting current of the cathodic reduction of ferricyanide on nickel. The electrolyte used was 0.05 M ferricyanide and .10 M ferrocyanide in 2.0 M sodium hydroxide operating at 23°C. The wiping velocity ranged from 0.3 to 50 cm/sec over an electrode length that was varied from 0.2 to 20 cm. The two nets used to wipe the electrode were composed of threads of thickness 80 and 250 μm and with an inter-thread distance of .5 and 2.5 mm respectively. These nets of synthetic tissues were run continuously over the two electrodes which were separated by 5 cm. The mass transfer results were summarized in terms of two dimensionless correlations of Sherwood number (Sh_L) as a function of Reynolds number (Re_L based on electrode length), electrode length (L) and tissue thread thickness (d") or spacing (d) given below:

$$Sh_L = 29.45\ (Re_L L/d)^{.369}$$ nets moving upward

$$Sh_L = 25.07\ (Re_L L/d)^{.377}$$ nets moving downward

$$10 < \frac{Re_L L}{d} < 3 \times 10^7$$

The equivalent thicknesses of the diffusion layer ranged from 4.4 to 95 μm and was compared with the 1 μm thickness obtained from bulk turbulent flow in a thin gap (0.5 mm) electrochemical flow channel [52] (which requires a large power input). From a practical standpoint, wiping accelerated mass transfer as much as laminar channel flow operating at a flow velocity equal to the wiping velocity and having the plate distance approximately that of the thread thickness (laminar flow gives 1/3 dependence on Re).

The concept of promoting turbulence in electrochemical flow channels was further studied by F. B. Leitz and L. Marincic for Ionics Inc. in 1974 [53]. This work was later published in 1977 [54]. Again the aim of their work was to use large obstacles (half the channel gap) of well defined shape to promote turbulence at lower flow rates. Since their goal was optimization, they evaluated the increased pumping costs associated with the obstacles through pressure drop measurements. The hydrodynamics were fully developed channel flow between the two electrodes that formed a cross section 1.0×10^{-3} m x 6.35×10^{-3} m. The obstacles were triangular, circular and rectangular in shape and placed in either the attached, detached, or opposed

position. They blocked half of the cross sectional area to flow and extended fully across the channel between the side walls. The fluid velocity was varied between .25 and 1.00 m/sec, corresponding to laminar flow in the unobstructed channel. The mass transfer was measured using the limiting current method with a specially constructed electrode divided into 1000 unique microelectrodes. The segmenting of the electrode allows local mass transfer rates to be measured as a function of position. The potassium ferricyanide/ferrocyanide electrolyte was used in 0.1 N potassium hydroxide. Because they used a segmented electrode, local current densities (mass transfer rates) were obtained at different positions upstream and downstream from the promoter for different flow rates. Consistently, a dramatic rise in mass transfer was observed at the obstacle, and a slow decrease to pre-obstacle values was observed further downstream. Integrating the local values gave average mass transfer data which were correlated in dimensionless form for each type of promoter. The general form of the correlation was:

$$Sh = \text{constant } (Sc)^{1/3} \ (Re)^{a} \left(\frac{D_e}{\Delta l}\right)^{b}$$

The 1/3 dependence on Schmidt number was assumed; not established experimentally. The Reynolds number dependence (a) varied from .343 to 1.09 and the parameter b varied from .153 to .531. The channel length does not appear; however, the channel equivalent diameter (D_e) and promoter spacing (Δl) are parameters in the correlation.

Pressure drop measurements were used for a cost optimization. It was observed that the optimum spacing ($D_e/\Delta l$) was 0.12 for the promoters. Using pumping power and cost considerations, the use of turbulence promoters gave a significant improvement over purely laminar flow in the channel. The detached cylindrical promoters gave the lowest costs over the broadest range of Reynolds numbers, approximately a doubling of the mass transfer over the unpromoted channel. This study showed the utility of flow obstacles for not only increased mass transfer, but also as overall energy savers when considering the very large fluid pumping cost of producing turbulence by high fluid flow rates. It should be remembered that Leitz and Marincic used obstacles that were large in size when compared to the cross section to flow of the channel (promoters occupied one half the channel gap).

The development of a new type of electrochemical cell utilizing the concept of increased mass transfer in a smaller reactor came in 1975 with the introduction of the "Swiss Roll" cell by P. Robertson, F. Schwager and N. Ibl [55]. This cell consisted of alternating layers of thin electrodes separated by a thin cloth net. This sandwich was then rolled creating a very dense reactor with electrodes closely spaced but separated by a cloth net. The reactant was pumped through the rolled cell in the axial direction; mass transfer was enhanced by the turbulence promoting cloth net separator. Due to the geometry and cloth, this early cell provided a nearly uniform current distribution. Limiting current studies (5 mM ferricyanide/10 mM ferrocyanide in 0.5 M KOH) and pressure drop measurements were performed with the cloth

separators in a parallel plate channel. The flow regime was in the transition between laminar and turbulent flow; mass transfer rates were proportional to the velocity raised to the 0.5 to 0.8 power. The cloth separators (teflon or polypropylene) gave higher mass transfer rates when compared with an empty channel utilizing the same pumping power.

Application of this "Swiss Roll" cell was shown by Robertson and Ibl in 1977 [56]. Here the cell was used to remove copper from dilute synthetic waste waters. For this cell, two different separator cloths and one ion-exchange membrane were used in the electrode sandwich. The cloths had mesh openings 1680 and 250 μm, thread thickness 800 and 200 μm, and mesh count 4.03 and 22.2 cm^{-1} respectively. In earlier work Schwager [57] showed that all the cloth separators could be represented by the following mass transfer correlations:

$$Sh = 0.15\ (Re)^{0.82}\ (Sc)^{0.33} \qquad 5 < (Re) < 80$$

$$Sh = 1.25\ (Re)^{0.34}\ (Sc)^{0.33} \qquad 80 < (Re) < 1000.$$

The copper concentration was lowered to a minimum of 1 ppm in batch experiments. Through an extensive operating and pumping cost analysis, it was concluded that a large Swiss Roll cell plant would be competitive with other waste water treatment technologies. In the introduction of their paper Robertson and Ibl reference other electrochemical processes that employ various methods for increasing mass transfer rates. These include use of packed beds for copper [58,59] and antimony [60] recovery or for oxidation of ferrous ions to ferric ions [61]. Also referenced was the use of fluidized beds for copper

recovery [62] and a U.S. patent by E. I. du Pont de Nemours in 1975 issued for a cell similar to the Swiss Roll cell [63].

In March of 1983, an industrial application of the "Swiss Roll" cell was reported [64] for the production of an intermediate* in the synthesis of vitamin C by Hoffmann-LaRoche. The report describes a large scale rolled electrode sandwich with mass transfer separator cloths. Currently, a 30 m^2 cell is used; eventually an anode of several hundred square meter area is to be employed.

In 1974 A. A. Sonin and M. S. Isaacson [65] suggested a method for evaluating the performance of electrochemical flow systems. The method rates the process on the basis of product yield and energy input. The terms are in dimensionless form so as to be independent of system scale. The cost equation is given below:

$$\dot{K} = k_c A + k_{ej} A\Phi + k_p \frac{\Delta P}{L} VhA \quad (\$/\text{sec})$$

The first term on the right represents capital costs; the second represents costs associated with electrical resistive losses; and the third term represents pumping cost. The cost coefficients (k_c, k_e, k_p) are assumed to be independently known and independent of current density and flow rate. Also the pressure drop is assumed to occur mainly in the reactor. The procedure of optimization is to first obtain a relation for the Sherwood number as a function of

---

*Oxidation of diacetone-L-Sorbose (DAS) to diacetone-2-keto-L-gulonic acid (DAG).

friction factor. This is done through mass transfer and pressure drop measurements. Then this relation is used in the presented model. Minimizing the cost produces the optimum operating point. From preliminary results applied to electrodialysis, they show the advantage of using large turbulent promoters and that these are more effective as the reactant concentration is lowered. Sonin and Isaacson reference two publications that used turbulence promoters not mentioned in this review. These are Rosenberg and Tirrell in 1957 [66] and Kitamoto and Takashima in 1971 [67].

Evaluation of this optimization technique with experimental electrodialysis results was done by Isaacson and Sonin in 1976 [68]. Here they empirically obtained Sherwood number and friction factor correlations. Besides their own data using strip type eddy promoters, they used the previously mentioned correlations by Winograd et al. [49], Hicks and Mandersloot [32], and Marriott [35]. Isaacson and Sonin used a 3.7 cm wide channel with a 0.38 cm electrode gap. Limiting currents were measured for the electrodialysis system containing .01 N KCl. The eddy promoters were non-conducting cylindrical rods 0.167 cm in dimeter (approximately one-half the channel thickness), and were placed in the center of the channel. The promoter rod spacing was varied from 2 to 63 channel thickness. The pressure drop was measured with a differential manometer. The mass transfer and pressure drop results were correlated in dimensionless form. It was observed that a spacing to channel height ($\Delta l/h$) of 4 gave the best enhancement to mass transfer. The correlations obtained for this geometry were:

$$Sh = .12\ Sc^{1/3}\ Re^{.80} \qquad \lambda = \frac{99}{Re} + .29$$

The 1/3 Schmidt number dependence was assumed. The conventional friction factor is given by λ. These equations are valid for only the "fully effective" flow regime ($400 < Re < 1400$). Three regimes were observed: low (below Re 140 to 250) where there was little effect; middle (higher Re) where Sh changed rapidly with Re; and the fully effective regime (Re above 300-400) where the mass transfer power law held (turbulent). By obtaining the dependence of Sherwood number on a modified friction factor the optimization method described earlier was used. It was observed that a spacing ratio $\Delta l/h = 4$ yielded the lowest operating cost at all feed concentrations. When $\Delta l/h$ was 2 higher costs were yielded (not as helpful). Their results compared closely to that of other workers who also used large eddy (turbulence) promoters.

A. Storck and F. Coeuret [69] in 1977 also investigated large cylindrical turbulence promoters. However, in their study the limiting current technique was used to measure local mass transfer rates to 21 segmented microelectrodes that were aligned in the flow direction, and flush fitted in the cathode. The electrolyte was 5×10^{-3} M potassium ferricyanide and 5×10^{-3} M potassium ferrocyanide in 0.5 N sodium hydroxide. The channel provided a cross section to flow of 50 x 10 mm. The cathode was only 30 mm wide so as to not contact the side walls. The two promoter sizes studied were made of PVC and had diameters 5 and 8 mm. They were positioned in the center of the

channel gap (notice the distance from the wall was 2.55 and 1 mm respectively). The small promoters were spaced 2.5 mm and the large ones spaced 2, 7, and 22 mm apart (inter promoter spacing - not center to center). The flow regimes studied ranged from the laminar to the beginning of the turbulent regime based on the unobstructed channel cross section area. The large cylinder (8 mm) results showed a very symmetric mass transfer (current) distribution from promoter to promoter. The mass transfer rates were highest directly under the promoter (where the velocity was the greatest). The small promoters (5 mm) gave similar behavior, though the mass transfer rates were not symmetrical and gradually decreased from promoter to promoter. A model was also presented that describes the unique result of a symmetric boundary layer thickness between the centers of neighboring promoters.

The results of this study were extended and compared with other work in a 1978 publication by A. Storck and F. Coeuret [70]. The method of economic evaluation used for the comparison was the one developed by Sonin and Isaacson [65,68] already described in this review. Besides the large cylindrical promoters of their earlier study (.8 cm cylinders in a 1.0 cm channel, intercylinder distance of 1 cm), Storck and Coeuret looked at three other mass transfer enhancing possibilities for the 1 cm gap channel: 1) increasing the liquid flow rate in the unobstructed channel; 2) flowing the electrolyte through a fixed packed bed of spherical glass beads of diameter 1 mm with a porosity of 0.4; and 3) flowing the electrolyte through a

fluidized bed of 1 mm spheres of glass or stainless steel. An important result is that the promoters or obstacles induce a more uniform distribution of local mass transfer rates. The open channel has a highly non-uniform distribution with the largest rates at the leading edge. After performing the cost evaluation, the fixed bed seemed more economical at lower velocities and the open channel at higher velocities. Storck and Coeuret conclude that mass transfer improvements by obstacles do not reduce the operating cost of the process and furthermore, the added pumping power to such systems (by obstacles) should affect the flow near the transferring wall (implying the benefit of efficient mixing near the wall).

This result is not surprising since their obstacles were very large and very closely spaced and lead to extremely high pressure drops and energy requirements. Furthermore, the advantage of obstacles or turbulence promoters probably breaks down as the flow rate is increased to where the channel would be operating in the turbulent regime in the absence of the promoters.

The previously mentioned economic optimization method and cost expression by Sonin and Isaacson [65,68] was again used in 1979 by J. Shen and R. Probstein [71] to study turbulence promotion in an ultrafiltration process. Here an increase in permeate flux (mass transfer) is desired; however, the additional energy input caused by the obstructions must be evaluated to optimize the complete process.

They reference other methods for flux augmentation for ultrafiltration including the work of Thomas and Watson in 1968 [72] who inserted a wire spiral that was separated from the tube surface;

Dejmek et al. in 1974 [73] who purified whey protein by an ultrafiltration technique using twisted tape inserts that were superior to volume displacement rods; and, the use of a Kenics static mixer by Pitera and Middleman [74] in 1973 for studying laminar flow and by Copus and Middleman [75] in 1974 for studying turbulent flow. However, a systematic and quantitative study of turbulence promoters in ultrafiltration was lacking. Experimental data was obtained in a flow channel 3 in. wide and with a height (gap) of .38 cm. The turbulence (eddy) promoters were stainless steel circular cylinder rods of diameter approximately 46 percent of the channel height. The interpromoter spacing (Δl) to channel height (d) ratio was varied from 2 to 63. The ultrafiltration working fluid was bovine serum albumin (BSA) in .15 M saline water. Two types of flat sheet membranes were used (UM-10 and polysulfone by Abcor Inc.). The experiments were performed in the laminar flow regime with Reynolds numbers ranging from 100 to 1500. The mass transfer rates and pressure drop results are given by the following correlations for the $\Delta l/d = 4$ case.

$$Sh = .072\ Sc^{1/3}\ Re^{.729} \qquad \lambda = 3.383\ Re^{-.312}$$

The one-third dependence on Schmidt number (Sc) was assumed. The Darcy friction factor is given by λ. It is important to note the transfer rates decreased when the spacing ($\Delta l/d$) was reduced to 2 (4 was the best). This agreed with earlier mass transfer results [68,49,72] and heat transfer results with twisted tape inserts by Bergles [76] and Seymore [77]. These results were inserted into the cost optimization

equation and shown to be superior over the unobstructed channels. Another important factor in ultrafiltration is the turbulent promoters' ability to create high fluid shear near the wall, reducing the concentration polarization due to filtrate buildup. Although these large cylindrical turbulence promoters brought about an improvement over an unobstructed channel, it was shown that a considerably greater reduction in product cost is theoretically attainable.

Work in this laboratory dealing with turbulence promoters was completed by K. Hanson in 1979 [2]. Based on earlier observations in 1975 by F. McLarnon [1], the concept of using turbulence promoters small compared to the electrode separation was investigated. A traveling dual-beam laser interferometer was used to directly observe the mass transfer boundary layer during copper deposition below the limiting current in a flow channel. This technique allowed the observation, in situ, of local mass transfer rates in the vicinity of single obstacles. The flow channel had a square cross section (.5 x .5 cm) with copper electrodes forming the top and bottom surfaces. Three different shapes of obstacles were used: cylindrical, rectangular prism, and triangular prism. The 0.762 mm high and 5 mm long electrically insulating promoters occupied only approximately 2 percent of the square channel cross section. These obstacles were either attached to the cathode or placed .762, 1.524 or 2.286 mm from the cathode surface. The electrolyte used was .05 M aqueous copper sulfate, without supporting electrolyte. Flow rates in the laminar regime were investigated. Local plots of boundary layer thickness show the mass transfer enhancing properties of the promoters.

Though no pumping power information was obtained, important conclusions were drawn from the results. The triangular obstacle showed the greatest tendency to decrease the diffusion layer, while the cylindrical obstacle produced the smallest effect. There tended to be better mass transfer enhancement as the obstacle was moved closer to the surface. The obstacles affected the boundary layer thickness for a substantial distance downstream; this recovery distance had strong dependence on Reynolds number (flow rate). The obstacles also had a pronounced effect on the copper deposit morphology, yielding information about the hydrodynamic flow patterns around the obstacles. The concept of producing a more uniform current distribution over the surface by attaching several obstacles was presented along with the idea that the obstacle acts as a new pseudo leading edge for mass transfer.

In 1980 F. Schwager, Roberston, and Ibl published a paper [78] describing pressure drop and mass transfer results for parallel plate channel experiments using the (woven plastic) cloth-type eddy promoters that were used in the "Swiss-roll" cell experiments described earlier [55,56]. The cloth promoters were placed between the top and bottom plates of the electrochemical flow channel. Mass transfer rates were measured using the limiting technique. Different concentrations of ferricyanide ion and ferrocyanide ion were used in sodium hydroxide supporting electrolyte. The cloth separators used had fiber diameters ranging from .0203 to .0800 cm, fiber separations ranging from .0552 to .744 cm and porosities ranging from .702 to .912 respectively. Because the cloths were sandwiched between the electrodes, the

hydraulic diameter of the channel varied from .026 to .192 cm. Mass transfer rates were measured for Reynolds numbers (Re) between 1.0 and 3000. The Schmidt number (Sc) was also varied in the range of 800 to 18500 in studies involving two of the separators. In earlier studies the Sherwood number (Sh) was always assumed to vary with the one-third power of Sc. They experimentally determined an exponent of .35 ± .02, confirming the validity of this assumption over the range investigated. The thinner cloths gave higher mass transfer enhancement than the thicker ones. The mass transfer data were correlated as follows:

$$Sh = .26\ (Re)^{0.62}\ Sc^{1/3}$$

A correlation based on a cloth promoter parameter, defined as channel hydraulic diameter divided by fiber separation (d_h/s_m) yielded:

$$Sh = 1.38\ Re^{.483}\ Sc^{1/3} \left(\frac{d_h}{s_m}\right)^{.531}$$

This correlation agrees well with one based on Ruckenstein's surface renewal model [79]. Schwager et al. show, through power considerations, that the pumping energy required for a given mass transfer rate is considerably lower for cells with the cloth nets than for the corresponding unobstructed flow channel with laminar or turbulent flow. The improvement in the stirring efficiency provided by cloth separators was highest at low flow rates--corresponding to the laminar flow regime. Moreover, this energy improvement occurs even though the

cloth nets provide a large resistance to flow. The current is more uniformly distributed with the fiber cloths. However, when exposed photographic film was placed on the electrodes and electrolyte replaced by developer, the highest mass transfer rates were observed around the leading edge of the promoters.

Additional experimental results by Storck and Hutin were presented in 1980 [80]. Two new turbulence promoting obstacles were investigated in the flow channel used for earlier work with larger cylindrical promoters [69]. The cell provided a 5 x 1 cm cross section to flow. They used platinum plated copper electrodes and a 30°C electrolyte of equimolar ferricyanide/ferrocyanide ions in sodium hydroxide (500 mol/m^3) for the limiting current measurements of overall mass transfer rates. The pressure drop was measured with differential air manometers. Compared to their earlier studies much smaller flow obstacles were used. However, flow rates were quite high and limited to Reynolds numbers above 2100. At these flow rates turbulence would occur in an unobstructed channel. The new promoting schemes included the net type PVC mesh promoters used by other workers [55] with mesh openings from 5 to 50 mm and wire diameters from 0.2 to 1.0 mm and also small diameter (0.7 to 3 mm) cylindrical wires spaced 25 to 50 mm apart. These small promoters were placed against the transfer surface (unlike the earlier work with the large cylinders which were placed in the middle of the channel). The results showed that the mesh-type and small wire promoters gave good mass transfer enhancement (from a 1.7 to a 3 fold increase in the rate of mass transfer at a constant fluid

flow rate). The goal of Stock and Hutin's study was to compare these results with previous work, with regard to energy requirement. It was found that, within a range of 50 percent, all the promoters could be characterized by:

$$k = 4.57 \times 10^{-5} \left[Q_v \frac{\Delta P}{L} \right]^{.217}$$

where k is the mass transfer coefficient and the quantity $[Q_v \ \Delta P/L]$ is an pumping energy input term (mechanical power dissipated). The mesh-type cloths and small cylinders showed better effectiveness by this method. However, it was concluded that an unobstructed channel was the most effective. This is not too surprising since the experiments were done at flow rates higher than those required for transition into turbulence in an unobstructed channel without promoters.

Mass transfer work by Moscicka and Westwal in 1972 [81] and heat transfer work by Miyashita et al. in 1976 [82] and Sparrow and Ramsey in 1978 [83] were referenced by Storck and Hutin involving the use of turbulence promoters.

In 1981 Storck and Hutin published another paper dealing with improvement of a copper recovery process through the use of turbulence promoters in an electrochemical reactor [84]. The same 50 x 10 mm flow channel was used with the large (8 mm diameter) cylinders placed in the center of the channel and spaced 50 mm apart. Copper cathodes and an electrolyte of 5×10^{-4} molar copper sulfate, .1 M sodium sulphate and .1 M sulfuric acid were used. The cell performance was observed at flow rates of 22.5 and 5 cm/s (for an unobstructed channel

with water flowing these velocities correspond to Reynolds numbers of 3780 and 840 respectively). The favorable effect of the large cylinders was clearly shown. The copper concentration dropped much faster and higher Faradaic yields were obtained with the promoters (the limit is 1 ppm). An approximate plug flow model that gave results in agreement with the data was given for the higher mass transfer rates of the promoted channel. The unobstructed channel always had a larger energy consumption when compared to the turbulence promoted channel. The beneficial effect of flow obstacles toward process applications was shown by this paper where cylindrical promoters occupying one half the channel gap were used.

In the same journal Storck and Hutin also present a more general article on turbulence promoters in electrochemical cells [85]. This article presents mass transfer and friction factor (if obtained) correlations from past work related to turbulence promoters. Results were provided from their previous work on the overall effect of: 1) large cylinders placed in the channel center; 2) small cylinders on the transfer wall; and 3) mesh-type promoter placed on the wall [80]. Furthermore, results on the local effects of these obstacles were demonstrated. These local mass transfer effects were obtained using the limiting current technique on 48 isolated platinum microelectrodes (5 mm diameter) and an electrolyte of ferricyanide and ferrocyanide in sodium hydroxide.

Results in the form of mass transfer coefficients were plotted as a function of position around the 3 types of promoters. These showed

a larger wake effect at higher flow rates. The smaller obstructions were mainly studied in the turbulent flow regime. The enhancing effect of many evenly-spaced obstacles is shown through the periodic reproduction of the elementary local mass transfer rate pattern. For the small wires placed on the wall, a maximum in mass transfer is observed both upstream and downstream close to the obstruction. The correlation developed earlier for the large (8 and 5 mm) cylinders placed in the center of the 10 mm gap channel is:

$$Sh = 1.19\ (Re)^{.61}\ Sc^{1/3} \left(\frac{H}{e}\right)^{.5} \left(\frac{d}{H}\right)^{1.5}$$

Here the channel thickness (H), large cylinder diameter (d), and cylinder spacing (e) are additional parameters. No correlation for the small wires operating below the fully turbulent regime was given.

Following theories on turbulent flow in roughened channels, the fully turbulent regime was characterized by $d^+ > 50$ and the correlation is as follows:

$$\frac{\sqrt{f/2}}{St} = 389.5\ (d^+)^{.26}$$

where the Stanton number (St) and roughness parameter ($d^+ = V_0 d/\nu$) are related to the friction factor (f). (V_0) is the friction velocity and (d) is the small cylinder diameter.

An extremely interesting article was published by Kang and Chang in 1982 [86]. These workers experimentally observed and numerically analyzed the effects of large rectangular turbulence promoters in a

parallel plate channel operating in the laminar flow regime. The specific system they modelled was 2-dimensional mass transfer in a flow channel with promoters (side wall effects are neglected in a flat channel). The promoters had heights equal to one-half the channel gap and extended in the flow direction twice the gap separation distance. These rectangular obstacles were placed in either a zig-zag (on opposite walls) or a cavity-type (all on the lower wall) arrangement. The spacing between the promoters was 3.5 or 5 times the channel gap. Regardless of the geometry, no mass transfer was assumed to occur through the promoter or through the wall directly opposite the promoter. The Reynolds number was varied from 50 to 500 and Schmidt number from 20 to 2000. The boundary conditions include a zero wall velocity and a zero concentration of reactant at the electrode surface. The size and shape of eddies formed were computed along with local and overall mass transfer rates (the pressure drop was not presented). With the cavity-type promoter and a promoter spacing to channel gap ratio of 5, eddies were observed before and after the promoter. With increasing Reynolds number these eddies grew (the upstream eddy was smaller) and turned in opposite directions until the upstream eddy disappeared (Re = 100) and the inter-promoter spacing was filled by one large recirculation zone. With the zigzag arrangement two eddies were always present. As the flow rate increased the size of these eddies increased and the downstream eddy elongated in the flow direction (this behavior was observed with the cavity arrangement at Reynolds numbers below 50). Mass transfer rate was higher where the

velocity gradient was larger. The rate was more enhanced by the zigzag geometry and this difference increased as Reynolds numbers increased.

The overall mass transfer rates were correlated for a spacing to height ratio of 5 as follows:

zigzag $\quad Sh = 0.519\ Sc^{.376}\ Re^{.475}$

cavity-type $\quad Sh = 1.069\ Sc^{.376}\ Re^{.294}$

$$10^3 \leq (Sc)(Re) \leq 4 \times 10^5$$

It was noted that the zigzag promoters gave a correlation similar to those experimentally determined by others [68,50,32,65]. Also the correlation shows the beneficial effect of the zigzag over an unobstructed channel (the Reynolds number is raised to the 1/3 power in the unobstructed channel flow). Kang and Chang validated their model by comparing the eddy lengths to those observed experimentally with dye visualization. Comparison was quite good for Reynolds numbers from 20 to 150. It was further shown that instability in the recirculation zones occurred at a Re of 250-300 which then lead to early transition into turbulence for this channel with these large promoters (one-half the gap).

The plate and frame concept was previously presented as an efficient heat exchanger design [35]. In February of 1983 the mass transfer enhancing characteristics of an electrochemical cell design, based on the turbulence promoting plate and frame principle, were presented [87]. The ElectroSynCell (ESC) was developed by the Swedish National Development Company (SU-cell). The cell is constructed by

placing a plexiglas grid between the electrodes. The experimental results presented in this paper compared the mass transfer characteristics of a single grid electrode unit to turbulence promotion by cylindrical rods or by an expanded metal electrode (mesh size 10 x 5 mm). The mass transfer rates were obtained by measuring the limiting current of ferricyanide in 1.0 M KOH on nickel electrodes. The cell provided a cross section normal to the flow of 12 x 154 mm and an inter electrode gap of 9 mm. The 5 or 7 mm diameter cylindrical rods were positioned in the center of the channel. The Reynolds number was varied from 70 to 800 but no pressure drop data were reported. The optimum spacing for the rods was 20 mm for both diameters. The SU-grid yielded three to six times higher mass transfer rates over the channel with flat electrodes. The grid performed better than either the rods or the expanded metal and represented by the correlation:

$$Sh = 5.57\ Re^{.40}\ Sc^{1/3}$$

$$70 < Re < 800$$

The 1/3 dependence on Schmidt number was assumed. The 0.40 exponent on Reynolds number appears suspiciously low when compared to their other correlations.

The cells are manufactured in two sizes with the large (ESC) having approximately a 0.75 cm grid mesh and the small (MP) cell having approximately a 0.30 cm grid mesh [88]. The electrode gap is given as 5 mm for the ESC and 6 mm for the MP. Also given in the company pamphlet is a pressure drop of 8-51 KPa per module of ESC cell. The module may have a flow rate of 65-195 liters/min. However, electrolyte flow per cell is given at 5-15 liters/min. It is important to

note that the grid extends between the two electrodes and presents a large barrier to flow.

At the completion of this thesis, in August of 1983, experiment results by W. W. Focke [89] dealing with mass transfer enhancement by semicircular cylindrical turbulent promoters were presented.

The flow channel was 50 mm wide, with a gap of either 5.05 or 8.08 mm. The eddy promoters were half cylinders with a height equal to half the channel gap and were placed alternately on opposite walls of the channel. Promoter spacing to promote height ratios of 12, 36, and 108 were used. Local values of mass transfer rates were obtained by measuring the limiting current for the reduction of ferricyanide on an array of strip electrodes. Potassium carbonate was used as the supporting electrolyte. The ferricyanide concentration was varied from 0.005 to 0.015 M. Using a rotating disk, the following expression for the ferricyanide diffusivity was obtained:

$$\frac{D_i \mu}{T} = 2.29 \times 10^{-15} \qquad Kg(sec)^{-2}(^{\circ}K)^{-1}$$

A differential pressure transmitter was used to measure pressure drop. Both the laminar and turbulent regimes were investigated; however, emphasis was placed on the turbulent promoting ability of the large obstacles.

Focke presents a qualitative description of the effect on the flow pattern and separation of a backward-facing step as the fluid velocity is increased. A downstream recirculation zone is described which

elongates along the flow direction with increasing Reynolds number in the laminar regime.

The experimental results show this growth when the reattachment point is assumed to coincide with the largest downstream local mass transfer rate. With increasing flow rate, the length of this point increased to approximately 15 promoter heights before decreasing. Minimum rates were observed directly upstream and downstream from the obstacles. The promoters were electronic conductors because large mass transfer rates were measured at their location. Transition to turbulence occurred at lower Reynolds numbers with larger promoters or closer spacing. The maximum reattachment length was observed to occur at lower Reynolds numbers as the promoter spacing was decreased. A one-third dependence of Sherwood number on Schmidt number was valid for the experimental data. For the turbulent flow regime the following correlation was obtained:

$$Sh = 0.57\ Re^{0.65} Sc^{0.33} \left(\frac{d_h}{P}\right)^{0.40}$$

The promoter spacing (P) and channel equivalent diameter (d_h) were used. The turbulent flow results found good agreement with turbulent flow theory and the mass transfer similarity function. The pressure drop results were only presented in the form of friction factor plots. Though most of the study dealt with transition to turbulence, the effects of the promoters on the laminar flow recirculation zone length agree with results of this study (this will be described further in a later section).

Other Methods for Achieving High Mass Transfer Rates

Most of the previous methods for improving rates of mass or heat transfer described in this review have been achieved by modifying the flow channel or the duct geometry. Obstructions and other roughening agents placed in the flow path have been successfully used to increase the mass or heat flux through a thinned diffusion layer. Besides the flow-through schemes discussed earlier, other transfer enhancing techniques have been investigated.

In this laboratory it has been shown by D. Roha that movement of suspended inert particles increases mass transfer rates in a stirred system [90]. His work, completed in June 1981, used the limiting current technique with ferricyanide. Roha measured mass transfer rates to a disk electrode rotating in a suspension of micron-sized particles. A 0.56 cm or 1.41 cm diameter rotating disk was alternately used. The particles were spherical glass beads and had size distributions in the range of: 1-5, 5-10, 8-20, 0-25, 44-53 and 61-74 μm. The disk was rotated at approximately 387 to 2800 rpm and the fraction of particles varied from 0-40 percent by volume. At a given rpm, the limiting current could be raised to a value over three times higher than that obtained without particles. The increase was greater at higher rotation speeds and with the larger disk electrode. The maximum increase in current was observed with approximately 10 μm sized particles.

Roha referenced other methods for increasing mass transfer; these will be briefly mentioned. Electrodeposition rates have been increased

by using spray nozzles which direct jets of electrolyte towards the cathode [91-96 and recently 97]. Flow channels with a very thin electrode gap (millimeters) have been operated at very high flow rates to produce high current densities [98-102]. Very high current densities have also been obtained by mechanically contacting (driven by an external source) the electrode surface with cloths, brushes, wipers, honing stones, or abrasive belts [103-110]. Increased mass transfer to electrodes has been achieved by sonic or ultrasonic vibrations [111-115]. Induced motion caused by magnetic fields have also been studied as a method for increasing transfer in electrolyte soutions [116-118]. Creating fluid motion by a sparging gas through the solution has been used effectively for increasing transfer rates [119-121]. The addition of solid particles has also found many mass transfer applications including fluidized beds [122-135]. Packed beds or porous electrodes also give high rates of mass transfer [167-168].

More recent studies not included in Roha's review include measurement of mass transfer rates to a spherical particle in a stirred tank reactor [137]. A novel electrochemical reactor design, utilizing oxygen evolution at the counter electrode [138] produces the effect of gas sparging without an external gas source. The evolved gas produces motion that increases the transfer 2 to 5 times over natural convection. A study of different flow patterns in the chlorate cell to overcome hypochlorite mass transport limitations has been presented [139]. The maximum mass transfer has been shown to occur at the point of flow reattachment in a cell where the cross sectional

area was suddenly increased [140]. A recent review of the vibrating wire electrode has recently been published [141]. Drag reducing polymers have been added to the electrolyte in a flow cell in an attempt to reduce the flow drag more than the reduction produced on the limiting current [142]. A trickle tower packed with Raschig rings was used for scavenging metals [143]. Nodulation of electrodeposited copper due to suspended particles (non-conductors and conductors) has been reported [144]. Finally, laser-enhanced electroplating has been described recently [145, 146]. The application of this method for precise localized deposition is on the horizon.

EXPERIMENTAL APPARATUS

The purpose of this investigation was to observe the effect of small flow obstacles on the limiting current and pressure drop in the square cross section electrochemical cell used for an earlier interferometric study [2] in this laboratory. That study used a double beam laser interferometer to obtain direct images of the mass transfer boundary layer in copper deposition from a copper sulfate electrolyte. The flow channel and holding tank were the only equipment items from the previous study that were used again in this study. The adaptation of the earlier system for limiting current and pressure drop measurements included:

1. Construction of a plumbing system suitable for the present study;
2. Construction of nickel electrodes for the limiting current measurements;
3. Adaptation of the flow channel for measurements of pressure drop;
4. Obtain and assemble the necessary electronics and other equipment for the measurements; and
5. Manufacture the small obstacles and develop a method for spacing and attaching them to the electrode surface.

Electrolyte Flow System

A diagram of the flow system is presented in Fig. (7). The electrolyte solution was prepared in the lower tank. This solution was then pumped up to the elevated holding tank. Electrolyte flow

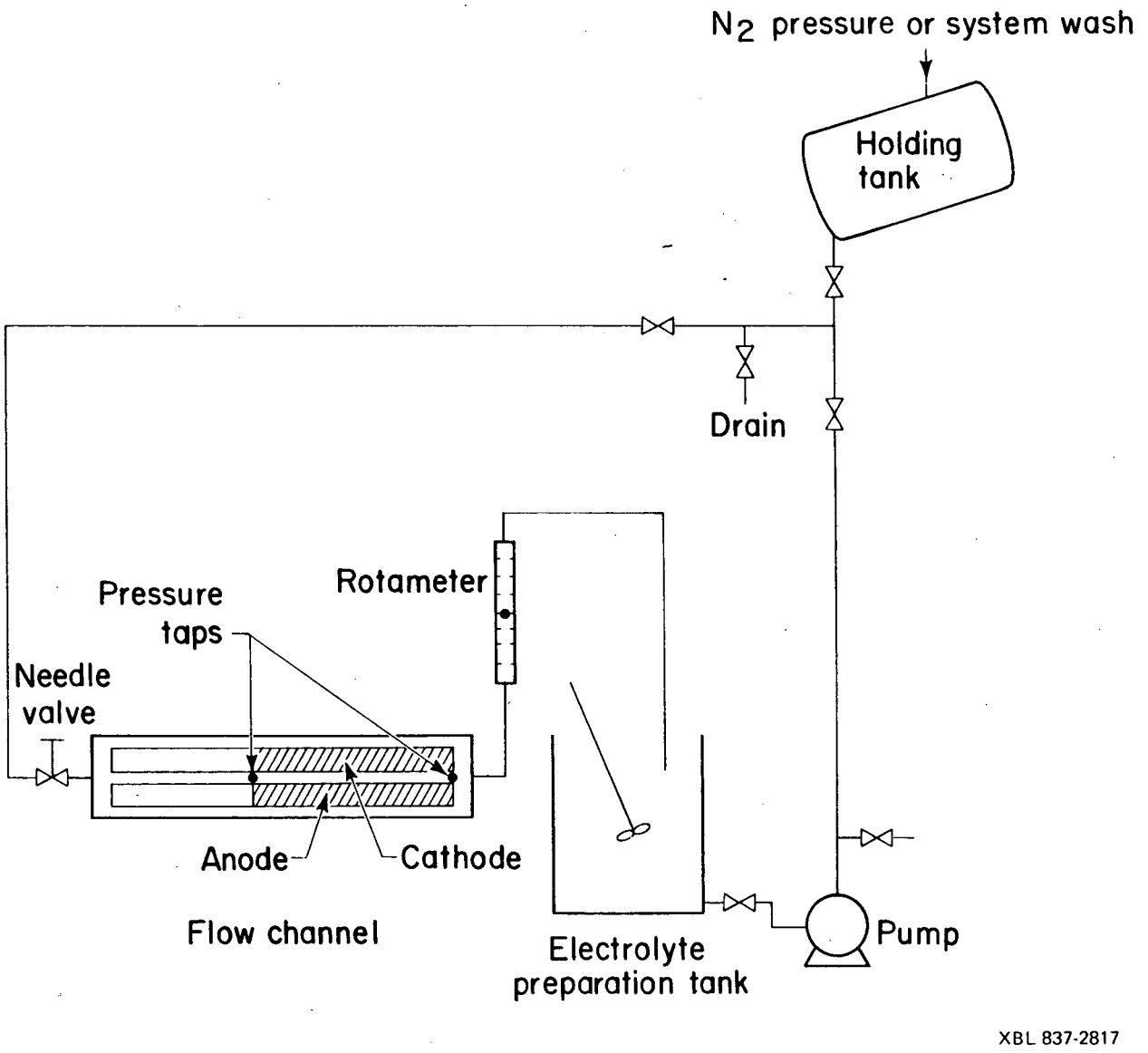

Fig. 7. Schematic of flow system.

through the channel was gravity driven. However, if higher flow rates were needed extra pressure could be applied to the holding tank from a nitrogen gas cylinder. A needle valve was used to adjust the flow rate, which was measured by a rotameter. Installing a number of ball valves produced a versatile system and enabled drainage and by-pass operation.

All connectors (Fast and Tite®) and tubing (Parflex®) were black polypropylene (150 psi max at 75°F) materials obtained from Parker Hannifin Corp. The connectors were leak-proof; Teflon® tape was used on all threaded fittings. The electrolyte preparation tank was polyethylene. All valves were made from polypropylene and purchased from Hayward Valve Company. A Doric Model 410A Trendicator (accurate to 0.1°C) was used to measure the electrolyte temperature. A type K thermocouple inside a stainless steel thermocouple well was inserted into the 90° elbow following the flow channel. Gilmont flowmeters (rotameters) were used for the flow rate measurements. Specifically, flowmeter No. 3 with a stainless steel float and flowmeter No. 4 with a glass float were used. Electrolyte contacted only Teflon and glass in the flowmeter. Calibration of the flowmeter was performed with the aid of a stopwatch and graduated cylinders.

Flow Channel

A cross section of the flow channel is shown on Fig. 8 (not to scale). The electrolyte passes through the approximately .5 cm square cross-section channel (actual effective hydraulic diameter (D_e) = 0.46 cm) which is formed by electrodes on the top and bottom surfaces

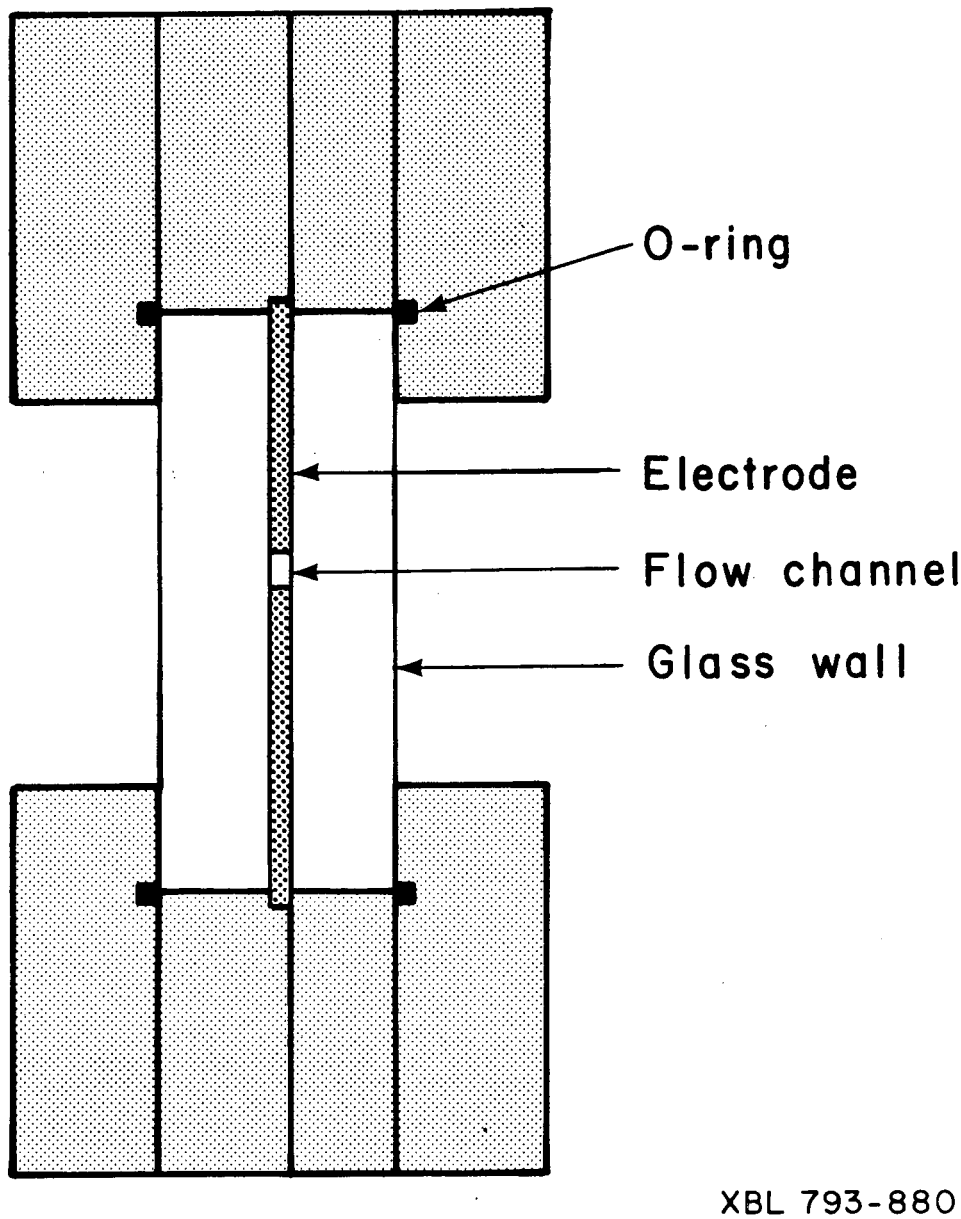

Fig. 8. Cross-section of flow channel. Note square geometry.

and a glass wall and plexiglas wall forming the sides. This produces the square duct geometry that is also shown in Fig. 1. A special large, soft o-ring (a 3/16" neoprene tube inside a 5/16" tube) seals the channel [2]. A fully developed velocity profile is assured by a 55 cm long plexiglas entry region with the same geometry as the following active electrode region. The nickel electrodes constructed for the limiting current measurements are shown on Figs. 9 and 10. Both pairs of electrodes are .476 cm (3/16 inch) wide and have an active length of 50.8 cm (20 inches). The electrodes shown in Fig. 9 were used only in the larger (.160 cm) obstacle study - composition (measured by x-ray spectography) of 95.96 Ni, 3.03 Fe, 0.75 Al and 0.26 Cr. The electrodes used in the other experiments (Fig. 10) were fabricated from Nickel 200. The flow channel is assembled by first inserting the electrodes. They are held in place by 3 stainless steel screws sealed with o-rings. These screws are also used as electrical connections to the electrodes. The electrodes are sandwiched between the glass channel walls and acrylic shell shown by Fig. 11. The entire assembly is then bolted together (Fig. 12). The entry region can be seen to the left of the channel in Fig. 12.

Electrical System

A schematic of the equipment used for the limiting current measurements is shown in Fig. 13. A PAR 371 potentiostat was used for potentiostatic control of the potential applied to the working electrode (cathode). An ammeter (Data Precision Model 1455) was used to measure the current passing through the cell. Limiting current curves

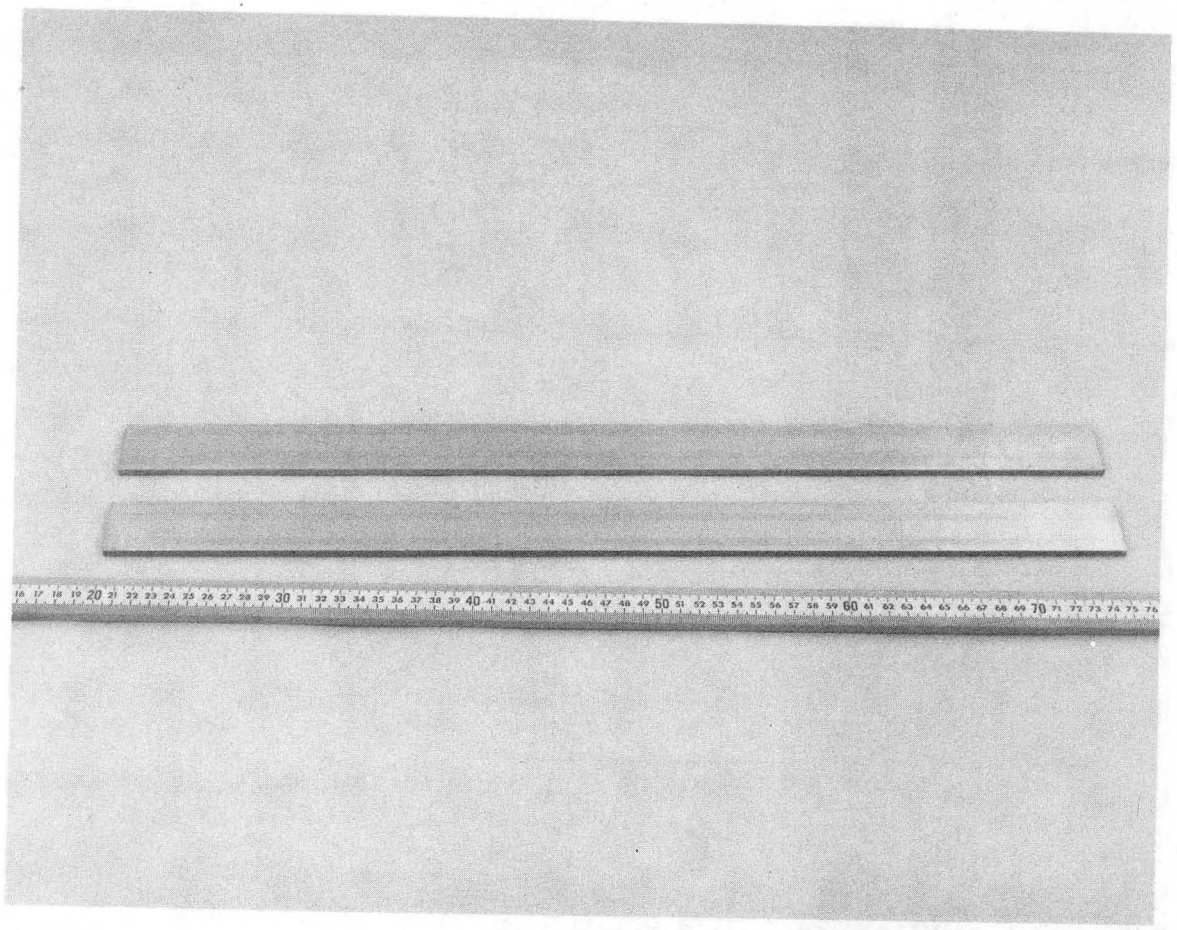

CBB 832-1495

Fig. 9. Nickel electrodes used for the experiments with the 0.16 cm obstacles.

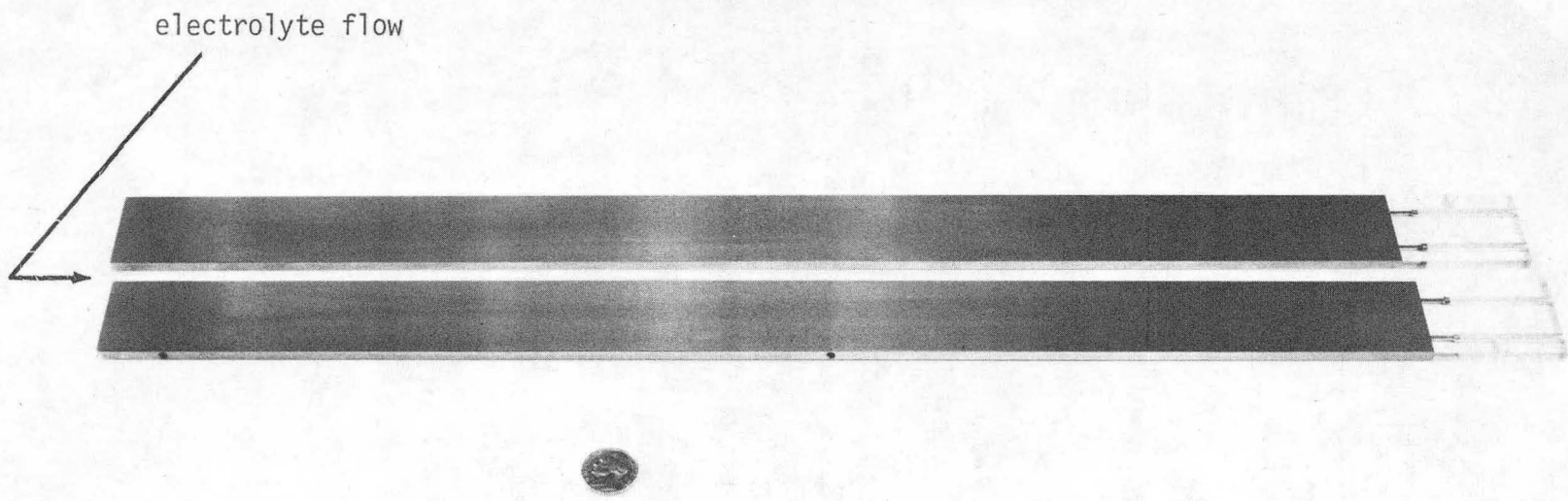

XBB 833-1734A

Fig. 10. Nickel electrodes. Active surfaces are between the electrodes.

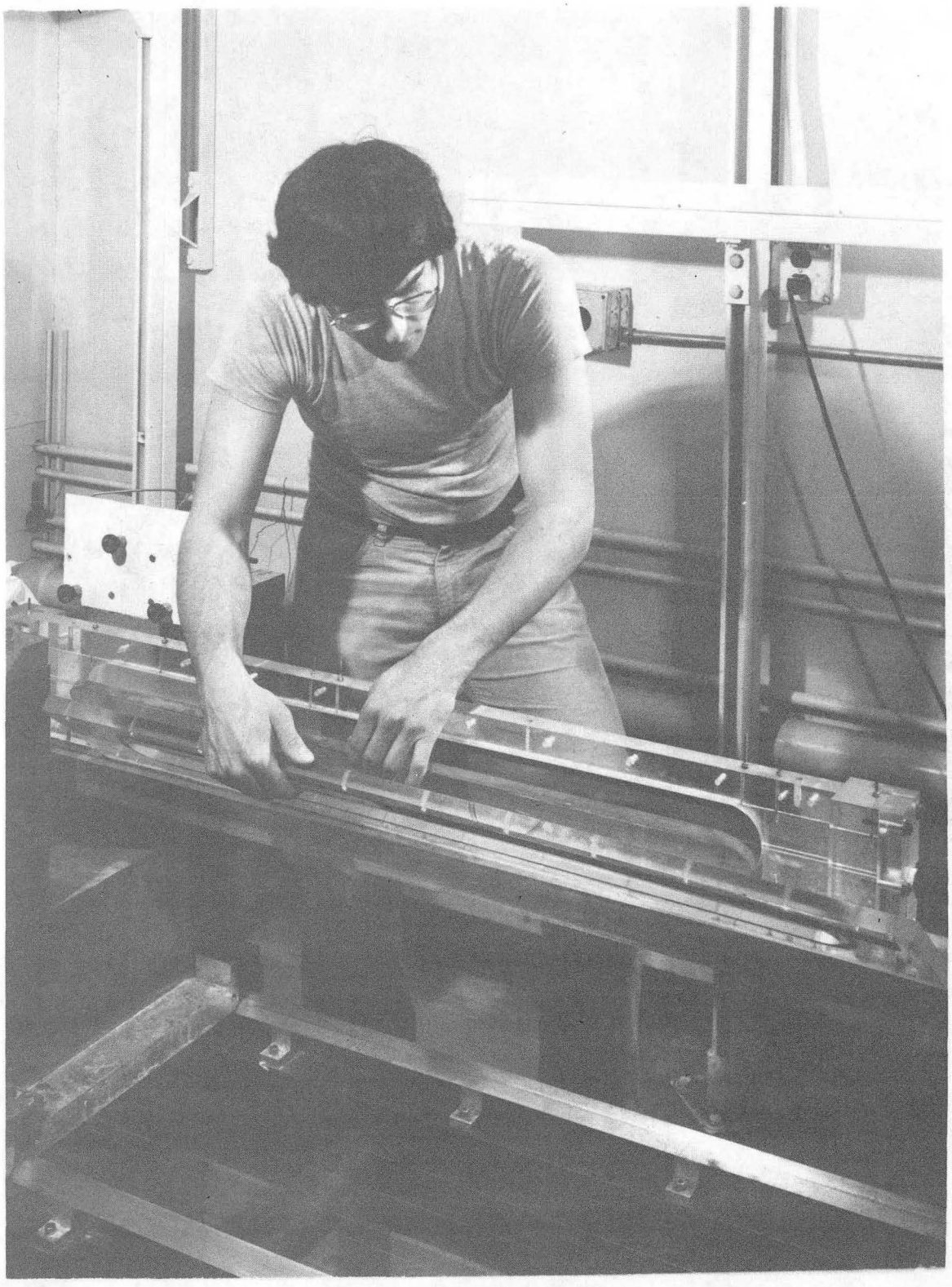

CBB 832-1701

Fig. 11. Flow channel assembly. Electrodes are in place. Glass side wall (left hand) and acrylic shell (right hand) are shown.

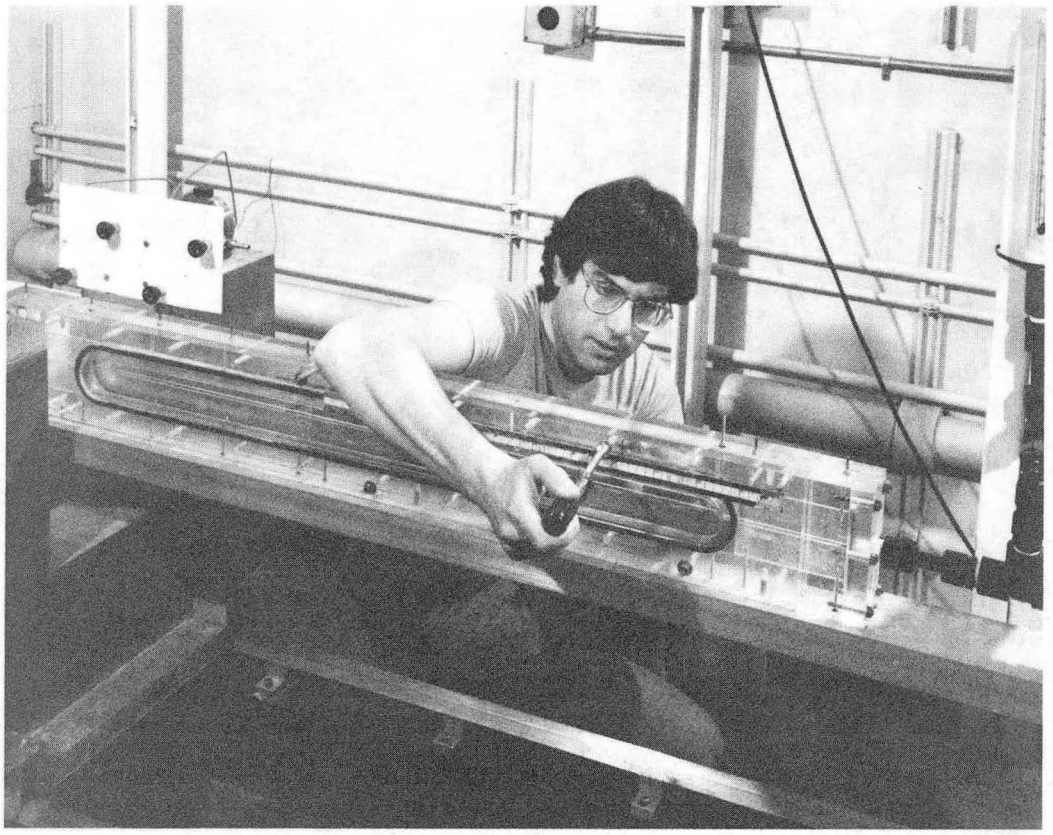

XBB 832-1699

Fig. 12. Assembly of the flow channel, bolting the acrylic shell.

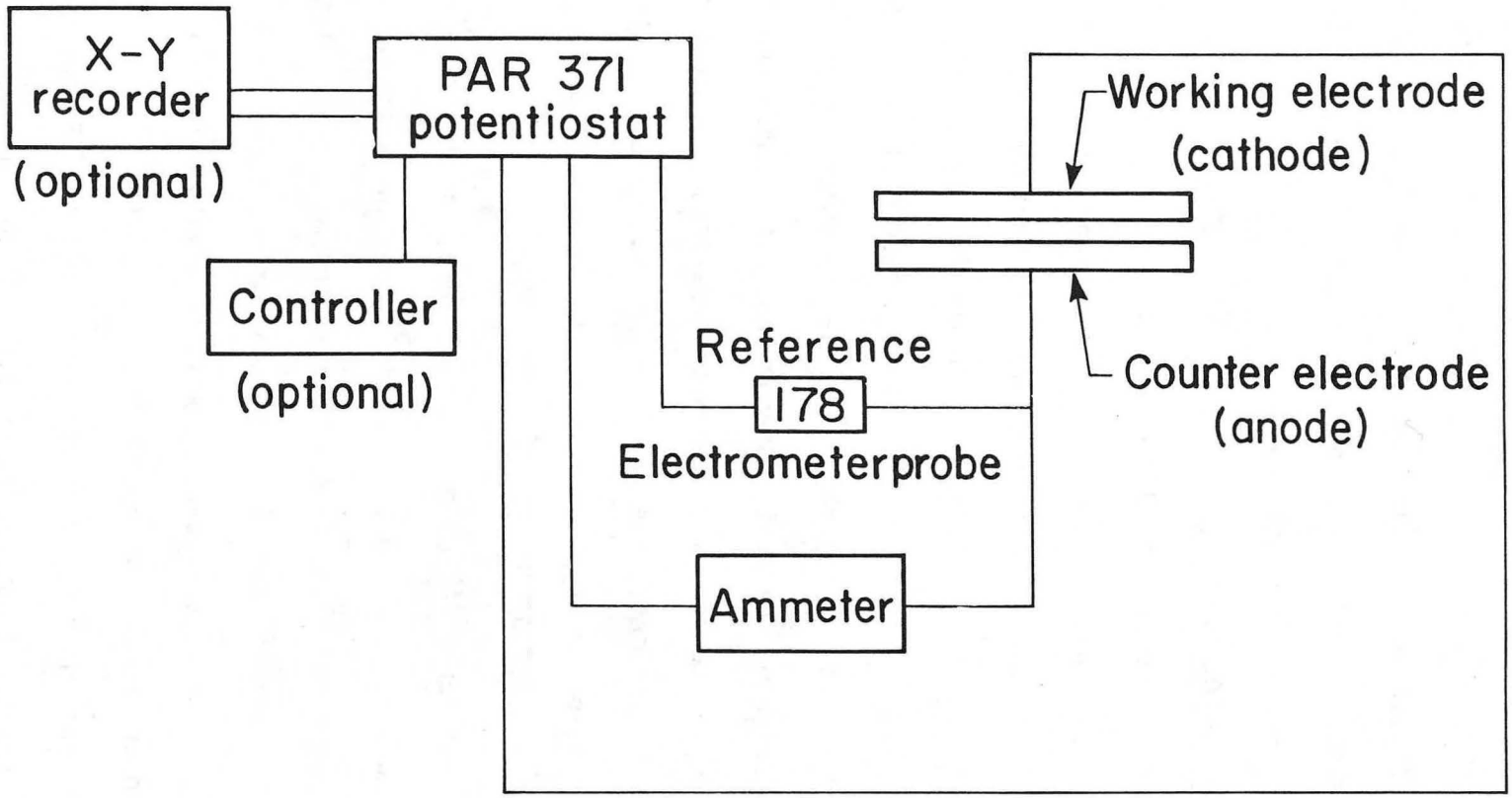

XBL 837-2885A

Fig. 13. Schematic of the experimental electrical components.

were obtained using a potential ramping device (controller) built in house by Mr. J. Severns (No. 7S 2481) and a Gould X-Y recorder (Model 3054 with time base). Since an absolute value of the applied potential was not needed, the counter electrode (anode) was used as the reference for the potentiostat.

Pressure Monitoring System

Two pressure taps of 0.074 cm diameter were machined into the plexiglas side wall 50.8 cm part and halfway between the electrodes (Figs. 14 and 15). (This plexiglas wall replaced one of the optical glass side walls used originally in the interferometric study.) Also shown in Fig. 15 is a capillary Teflon tube that can be connected to a reference electrode compartment. The pressure at the leading and trailing edge of the active channel was then transmitted by tygon tubing to open ended glass tubes (manometers) or a Validyne DP103 pressure transducer. The fluid piping and the electronic components for this diaphragm-type transducer are shown on Fig. 14 (a Keithley 179 TRMS Digital Multimeter was used).

For the larger (.160 cm) obstacle experiments, the pressure drop was calculated by measuring the difference in height between two vertical open ended glass tubes. The measurement of the liquid heights was performed with the aid of a cathetometer (shown in Fig. 16). This sighting instrument allowed very small liquid height differences to be measured accurately (to ±.005 cm).

The transducer was more convenient to use. Furthermore, it allowed transient data to be recorded. The transducer contains a

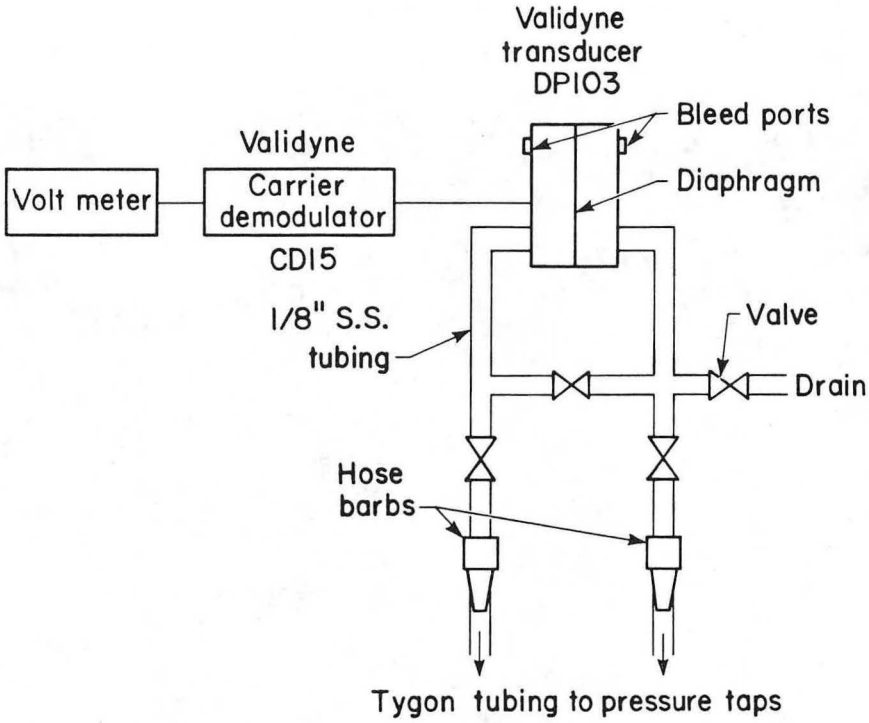

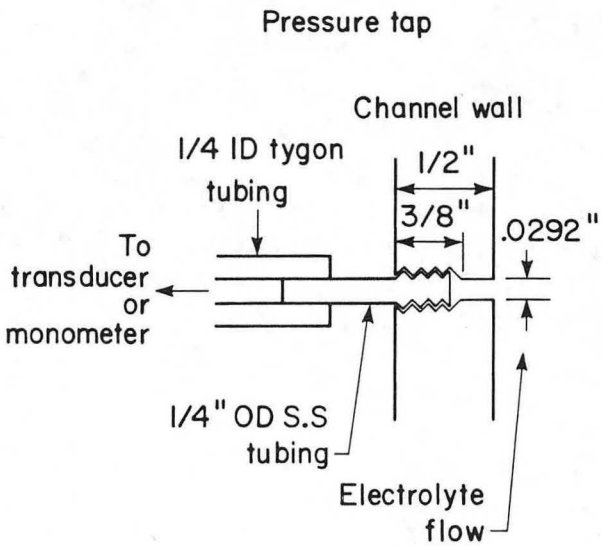

XBL 837-2884

Fig. 14. Pressure measuring system and pressure tap cross-section.

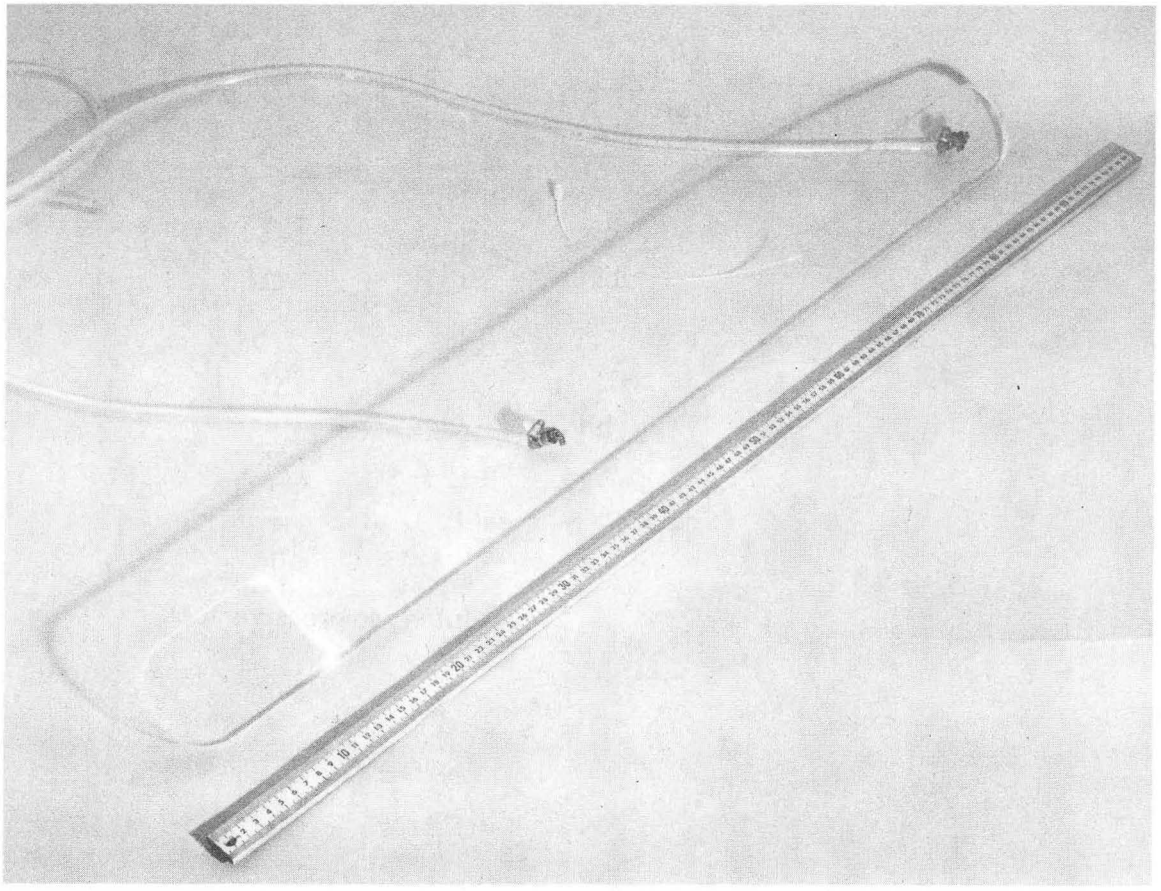

XBB 832-1500

Fig. 15. Plexiglas side wall. Pressure taps with tygon tubing and reference electrode connection are shown.

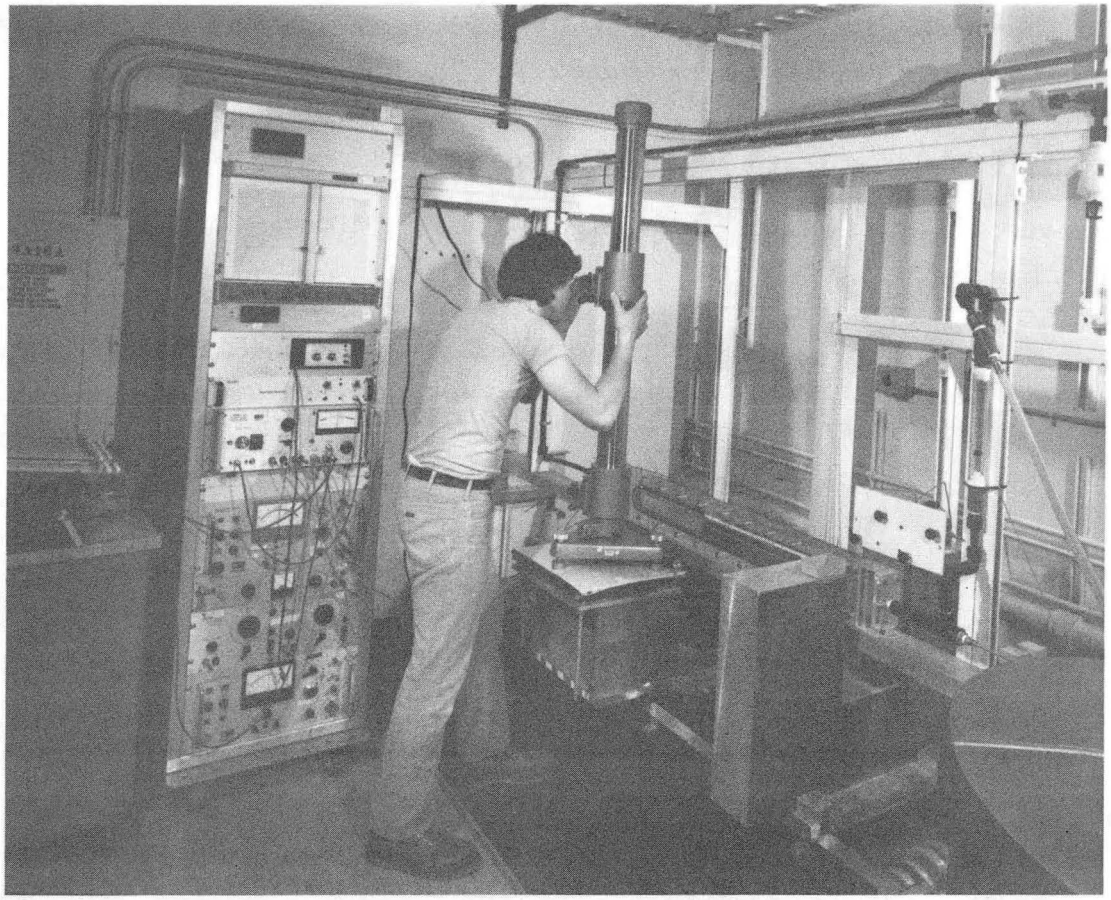

XBB 832-1697

Fig. 16. Electrical equipment rack, flow system, and cathetometer for pressure drop measurements.

metal diaphragm which undergoes a deflection in response to pressure differences. The deflection decreases a gap on one side of the diaphragm and increases a gap on the other side. The physical displacement and resulting magnetic reluctance variation is converted to a voltage output proportional to the applied pressure difference. The Validyne transducer was calibrated using the cathetometer and two vertical glass tubes (manometers) filled with water.

Electrode Preparation

The electrodes described earlier and shown in Figs. 9 and 10 were .476 cm (3/16 inch) wide and had an active length of 50.8 cm. All surfaces except those forming the active surface (24.2 cm^2) had to be electrically insulated. Attempts were made to coat the sides of the electrodes with Kynar , a vinylidene fluoride resin from Pennsalt Chemical Corporation. This failed because the Kynar did not adhere to the electrode (probably due to improper baking at the LBL paint shop). Finally, polyurethane proved successful. Varethane high gloss spray was used for the larger obstacle (.16 cm) experiments and liquid high gloss polyurethane from Ameritone (diluted by thinner) was used for the other experiments with the electrodes shown in Fig. 10. The polyurethane had to be reapplied after every second run because it peeled off the electrode. Differences between the two runs due to ineffective urethane coating were insignificant. Once the electrodes were coated they were polished using the right angle jig shown in Fig. 17. Silicon carbide paper with adhesive backing (from Buehler Ltd.) was placed on the flat metal surface. This surface was then slid back

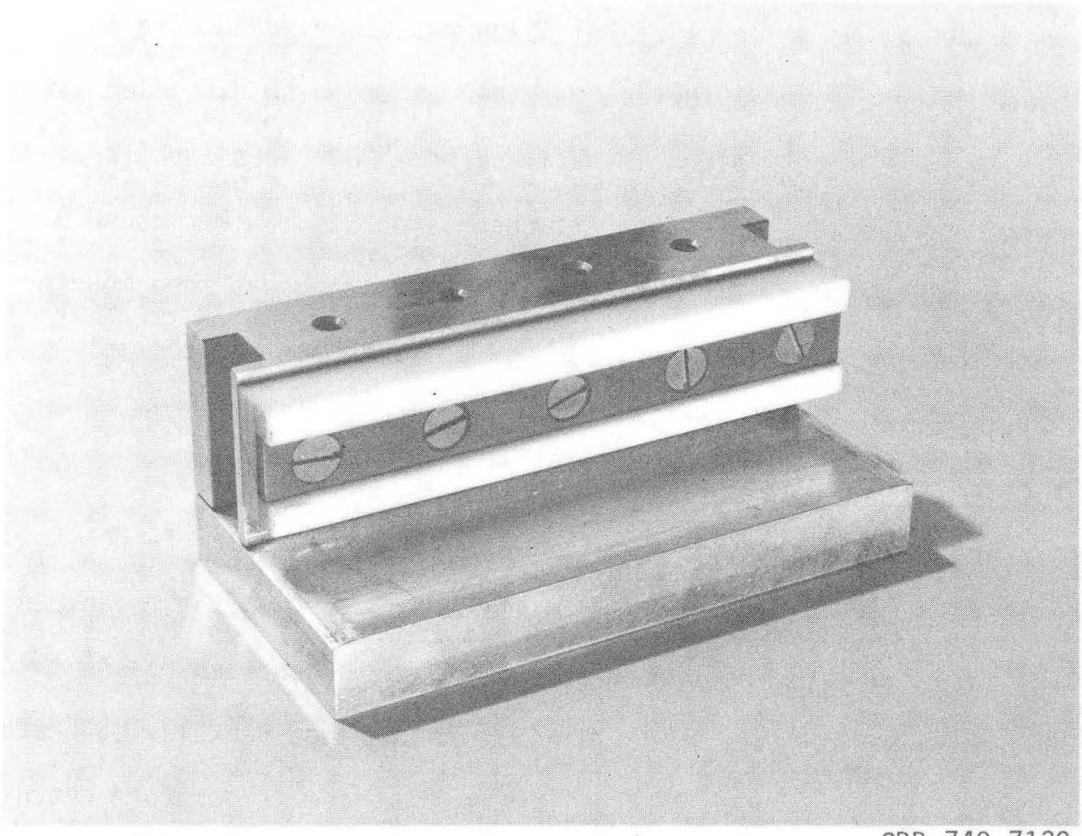

CBB 740-7139

Fig. 17. Electrode polishing jig.

and forth on the electrode with the Teflon guides contacting the electrode sides. A photograph of the jig in operation has been described by McLarnon [1]. Polishing was achieved down to 600 grit paper. The electrode surface was then rinsed with distilled water and then with isopropyl alcohol (Mallinckrodt .0004 residue after evaporation). The obstacles were attached using Eastman Permabond 910 Adhesive (cyanoacrylate ester) and the electrode was then mounted in the flow channel. The electrode was polished and new obstacles attached for every experiment.

Electrolyte Preparation

The 0.01 M potassium ferricyanide/0.05 M potassium ferrocyanide with an excess of sodium hydroxide electrolyte used for the experiment was prepared using demineralized water, which had been passed through an ion exchange resin in Building 62 of Lawrence Berkeley Laboratory. This water was allowed to equilibrate with room temperature overnight. A larger concentration of ferrocyanide ion was used to insure that the limiting reaction in the cell was due to the ferricyanide reduction and not to that of the ferrocyanide oxidation at the counterelectrode. (Diffusivity of ferrocyanide is lower than that of the ferricyanide ion.) Nitrogen gas was sparged through the solution before and after electrolyte make-up to remove dissolved oxygen. Thirty liters of fresh electrolyte were prepared for each run. The 30 liter solution batches were composed as follows:

For the large obstacle runs,

0.10 M NaOH sodium hydroxide (mw 40.0) (120 g)

0.05 M $K_4Fe(CN)_6$ $3H_2O$ potassium ferrocyanide trihydrate (mw 422.4) (633.6 g)

0.01 M $K_3Fe(CN)_6$ potassium ferricyanide (mw 329.25) (98.78 g)

All other runs,

0.30 M NaOH sodium hydroxide (mw 40) 360 g)

0.05 M $K_4Fe(CN)_6$ $3H_2O$ potassium ferrocyanide trihydrate (mw 422.4) (633.6 g)

0.01 M $K_3Fe(CN)_6$ potassium ferricyanide (mw 329.25) (98.78 g)

The chemicals were dissolved in 30 liters of water (measured by weighing) with the aid of a mechanical propeller. Reagent grade potassium ferrocyanide trihydrate and potassium ferricyanide were obtained from J. T. Baker Chemical Co. The sodium hydroxide pellets were obtained from Mallinckrodt Inc. The electrolyte was sparged with nitrogen for two hours before beginning the experiments.

Electrolyte Physical Properties

Both electrolyte solutions had a density (ρ) of 1.02 gm/cm^3. For the electrolyte used with the larger (.16 cm) obstacles (0.10 M NaOH), the viscosity (μ) was calculated using the empirical equation of Boeffard [147] given in terms of the species concentrations (C_i in moles/liter):

$$\begin{aligned}\mu(\text{cps}) = 0.96714 &+ 0.09622\, C_{NaOH} - 0.20528\, C_{Ferri} \\ &+ 0.090255\, C_{Ferro} + 0.05404\, C_{NaOH}^2 + 0.53303\, C_{Ferri}^2 \\ &+ 0.43505\, C_{Ferro}^2 + 0.23546\, C_{NaOH}C_{Ferri} \\ &+ 0.302585\, C_{NaOH}C_{Ferro} + 0.99923\, C_{Ferro}C_{Ferri}\end{aligned} \tag{27}$$

This equation was obtained for a 25°C electrolyte and using it could have introduced a ±3 percent error to the large (0.16 cm) obstacle calculations in which the electrolyte temperature was not regulated. This probable error was eliminated from the other runs by direct measurement of viscosity using a capillary viscometer.

Knowing the viscosity (μ), the diffusivity of the ferricyanide ion (D_i) was determined from the equation by Gordon et al. [14]

$$\frac{D_i \mu}{T} = (0.234 + 0.0014\Gamma) \times 10^{-9} \frac{cm^2 \text{ poise}}{sec\ ^\circ K} \tag{28}$$

where the ionic strength (Γ) is given by:

$$\Gamma = \frac{1}{2} \sum_i^m c_i z_i^2 \tag{29}$$

The transference numbers (t_+) were calculated using the following equation:

$$t_+ = \frac{c_+ z_+^2 u_+}{\sum_i c_i z_i u_i} \tag{30}$$

Using the ionic mobilities at infinite dilution given by Glasstone [148], Beoffard [146] obtained the following expressions for the transference numbers:

$$t_{Ferri} = \frac{C_{Ferri}}{C_{NaOH} \times 0.8189 + C_{Ferri} \times 1.7179 + C_{Ferro} \times 2.4293} \tag{31}$$

$$t_{OH-} = \frac{C_{NaOH}}{C_{NaOH} \times 1.2531 + C_{Ferri} \times 2.6442 + C_{Ferro} \times 3.7175} \tag{32}$$

Applying this equation to the electrolyte solutions in this study gave a ferricyanide transference number (t_{ferri}) of 0.0453 for the 0.1 M NaOH electrolyte and 0.026 for the 0.3 M NaOH electrolyte. A summary of the range of the electrolyte fluid properties is given below.

Composition	0.30 M	Sodium Hydroxide
	0.05 M	Potassium Ferrocyanide Trihydrate
	0.01 M	Potassium Ferricyanide

Temperature (°C)	Viscosity (μ) (cp)	Ferricyanide Ion Diffusivity (D_i) (cm^2/sec)	Schmidt Number (Sc)
22.8 - 24.2	1.02 - .990	6.82×10^{-6} - 7.12×10^{-6}	1353 - 1465

A procedure for the quantitative titration of the electrolyte is given in Appendix B. Titration showed the ferricyanide concentration differed by less than one percent before and after performing experiments and less than seven percent from the 0.01 molar value at the end of a day's experiments.

Obstacle Fabrication and Electrode Attachment

The flow obstacles used in this study were all rectangular in cross section and constructed from nonconducting materials. The dimensions of the three sizes shown in Fig. 18 are summarized below.

Obstacle Size	Dimensions (Perpendicular to Flow X With Flow X Across Channel)
Large	(.160 cm x .146 cm x .476 cm) or (.06315" x .0573" x .1875")
Small	(.0762 cm x .0825 cm x .476 cm) or (.030" x .032" x .1875")
Micro	(.0254 cm x .0825 cm x .476 cm) or (.010" x .032" x .1875")

The "Small" obstacles correspond to those used by Hanson [2]. The three different obstacles were all approximately square end-on; except for the "Micro", which had the same length in the flow direction as the Small but were only one third as high. (From here on the obstacle size will be capitalized.)

A qualitative comparison of the Small to the Large obstacles is shown by Fig. 19. The Large obstacles were Lucite (acrylic) machined to size using the jig shown in Fig. 20. A .060 inch square strip is held down by the metal bar and allen bolt; it is then sliced off into obstacles 3/16 inch long. This method was not used for the Small and Micro obstacles, rather these were punched from .030 and .010 inch thick cellulose acetate sheets. The punch, shown in Fig. 21, produced obstacles that were very smooth and clear on two opposing surfaces and dull on the others. The clear smooth surface was attached to the electrode allowing the dull surfaces to be perpendicular to the on-coming flow. The electrode was cleaned with isopropyl alcohol and the obstacles attached with Eastman Permabond 910 TM Adhesive (cyano-acrylate ester).

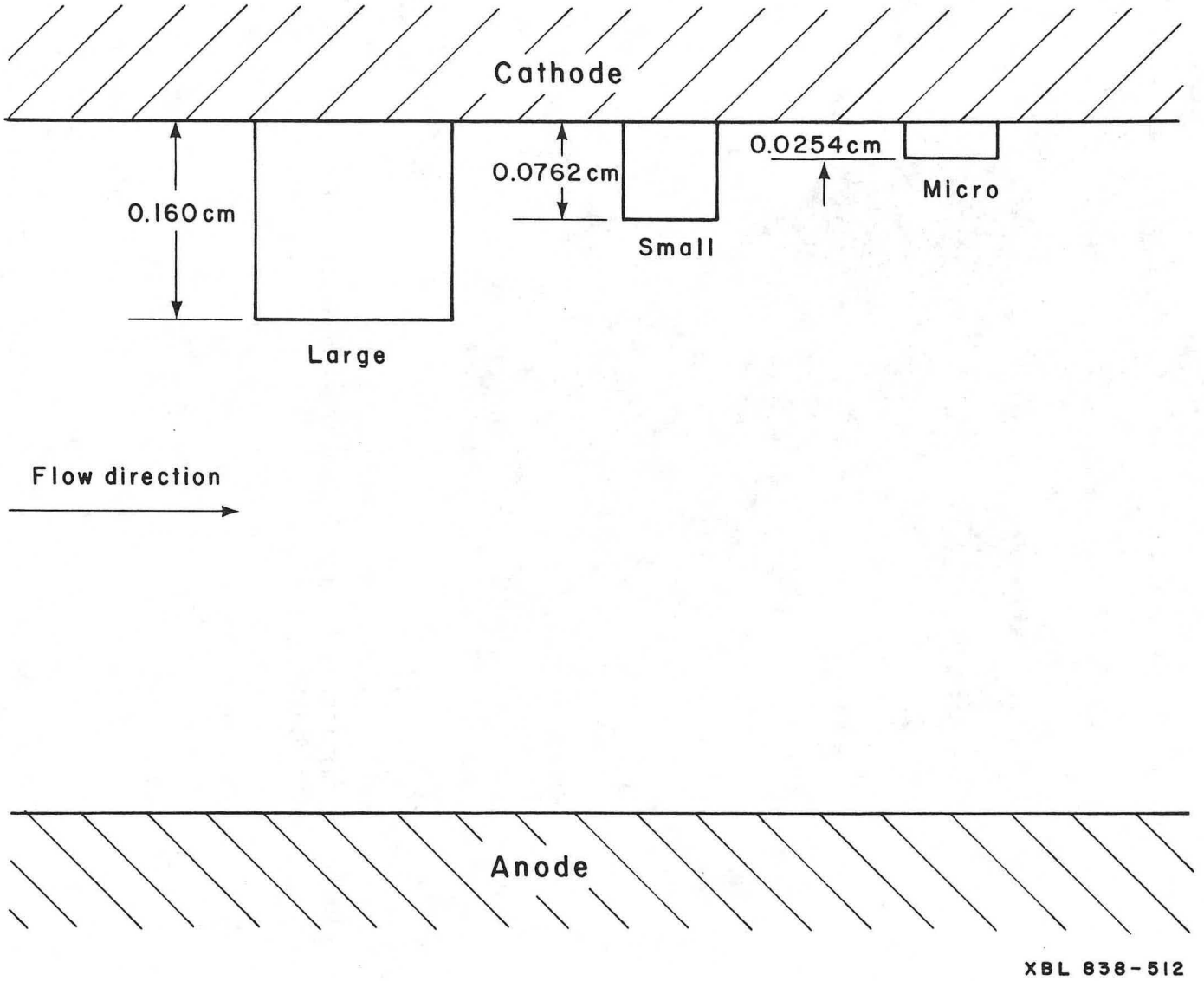

Fig. 18. Obstacle geometries.

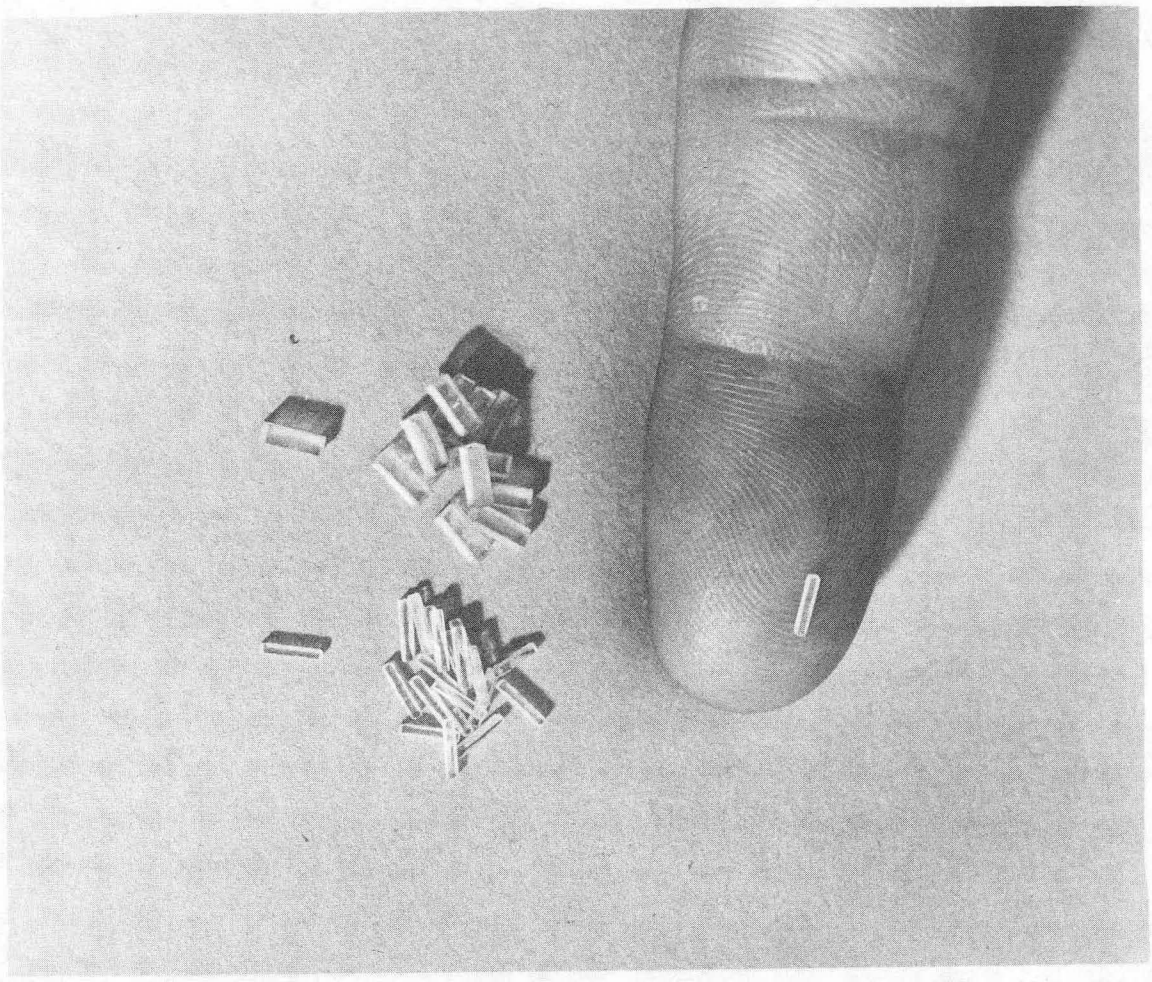

XBB 832-1498

Fig. 19. Comparison of Large (0.160 cm) and Small (0.0762 cm) obstacles.

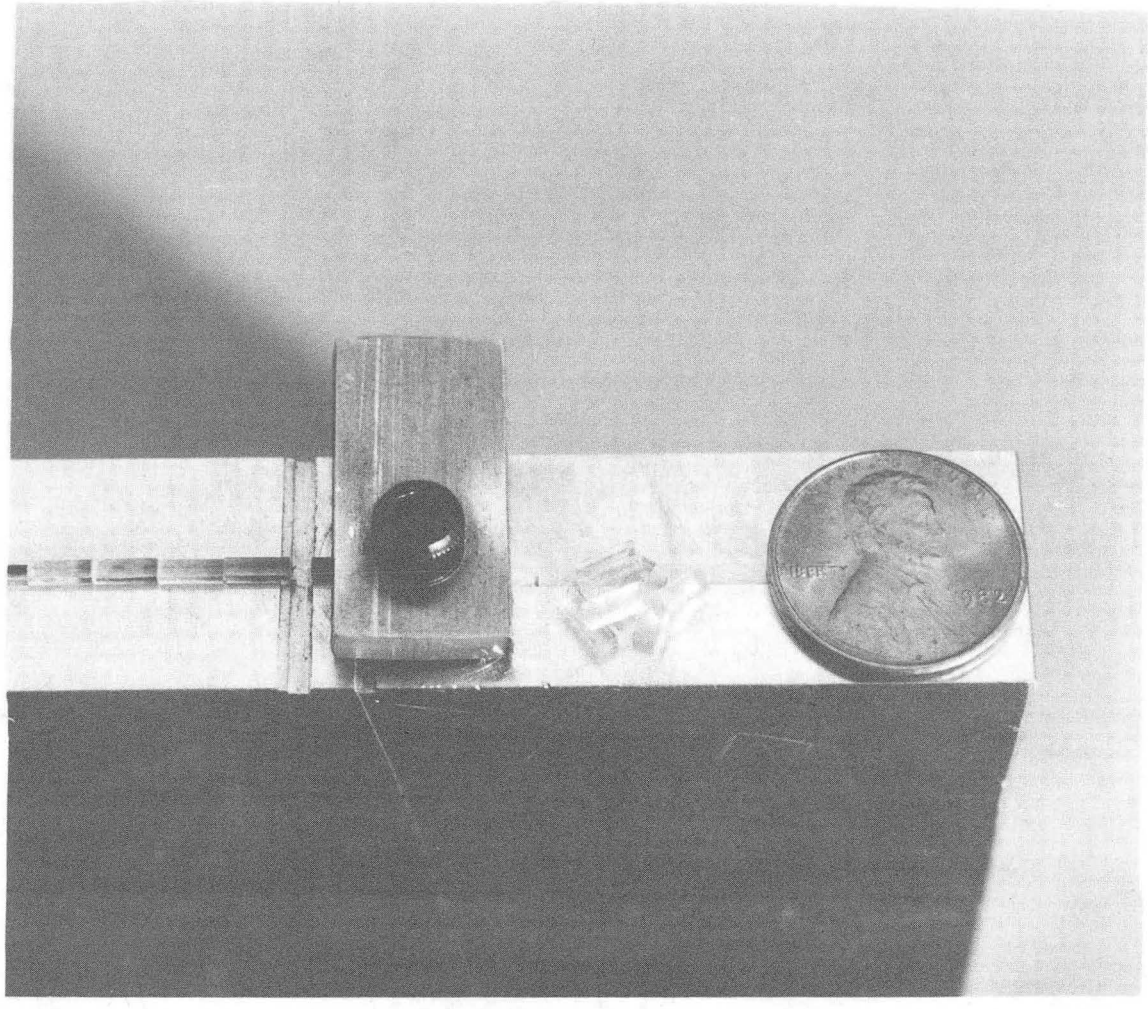

XBB 832-1496

Fig. 20. Large obstacle (0.160 cm) manufacturing jig.

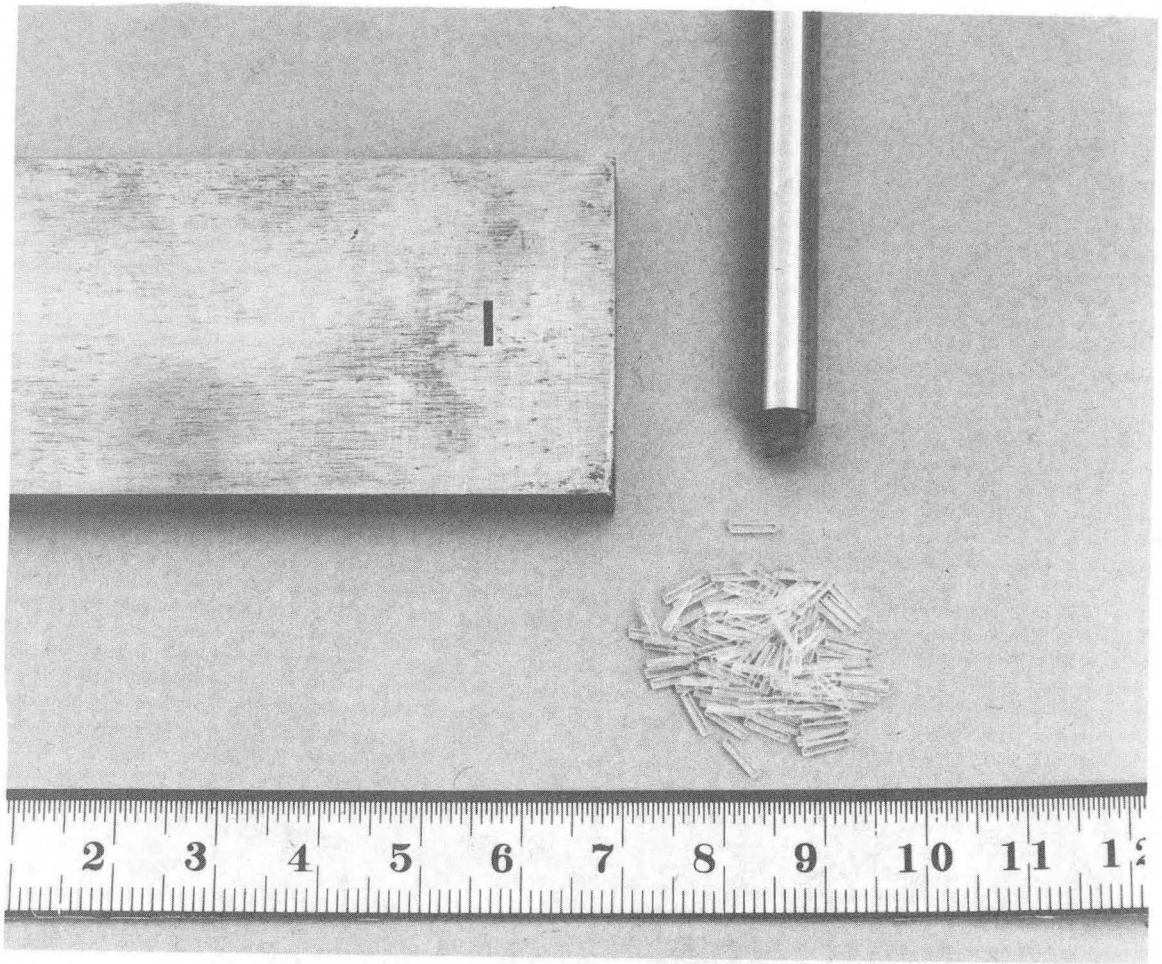

XBB 832-1499

Fig. 21. Small (0.0762 cm) and Micro (0.0254 cm) obstacle punch.

The spacing of the obstacles posed a problem. Specially designed spacers constructed from Teflon did not alleviate the problem because they could not be moved without also removing the attached obstacles from the surface. For this reason the obstacles were first spaced rather crudely. Using an accurate scale and a sharp razor blade, the electrode was lightly scratched where an obstacle was to be placed. Then using forceps, the obstacle, with a drop of adhesive smoothed on the bottom surface, was positioned on the scratch. This positioning was aided by clamping two pieces of plexiglas along the sides of the electrode. The plexiglas formed a slot in the electrode direction. The obstacle was then fitted into this slot perpendicular to the plexiglas and flush with the electrode sides.

After each run the obstacles were removed and the electrode repolished. The previous spacing placement scratches could not be seen after polishing. New obstacles were attached to a newly polished electrode for every run.

EXPERIMENTAL TECHNIQUES, PROCEDURES, AND CALCULATIONS

In this experimental investigation the effect of small flow obstacles on the performance of an electrochemical square duct reactor was studied. The obstacles increase the mass transfer rate, but also cause an increase in the required power to pump the electrolyte. To assess the advantage that may occur due to the placement of these obstacles in the flow channel, pressure drop and limiting current measurements were made. Also, the flow patterns around the obstacles were visualized and photographed.

Pumping Power - Pressure Drop Measurement

A fluid moves through a horizontal channel, duct, or tube because of an applied pressure difference. The fluid moves from the high pressure region to a lower pressure region. For a duct with a given length (L) the difference in pressure between the inlet and outlet becomes greater when the resistance to flow is increased. Flow obstacles provide resistance to fluid flow. The pressure drop ($\Delta P/L$) is the decrease in fluid pressure (ΔP) incured over the distance (L). By measuring pressure drop one obtains a measure of the resistance to flow and the power required to pump a fluid through the duct can be calculated.

In this investigation the pressure drop (ΔP) over the electrode length (50.8 cm or 20 inches) was measured via two small pressure taps in the channel wall. The pressure difference was then obtained by measuring the height difference in two glass tubes (manometers) or by reading a calibrated pressure transducer. The manometers were used

for the large obstacle experiments and were read using a cathotometer. The height difference Δh (cm) is related to the pressure by:

$$\Delta P = \rho g \Delta h \tag{33}$$

where the density (ρ) refers to the manometer fluid (which was the electrolyte). The acceleration due to gravity (g) was taken to be 976.77 dyne/cm^2. The electronic pressure transducer was calibrated using the cathetometer, water, and the glass tube manometers. For both devices gas bubbles had to be removed from the tygon transfer lines. For the manometers this was easy because the tubing was clear and the bubbles could be spotted. The transducer had to be bled to remove bubbles. This was accomplished by using the bleed screws provided for this purpose. The major advantages of the electronic transducer were its ease in use, large pressure range, voltage output, and response to transient behavior (DC to 1000. Hz). To monitor the transient behavior of the pressure in the channel, all air bubbles had to be out of the transfer lines. Bubbles would tend to dampen the response because they are compressible.

For laminar flow in a square channel it is shown in the Introduction (Eq. (3)) that the pressure drop ($\Delta P/L$) is related to the equivalent hydraulic diameter (D_e), fluid viscosity (μ) and fluid volumetric flow rate (Q) as follows:

$$\frac{\Delta P}{L} = 28.45 \frac{\mu Q}{D_e^{\,4}} \tag{34}$$

where

$$Q = (V_b)(D_e)^2 \tag{35}$$

A plot of the measured pressure drop (reproducible to ±0.03 cm H_2O) versus flow rate in the laminar regime (Re < 2100) produced a straight line. Evaluation of the slope using the appropriate fluid properties yielded a channel equivalent diameter that was 1.5 percent different than the valve obtained by direct measurement with a micrometer. A hydraulic diameter of 0.46 cm was used in all the calculations in this study.

The friction factor (f) is defined [150] as the proportionality constant between the force (F) applied in the flow direction to move the fluid and a characteristic area (A_{char}) multiplied by the kinetic energy (K.E.) of the fluid:

$$F = f\ (A_{char})(K.E.) \tag{36}$$

For a duct, the dimensionless Fanning friction factor (f) used in this study is then given by:

$$f = \frac{1}{4}\ \frac{D_e\ \ \Delta P}{\frac{1}{2}\rho\ V_b^2\ L} \tag{37}$$

The equivalent hydraulic diameter (D_e), fluid density (ρ) and fluid bulk velocity (V_b) are used to non-dimensionalize the pressure drop ($\Delta P/L$).

The actual power (P_p) per reactor volume (W/m^3) needed to pump the fluid at a certain linear velocity (V_b) m/sec is given by:

$$P_p = (V_b) \frac{\Delta P}{L} \tag{38}$$

For this equation the pressure drop ($\Delta P/L$) must now be in units of Newtons per square meter and V_b in units of meters per second. The power input increases drastically in the turbulent flow region. This is caused by a pressure drop approximately dependent on the velocity squared as opposed to the linear dependence in the laminar regime.

Mass Transfer Rates - Limiting Current Technique

In an electrochemical cell, when a potential difference is applied to the two electrodes and current is passed, a reduction reaction occurs at the cathode and an oxidation reaction occurs at the anode. As shown earlier (Eq. (11)), the current passed is related to the flux of charged species to the electrode. Due to the complex nature of electrochemical reactions, many factors influence the rate of the overall reaction processes. For a cathodic electrode process, the ions are transported toward the cathode by diffusion, electric migration, and convection (Eq. (8)). Near the electrode surface the convection is diminished. Excess "supporting" electrolyte (indifference) ions that do not participate in the electrode reaction provide the primary mobile species and suppress the induced migration of the reacting ion. Therefore the reacting ions move close to the electrode mainly by diffusion through the thin mass transfer boundary layer

located next to the electrode. At the electrode the following processes usually take place: adsorption, charge transfer, surface diffusion, and finally (with deposition) incorporation into the lattice.

The overall rate of the process is related to the slowest rate of the many individual steps. Because the process is not in equilibrium, energy must be supplied to drive the process. This energy is the voltage that must be supplied in excess of the thermodynamic equilibrium potential and it is the driving force for the reaction. This extra energy (called overpotential) is divided into three main components [151]: the ohmic overpotential produced by the electrolyte resistance, the concentration overpotential due to mass transfer limitations, and the activation overpotential which is the resistance to surface processes.

If the surface reaction steps are "fast" compared to the other process steps, the overall reaction will be limited by the transfer rate of material to the surface. In this case the reactant will react infinitely fast (relative to its rate of diffusion) once it arrives at the surface and its concentration will consequently become be zero on the surface. The "limiting" current condition has then been reached and increasing the overpotential will not increase the reaction rate above this limiting value (i_L). The current passed can then only be increased by affecting the surface reaction, bulk reactant concentration, or system hydrodynamics. Using the equations presented in the Electrochemical Mass Transfer section, the following equation can be derived for the mass transfer coefficient (k) in terms of the limiting current density (i_L) for a system with excess supporting electrolyte:

$$k = \frac{i_L}{C_b nF} \tag{39}$$

The limiting current technique is therefore an experimental method which measures mass transfer rates, which can then be correlated by means of dimensionless quantities. The technique has been used extensively to determine mass transfer rates in forced convection systems. Copper deposition mass transfer rates have been investigated in this laboratory by Hickman et al. in 1963 [153,154]. They made use of channel flow between two parallel plates to study the effect of buoyant forces on the process. Also in this laboratory, Landau in 1976 [155] used the copper deposition reaction to study forced convection mass transfer to a segmented electrode in channel flow. Unlike copper deposition studies, the ferri-ferrocyanide redox reaction does not affect the surface morphology (nothing is deposited). Mass transfer studies using this redox couple date back to Lin et al. in 1951 [156] who studied forced convection in an annular gap and in this laboratory by M. Eisenberg [157] in 1951. Eisenberg's work on mass transfer to rotating cylinders was published in 1954 [158]. Additional work in this laboratory includes that of Acosta in 1974 [159] who used the ferri- ferrocyanide system to study high rate electrolysis in a very thin gap parallel plate cell with controlled roughness under high flow rates. Roha [90] in 1981 used this redox reaction for his mass transfer study of suspended particles. Additionally, the work of J. Selman in the 70's [160,161] was devoted to developing the limiting current technique as a quantitative experimental tool. Besides the work in

this laboratory, the limiting current technique and specifically the ferricyanide reaction has been extensively used for mass transfer studies. The literature review section discusses the technique with regard to transfer enhancement investigations. As shown by Eq. (39), the limiting current density can be used to obtain a direct measure of mass transfer rates. However, the important assumptions used to obtain this result are summarized below.

1. The limiting current must be identified.
2. Reactant bulk concentration, diffusivity and number of electrons transferred per species reacted must be known.
3. The current must be due to the reaction of the species whose concentration is known (no other reactions).
4. The limiting current must be due to mass transfer limitations with no migration effects (fast surface reaction and excess supporting electrolyte).
5. The limiting reaction must occur at the electrode studied (not the counter electrode).
6. The calculated mass transfer coefficient (k) or Sherwood number (Sh) is independent of concentration.

For this study, all the above items have been considered and the technique adjusted to insure the assumptions hold in this system. The desired reactions are shown below and occur on the nickel electrodes.

<u>Cathode</u> - reduction of ferricyanide ion

$$Fe(CN)_6^{3-} + e^- \longrightarrow Fe(CN)_6^{4-}$$

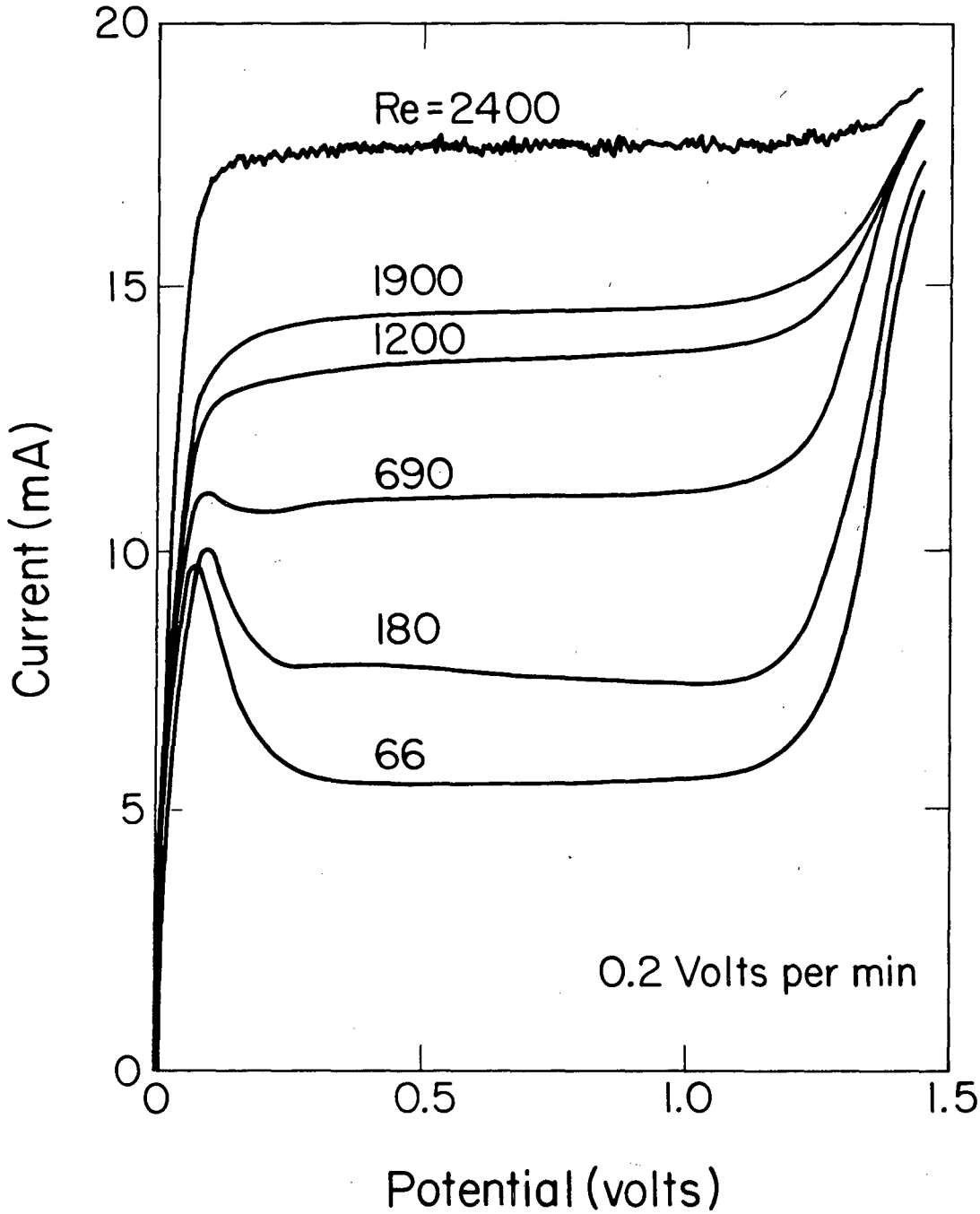

XBL 835-2634

Fig. 22. Limiting current curves for the unobstructed duct at various Reynolds numbers (Re). Sweep rate = 0.20 volts/min.

<u>Anode</u> - oxidation of ferrocyanide ion

$$Fe(CN)_6^{4-} \longrightarrow Fe(CN)_6^{3-} + e^-$$

$$(n = 1)$$

$$V^o = 0.36 \text{ volt}$$

Sodium hydroxide is used as the supporting electrolyte. The system is bubbled (sparged) with nitrogen to remove any dissolved oxygen. This insures the current passed goes to the redox couple, and not for oxygen reduction. A larger concentration of the ferrocyanide ion allows the ferricyanide reaction to reach its limiting rate first. Physical properties were determined by the methods previously explained.

Ferricyanide is a strong oxidizing agent; therefore, the apparatus was constructed from materials resistant to its attack. The decomposition of ferricyanide in alkaline solutions [147,158,159,174], and ferrocyanide when exposed to light [147,158,159] have been reported. For these reasons, fresh solutions were made for each run and the system was mainly composed of opaque materials. Poisoning of the electrode by cyanide was avoided by polishing the electrode before every run. The surface was polished and electrolyte prepared the same day as the experimental run.

The limiting current value can be obtained from polarization curves similar to those shown in Fig. 22. At time zero, a cathodic potential ramp is applied to the electrodes (cathode polarized negative with respect to hydrogen reference). As the potential increases so does the reaction rate and the current. At the limiting current

condition (I_L), the current becomes constant and a further increase in the cathodic potential produces no additional increase in reaction rate. Finally, as the electrode is further polarized, another reaction can occur (hydrogen evolution). The current passed to this secondary reaction produces the sharp rise at the higher potentials. It is important to realize the absolute value of the potential was not recorded because a reference electrode was not used. The resistance of the 0.3 M NaOH electrolyte produced an IR voltage drop of approximately 16.2 mV when a current of 50 mA was passed. This is not important because the mass transfer rate is related to the limiting current, not the potential at which it occurs. Figure 22 displays results for the unobstructed square duct operating at the Reynolds numbers (Re) shown. As the Reynolds number is increased, higher mass transfer rates are observed and higher limiting currents are achieved. At the lower flow rates a peak or local maxima is observed just before the plateau is reached. This maxima is a transient phenomenon and has been explained by previous workers [160]. It occurs at sweep rates that are "fast" compared to the rate of mass transfer through the boundary layer. Higher currents can be passed until the steady state shape of the mass transfer boundary layer is produced. P. C. Andricacos and H. Y. Cheh [162] have shown that the disappearance of the maxima, assuming an average Nernst diffusion layer thickness (δ_{avg}) is related by:

$$\sigma = \frac{nF\ \bar{V}\ \delta^2_{avg}}{RT\ D_i}$$

no hump $\sigma < 3$

hump $\sigma > 3$

where $\bar{V}$ is the potential ramp sweep rate (volts/sec). This relation shows that an average diffusion thickness can be calculated without knowledge of the electrode area or measurement of the limiting current value (further information can be found in Appendix A). Plots such as the one in Fig. 22 shall be referred to as "limiting current curves." These curves were qualitatively used to evaluate the effect of the flow obstacles.

Quantitative measurements of the mass transfer rates were obtained by measuring the limiting current using a potential step method. In this case, at time zero, a step in potential was applied to the electrodes. The magnitude of the step was chosen to be in the limiting plateau region of Fig. 22. A 0.5 volt potential step was used for the measurements involving large obstacles, and a 0.6 volts step was used for the others. The current response to this potential step is shown in Fig. 23 for different flow rates. The value of the current at long times (steady state) was used to calculate the limiting current density ($i_L = I_{ss}/A$). The time needed to reach the "steady state" current was longer at lower flow rates (Reynolds numbers). The curves also show the effect of the onset of flow turbulence on the current in the unobstructed square duct. This is shown by the large fluctuations of

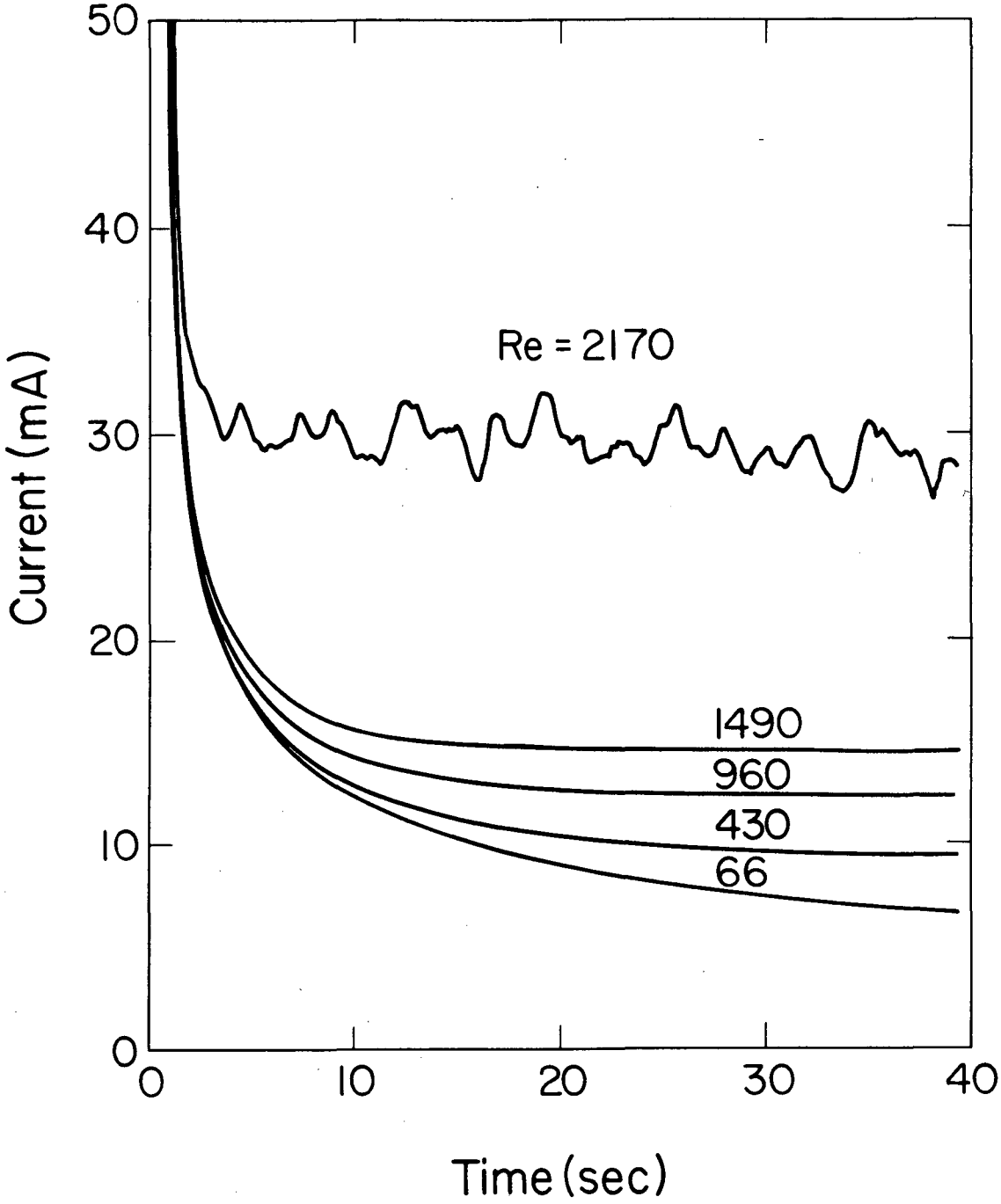

XBL 835-2633

Fig. 23. Current response to a potential step at time equal to zero. The magnitude of the step was in the limiting current plateau region. Effect of increasing Reynolds number (Re) is shown for the unobstructed duct.

the "steady state" current. These fluctuations were largest around transition to turbulence (Re = 2100 for a duct) and diminished as flow rate was further increased (notice Re = 2400 in Fig. 22). After the limiting currents were obtained, Sherwood numbers were calculated by using:

$$Sh = \frac{D_e \; i_L}{C_b D_i nF} \tag{40}$$

The above equation is derived from Eq. (20) using $C_b = 0$ at limiting current. An equivalent hydraulic diameter (D_e) of .46 cm, bulk concentration (C_b) of 0.01 M, and the appropriate active electrode area (A) were used.

Operation

The basic procedure used for the experimental runs in this investigation are given below. Details of the steps have already been described.

1. Coat the electrodes with urethane (day before).
2. Weigh out 30 liters of water (night before).
3. Sparge the water with N_2 gas.
4. Make up the electrolyte solution.
5. Sparge the electrolyte for 2 hrs with nitrogen.
6. Polish the electrodes to 600 grit with silicon carbide paper.
7. Rinse electrodes with distilled water.
8. Rinse electrodes with isopropyl alcohol.
9. Attach obstacles to cathode at desired spacing.

10. Mount electrodes in flow channel.
11. Seal the flow channel.
12. Throttle nitrogen through the flow system to remove air (1 min).
13. Pump the electrolyte to the upper tank.
14. Bleed and zero the transducer.
15. Obtain two limiting current curves and hold at hydrogen evolution for a few minutes.
16. Take data at different flow rates. At each flow rate measure limiting current, temperature, and pressure drop (allow for steady state hydrodynamics after changing flow rate). The flow rate was varied as follows: 10, 30, 50, 70, 90, 80, 60, 40, 20, 5, 15 on the rotameter scale.
17. Obtain qualitative limiting current curves.
18. Measure fluid properties (if needed).
19. Clean up.

Note: Eisenberg et al. [158] pretreated their electrodes by polishing, washing with CCl_4 and treating cathodically in a 5 percent NaOH solution at a current density of 20 mA/cm^2 for 12-15 min.

Errors

The greatest source of experimental error must be attributed to the flow meter. It was a ball type rotameter and gave a scattered calibration curve. The pressure drop and limiting currents were measured very accurately. Comparisons of the results with known unobstructed correlations were excellent. The reproducibility shown in the Results section, was quite satisfactory.

Flow Visualization

Experimental science is based on observations. In studying fluid mechanics, one can observe properties of the flow (e.g. pressure drop); however, the flow paths have the unique ability of being directly visualized. An excellent collection of flow visualization photographs can be found in An Album of Fluid Motion [163]. Some of the techniques used in this study to observe and photograph fluid motion are described in Flow Visualization by Wolfgang Merzkirch [164].

In this study, the flow was visualized by adding foreign material to the flowing fluid (milk, bubbles, Mearlmaid). To visualize and photograph their motion, a light source must shine perpendicular to the viewing direction. This dark field illumination was used so that only scattered light contributed to the image. In this investigation the obstacles were attached to a piece of plexiglas that was cut to the same dimensions as the cathode (upper electrode). This plexiglas spacer was then mounted in the flow channel replacing the cathode. The duct thus formed had the same dimensions as the duct used for the electrochemical experiments. The channel was illuminated from above by a floodlight whose light passed through the translucent plexiglas spacer and into the flowing fluid. The flow paths were viewed and photographed through the glass side wall.

To visualize filament lines, milk was slowly injected into the duct containing water as a flowing fluid. The reference electrode syringe was used for this purpose (Fig. 15). This method did not prove to be the best because the milk, injected manually, affected the bulk flow rate.

Small hydrogen bubbles produced the best photographs. For this technique, a wire or a small metal screen attached to a wire was placed upstream from the obstacles. Sodium hydroxide was dissolved in water and passed through the duct. By passing current between this electrode and the flow channel anode, hydrogen bubbles were generated on it electrochemically. These small bubbles after detachment followed the streamlines and produced white streaks when photographed. The bubbles were buoyant and accumulated near the cathode. Some of them became attached to the surface on the downstream side of the obstacle or in the corner of the duct. These attached bubbles affected the flow patterns. The bubble technique did not work well with the small obstacles since the bubbles were not small enough to follow the streamline pattern.

In another effort, neutrally buoyant solid micron sized flakes were added to water in order to observe particle paths and stream lines. The flakes used were (10-30 μm) x 6 μm Natural Pearl Essence crystals (guanine) manufactured for the cosmetic industry. Specifically, Mearlmaid AA obtained from the Mearl Corporation in New York was used. These small shiny particles produced excellent optical flow visualization; however, the photographs did not exactly reproduce what was seen with the naked eye (less clarity and detail). The particles did allow excellent observation of the flow patterns with the small and large obstacles. The interaction between closely spaced obstacles was also seen.

RESULTS

The experimental techniques used led to direct measurement of the limiting current and pressure drop at different values of the flow rate, obstacle spacing, and obstacle size . The obstacles were electrically insulating and attached directly to the electrode surface. The total number of obstacles used was varied between experiments. However, for a given experiment the selected number of obstacles were equally spaced along the entire electrode length. The placement of the first obstacle was measured downstream from the leading edge of the electrode with the obstacles evenly distributed along the length. (No obstacle was attached to the leading edge or downstream edge of the electrode.) The results are presented using the number of obstacles as a parameter. The number of obstacles and the inter obstacle distance (measured center to center) is summarized in the table below:

Number of Obstacles	Spacing (Center to Center)	
0	-	-
1	25.4 cm	(10 in)
3	12.7 cm	(5 in)
7	6.35 cm	(2.5 in)
15	3.175 cm	(1.25 in)
31	1.58 cm	(.625 in)
49	1.02 cm	(.400 in)

Without any obstacles (unobstructed) the electrode active area was 24.2 cm^2 over the length (L) of 50.8 cm. The channel equivalent hydraulic diameter (D_e) was 0.46 cm. Other obstacle spacing characteristics are shown below:

Large (0.160 cm) Obstacles — Obstacle Height/D_e = .348

Number of Obstacles	Obstacle Spacing / Obstacle Height	Obstacle Spacing / D_e	Active Electrode Area (cm^2)
0	-	-	24.2 cm^2
1	158.75	55.2	24.1 cm^2
3	79.37	27.6	24.0 cm^2
7	39.69	13.8	23.7 cm^2
15	23.44	6.9	23.1 cm^2
31	9.87	3.4	22.0 cm^2

Small (0.0762 cm) Obstacles — Obstacle Height/D_e = .166

Number of Obstacles	Obstacle Spacing / Obstacle Height	Obstacle Spacing / D_e	Active Electrode Area (cm^2)
0	-	-	24.2 cm^2
3	166.67	27.6	24.1 cm^2
15	41.67	6.9	23.6 cm^2
31	20.73	3.4	23.0 cm^2
49	13.39	2.2	22.3 cm^2

Micro (0.0254 cm) Obstacles Obstacle Height/D_e = .055

Number of Obstacles	Obstacle Spacing / Obstacle Height	Obstacle Spacing / D_e	Active Electrode Area (cm^2)
15	125.0	6.9	23.6 cm^2

The limiting current passed to the electrode (I_L, Amps) is plotted and not the limiting current density (i_L, Amps/cm^2). The limiting current density (i_L) is the total limiting current passed (I_L) divided by the active electrode area, which varies with the number of obstacles attached. This "process optimization" approach was taken because the effect of adding obstacles to the system as a whole was investigated. Although the obstacles cover only a small portion of the available surface area, this effect was taken into consideration when calculating the Sherwood number.

Limiting Current Curves

Limiting current curves were used in this study for qualitative observations of the obstacles' effect on mass transfer. The plots shown on Figs. 24 and 25 were produced using the Large obstacles (0.16 cm). The potential was manually increased by 25 mV increments (discrete steps) every 15 seconds. These steps gave the jagged spikes seen in Fig. 24. Figure 25 was smoothed by the illustrator (the spikes appeared in the original data). The additional limiting current curves shown on Figs. 26 through 31 were produced using a potential ramping

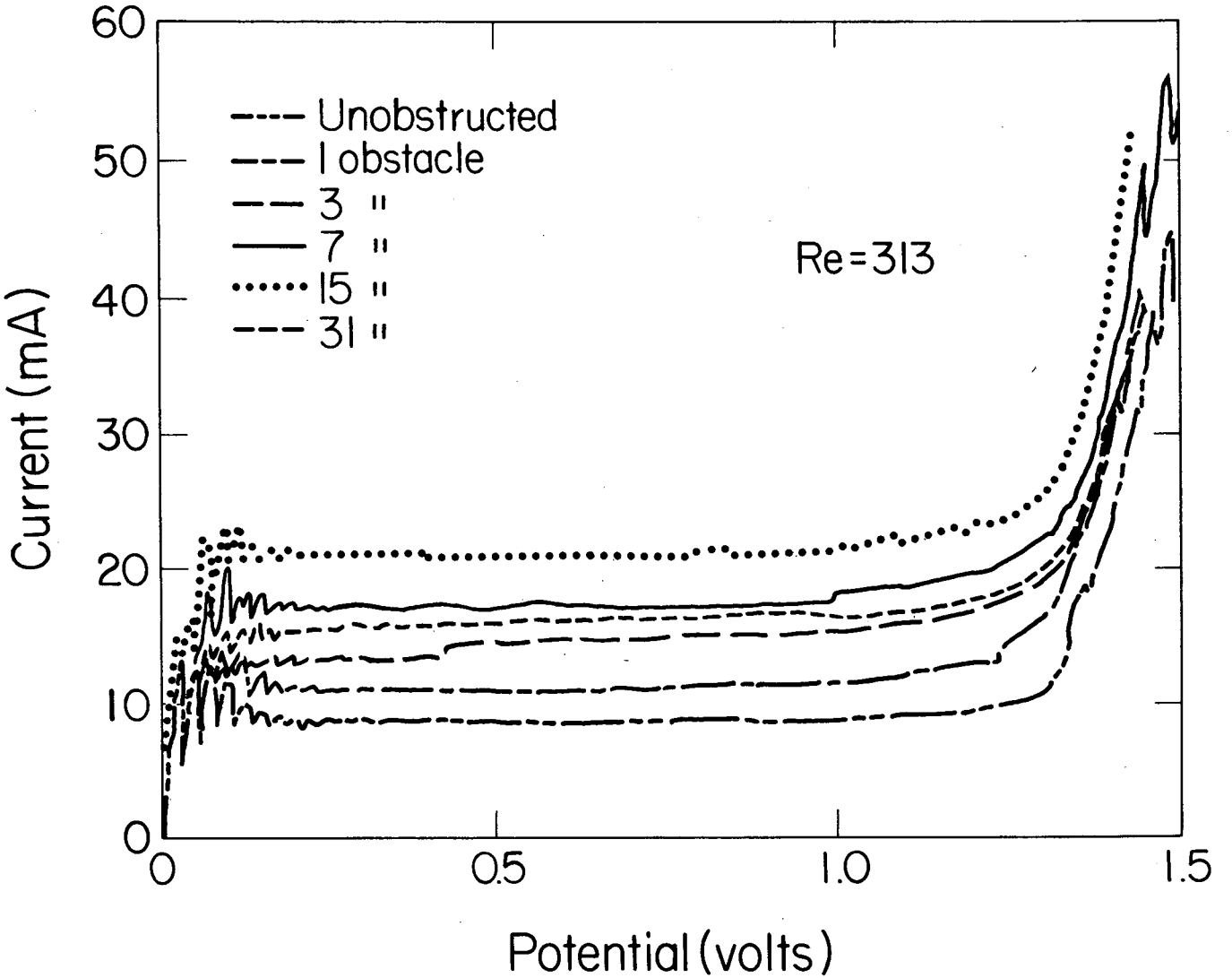

XBL 837-2886

Fig. 24. Limiting current curves for the Large obstacles (0.160 cm). Re = 313. 25 mV increments applied manually every 15 seconds.

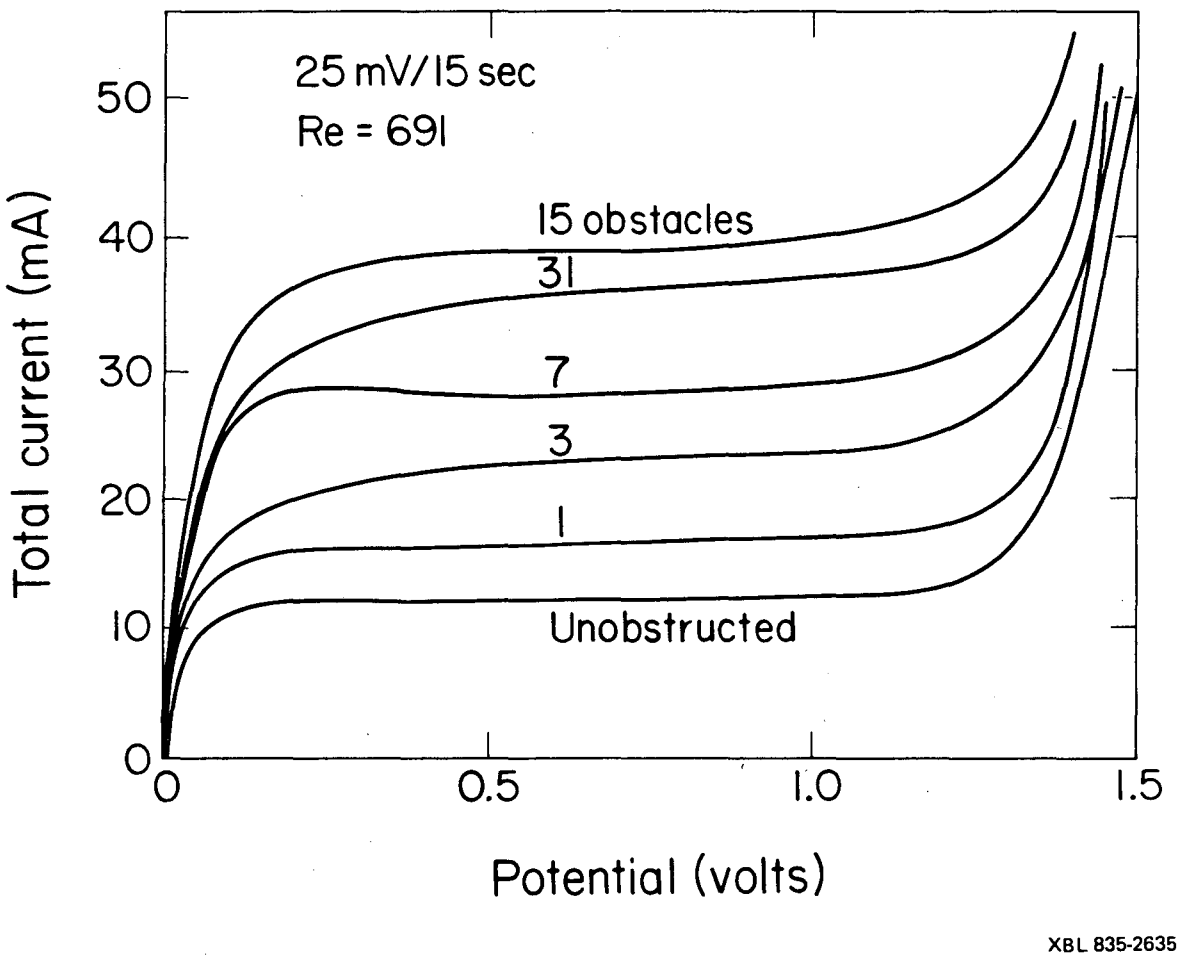

Fig. 25. Limiting current curves for the Large obstacles (0.160 cm). Re = 691. 25 mV increments applied every 15 seconds. Curves smoothed by illustrator.

device (controller) that increased the potential at a continuous rate of 200 mV/sec. The spikes that appear on these curves are "real" current spikes caused by turbulence. The obstacles used in Figs. 26 through 31 were all the Small (0.0762 cm) size.

The addition of obstacles is shown to produce enhancement to mass transfer (higher limiting currents). The enhancement increases with higher Reynolds numbers (flow rates) and with more obstacles (closer spacing). However, there is a limit to this effect, and an even closer spacing eventually yields less enhancement. This reduction in enhancement is shown for the Large (0.16 cm) obstacles on Fig. 24 and 25. In this case the addition of 31 obstacles (1.58 cm spacing) produces lower enhancement than the use of 15 obstacles (3.175 cm spacing). This reduction in total current passed is due to hydrodynamic interactions and not to a reduced active surface area caused by the additional obstacles. Calculating the limiting current density based on the surface not covered by obstacles yields: 0.870 mA/cm^2 and 0.681 mA/cm^2 at Re = 313, and 1.66 mA/cm^2 and 1.305 mA/cm^2 at Re = 691 for the 15 and 31 Large obstacles, respectively. At both flow rates, with 31 obstacles the current density passed to the active electrode surface is lower than the value with 15 obstacles.

Figure 26 shows limiting current curves for the unobstructed channel at different Re. Large fluctuations in current are observed for when the Reynolds number equaled 2460. These large fluctuations are absent at the lower Reynolds numbers and are probably due to the formation of turbulent flow in the channel. The turbulence also causes

large increases in the mass transfer rates resulting in a large increase of the value of the limiting current.

The large fluctuations observed with the unobstructed channel are absent in the curves with 3 Small and 15 Small obstacles (Figs. 27 and 28, respectively). Fluctuations are observed at the higher Reynolds numbers; however, they are considerably lower than those seen with the unobstructed channel.

The curves are replotted to show the effect of obstacles at a specific flow rate. Figure 29 provides the results for a Reynolds number of 300 (based on the unobstructed channel equivalent diameter). No fluctuations are observed, and the mass transfer enhancement caused by the obstacles is clearly seen. The effect of these Small obstacles at Re = 1000 is shown on Fig. 30. The enhancement due to the obstacles is larger at this flow rate, and slight fluctuations in limiting current are observed. These fluctuations seem to decrease at still higher Reynolds numbers. At Re = 1680 (Fig. 31) the magnitude of the fluctuations seen with 15 obstacles decreases from those observed at Re = 1000 (Fig. 30). At Re = 1680 the enhancement due to the obstacles is much larger than that observed at lower Re values. The 15 obstacles give a 3-4 fold increase of the limiting current over the unobstructed duct. These limiting current curves show the large effect that addition of Small obstacles can have on mass transfer at flow rates below "natural unpromoted" turbulence (laminar regime). Interestingly, this effect can be observed even when only one 0.16 cm high or three 0.0762 cm high obstacles are placed on the cathode surface that is 50.8 cm long.

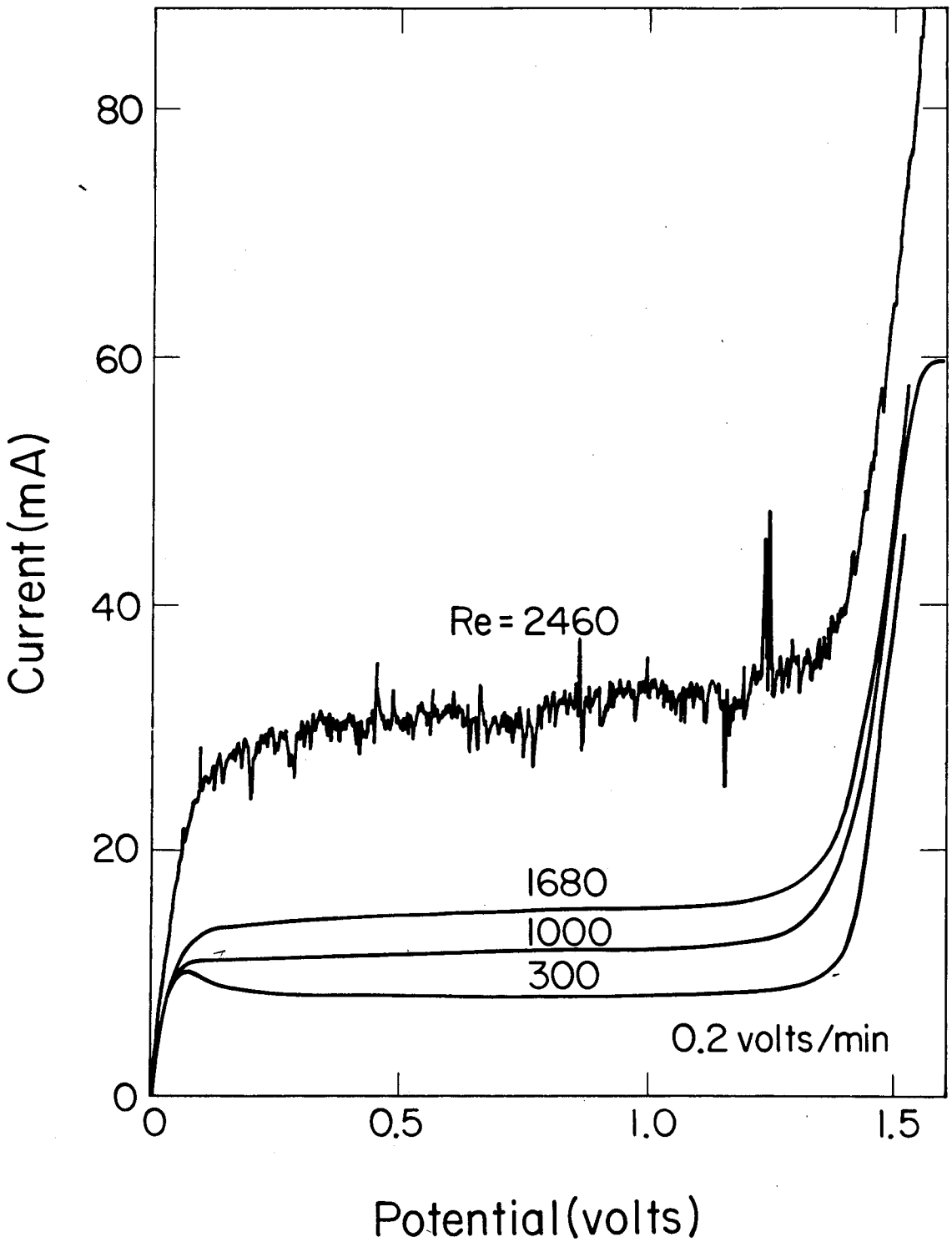

XBL 837-2764

Fig. 26. Limiting current curves for the unobstructed duct at different Reynolds numbers (Re). Note turbulence at Re = 2460.

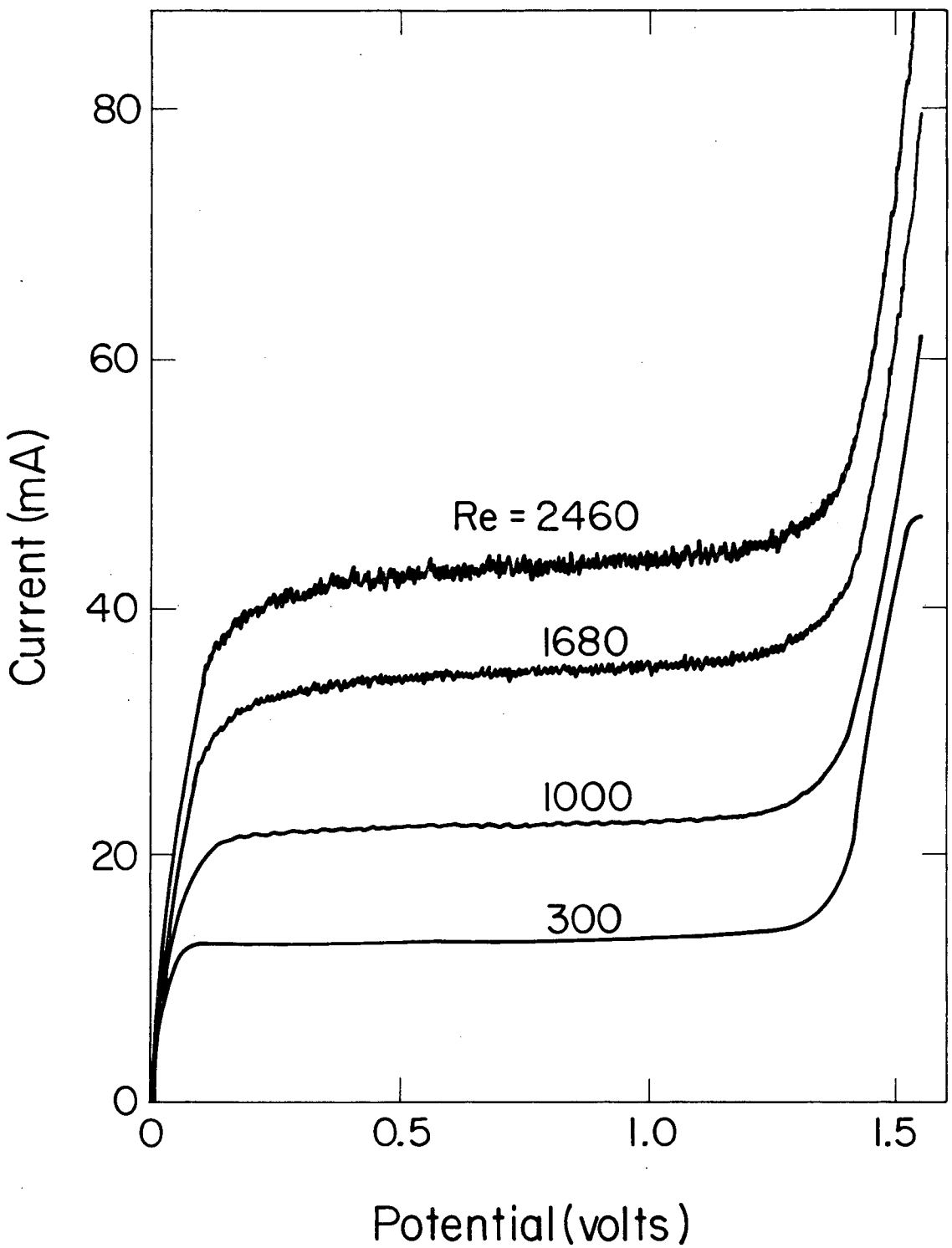

XBL 837-2771

Fig. 27. Limiting current curves for three Small obstacles (0.0762 cm) at various Reynolds numbers (Re). Note absence of large fluctuations of current.

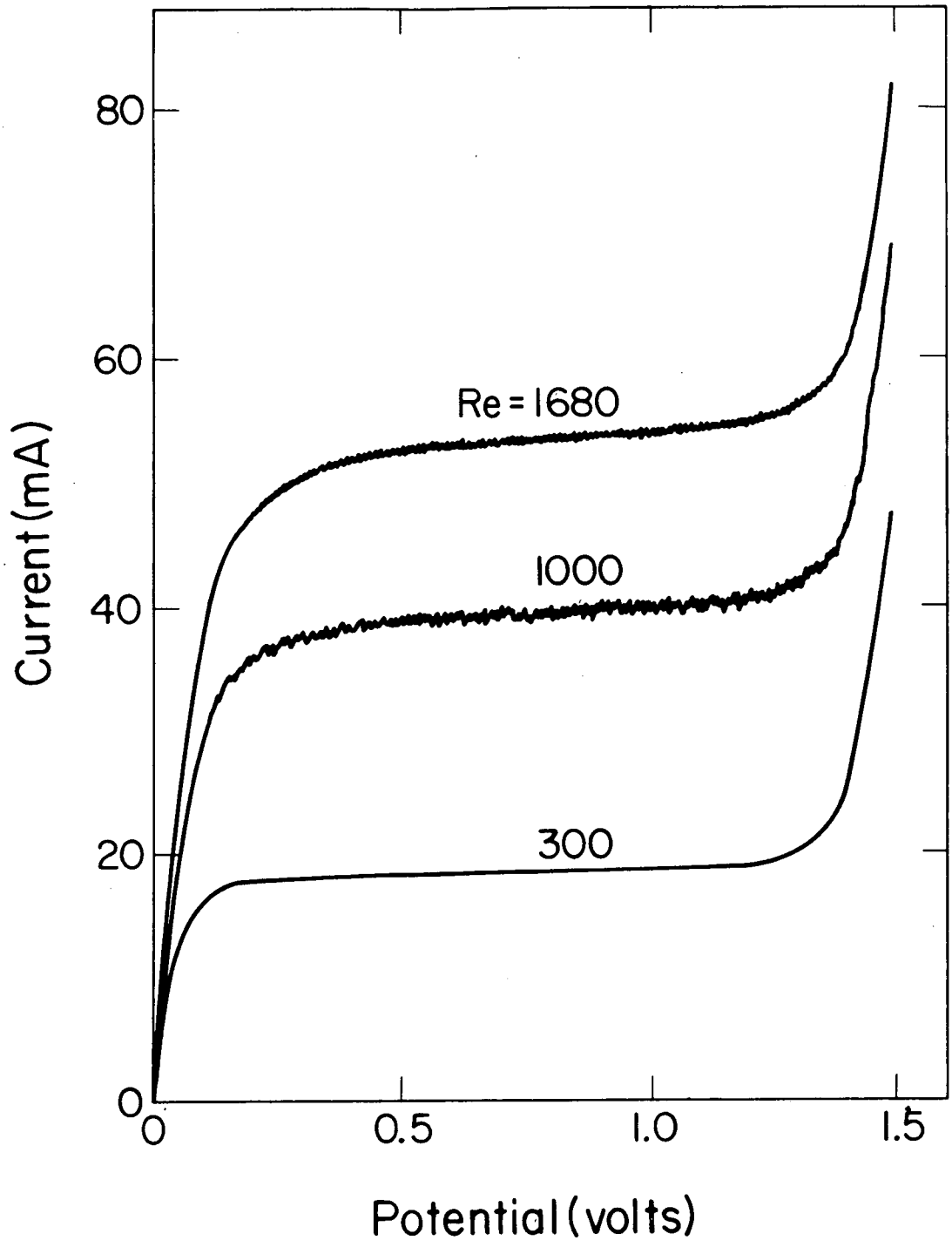

XBL 837-2770

Fig. 28. Limiting current curves for 15 Small obstacles (0.0762 cm) at various Reynolds numbers (Re).

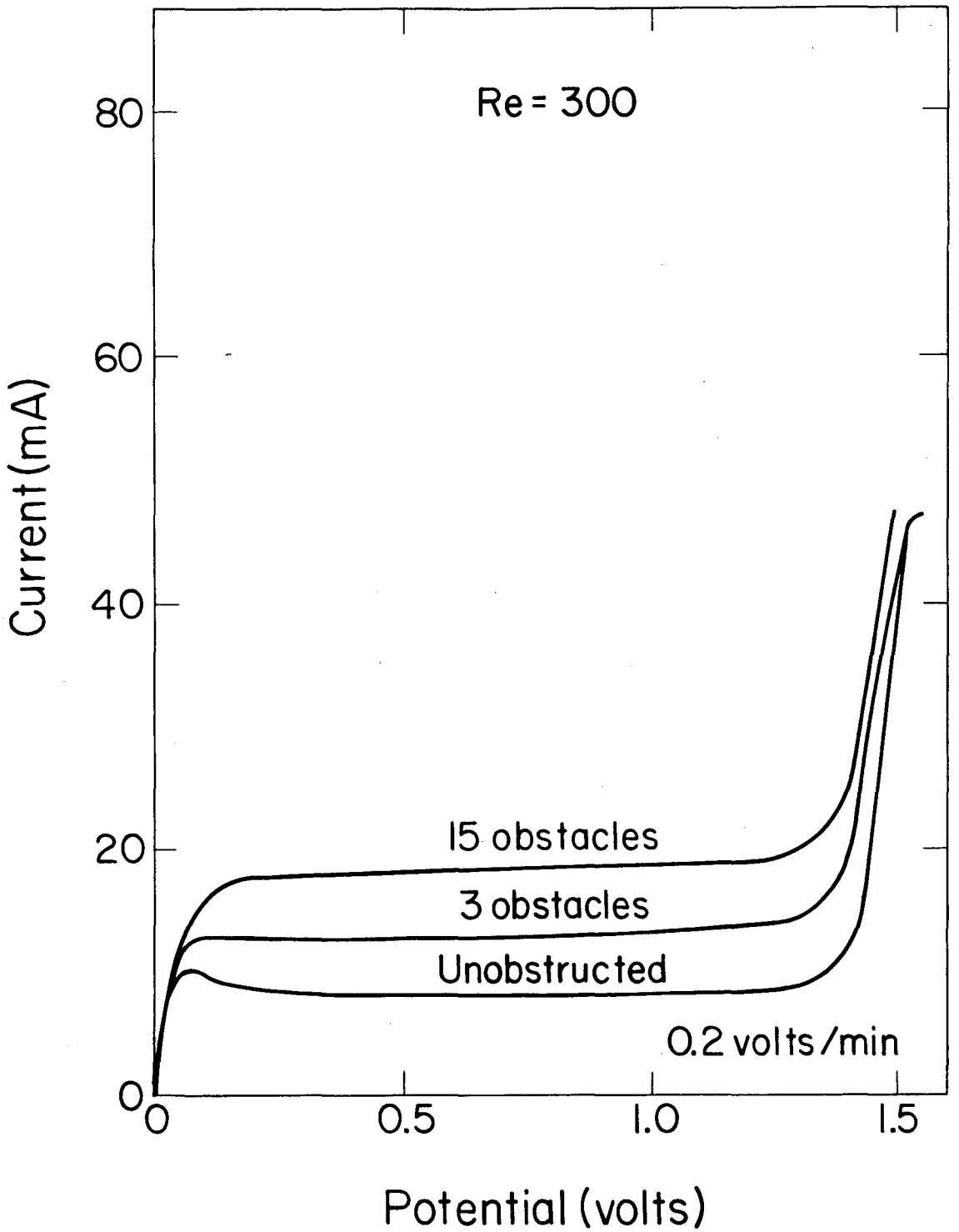

XBL 837-2774

Fig. 29. Limiting current curves for two spacings of Small obstacles (0.0762 cm) at Re = 300 relative to the unobstructed duct.

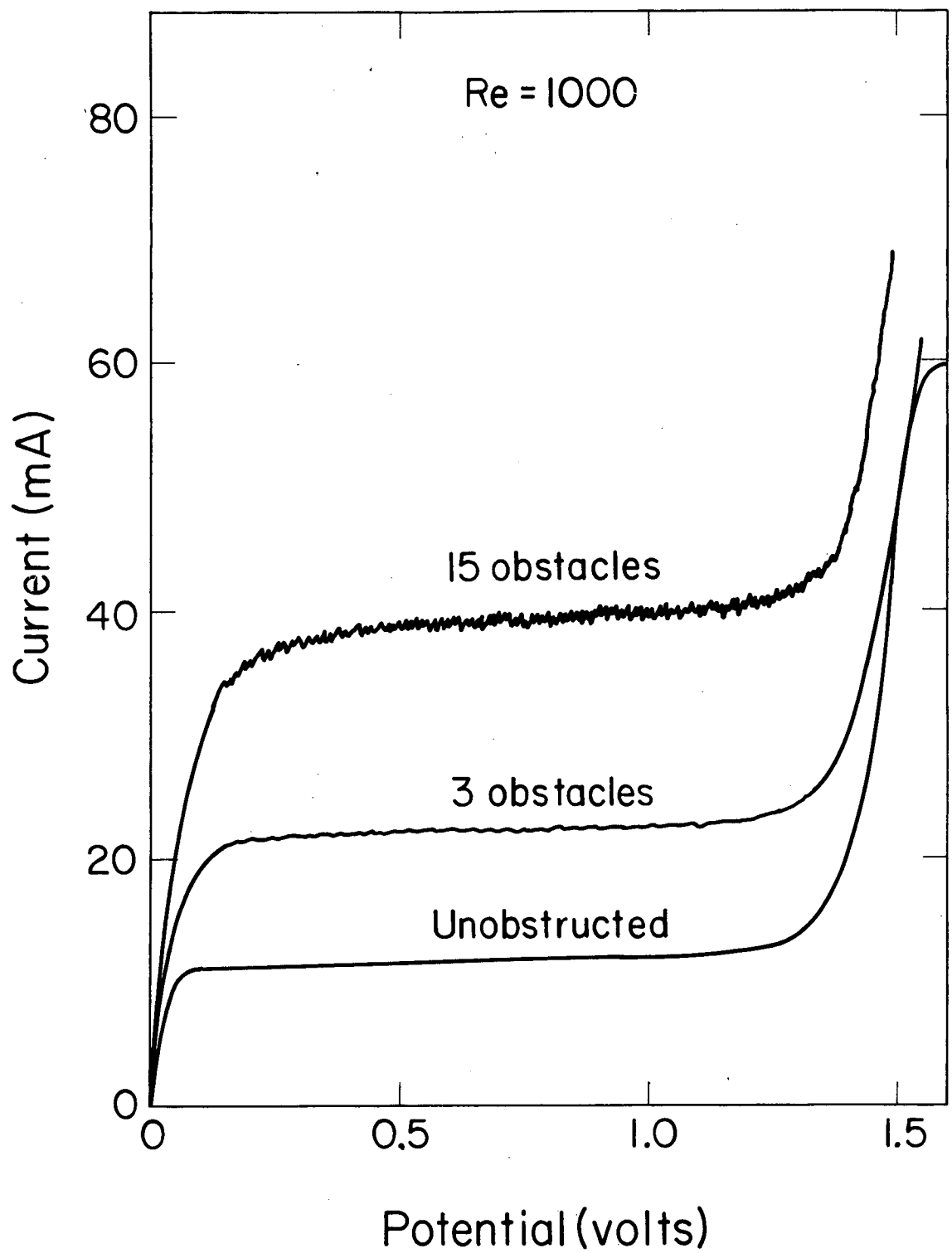

XBL 837-2775

Fig. 30. Comparison of limiting current curves for two spacings of Small obstacles (0.0762 cm) at Re = 1000 relative to the unobstructed duct.

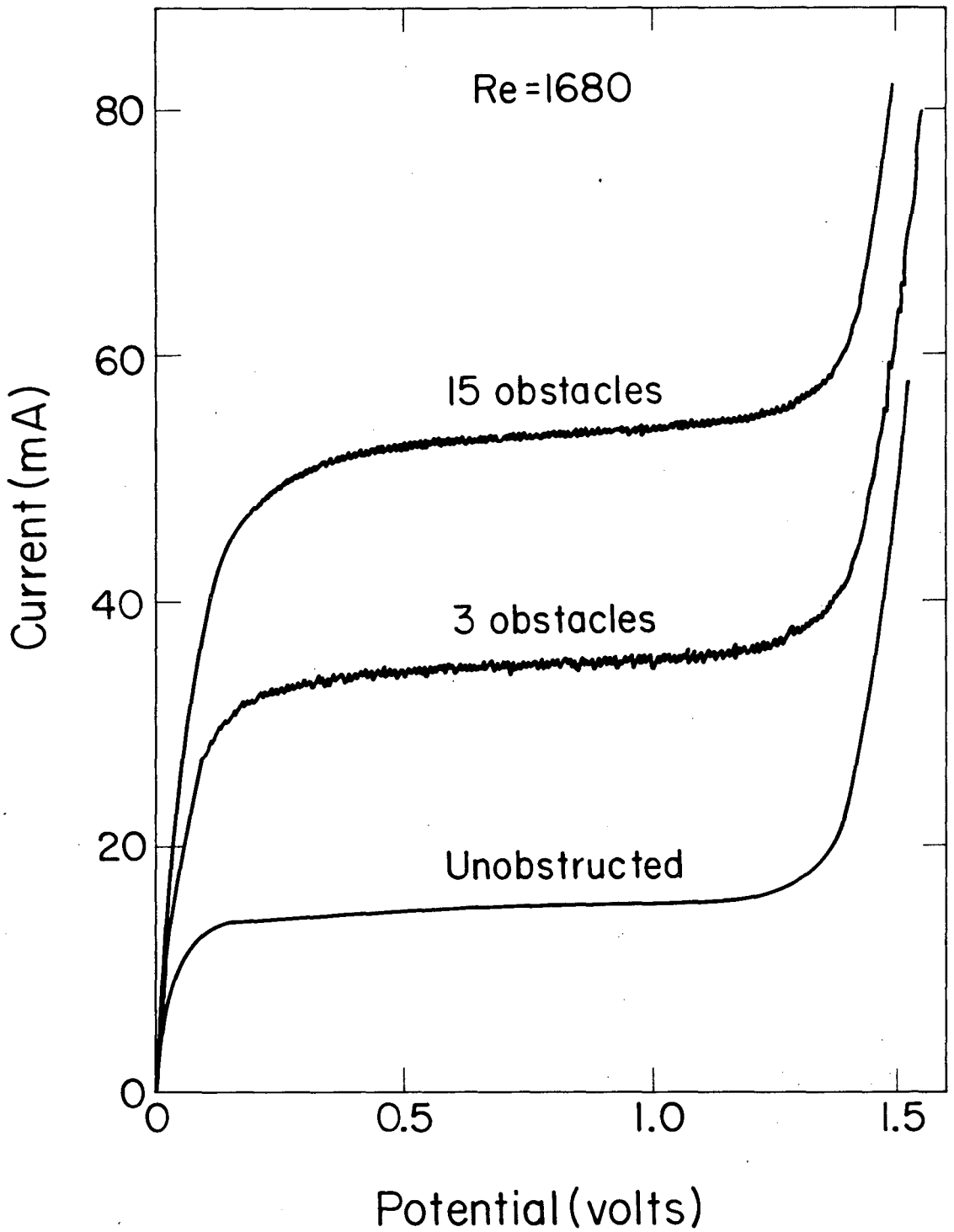

XBL 837-2773

Fig. 31. Limiting current curves for two spacings of Small obstacles (0.0762 cm) at Re = 1680 relative to the unobstructed duct.

Quantitative Mass Transfer Results - Limiting Current Measurements

As described earlier, the quantitative measurements of mass transfer rates were performed by applying a cathodic potential step to the working electrode (cathode). The magnitude of the step was chosen to be in the limiting current plateau region. Figure 23 shows the initial current response to such a step for an unobstructed channel. The value of the current reaches "steady state" with time. It is this "steady state" current (I_{ss}) that is plotted as the total limiting current passed to the cathode (I_L). Though they are called "steady state" currents, these currents fluctuated around a mean value - which was the value recorded. As seen in the previous curves, the current fluctuations are again observed above Reynolds numbers of 2100 (turbulent regime) in the unobstructed channel.

Figure 32 shows that large current fluctuations are seen in the limiting currents (I_{ss} or I_L) measured in the unobstructed channel. These fluctuations are largest in the flow regime transition region ($2100 < Re < 3100$) and decrease as "fully developed" turbulence occurs. The time scale was changed to show both the short and the long time transient effects. At a Reynolds number of 2120 a very interesting periodic behavior is observed. At this flow rate, long duration large current increases are observed which produce a unique, spiked behavior. These spikes might be due to the formation of a turbulent eddy at the leading edge of the electrode or "turbulent spot" elsewhere on the electrode which enhances mass transfer as it travels down the electrode. Other workers have observed (visualized)

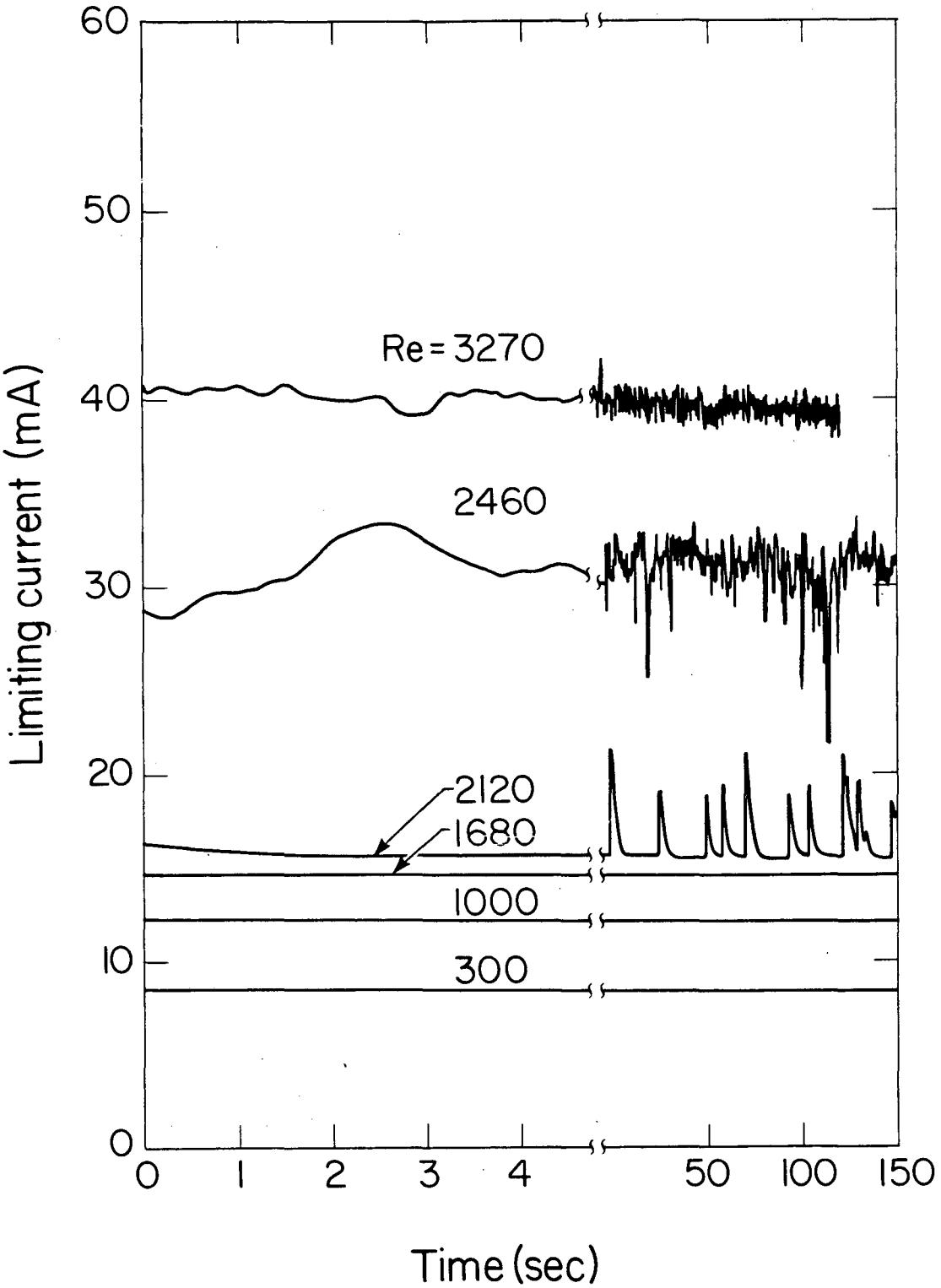

XBL 837-2760

Fig. 32. Fluctuation of "steady state" limiting current in the unobstructed channel at different Reynolds numbers (Re). Note periodic transition spikes at Re = 2120.

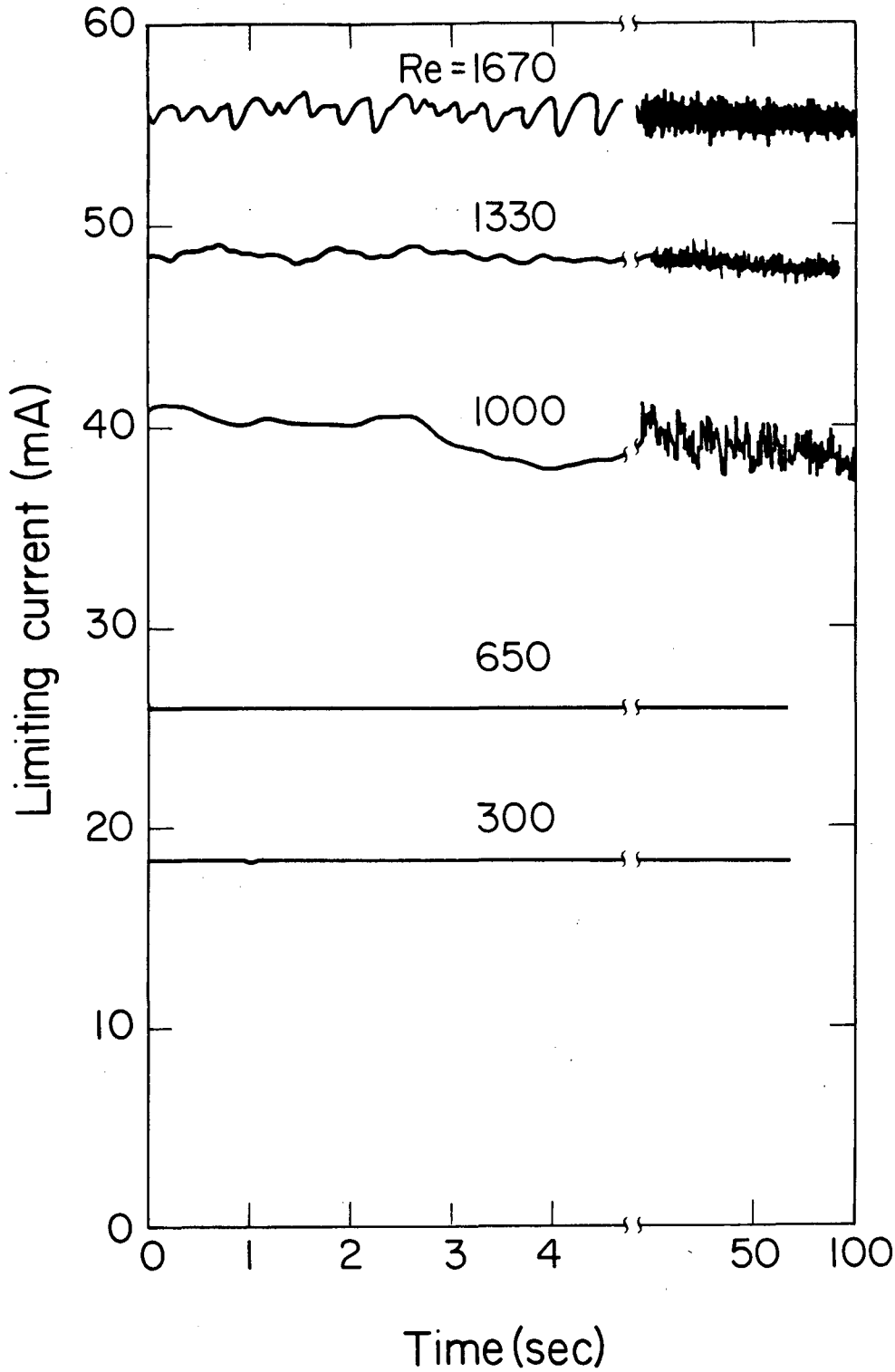

XBL 837-2766

Fig. 33. Fluctuations of "steady state" limiting current in the presence of 15 Small obstacles (0.0762 cm) at different Reynolds numbers (Re).

large disturbance eddies with flow in a pipe [169] and turbulent "sources" [175] or "spots" [176] with flow over a flat plate. This phenomenon builds and sheds periodically, giving rise to the individual current spikes. As flow rate is further increased, more turbulence is produced and the fluctuations become faster and more chaotic.

Figure 33 shows the effect that attaching 15 Small (0.0762 cm) obstacles to the electrode has on these fluctuations. Although fluctuations occur, the very large fluctuations seen in the unobstructed channel are absent in the presence of 15 obstacles. These fluctuations are produced at Reynolds numbers which would be considered in the laminar flow regime. These low Reynolds number fluctuations are probably caused by small eddies forming upstream and downstream from the obstacle.

Plots of the total limiting current (I_L) versus the flow rate as a function of number of obstacles are given in Figs. 34 and 35 for the Large (0.16 cm) and Small (0.0762) obstacles, respectively. In both figures, the unobstructed results are given by the solid dots. The transition into turbulence occurs at Re = 2100 for the unobstructed duct and this is manifested in a more rapid rise in the limiting current obtained. Significantly, in the presence of obstacles, this more rapid rise of i_L does not occur. Error bars are given in Fig. 35. Notice that the length of these error bars increases as the flow rate is increased. The effect of crowding obstacles too close together can be clearly seen. For the Large (0.16 cm) obstacles, 31 yields lower currents than 15 obstacles (Fig. 34). Similarly, 49 Small (0.0762 cm)

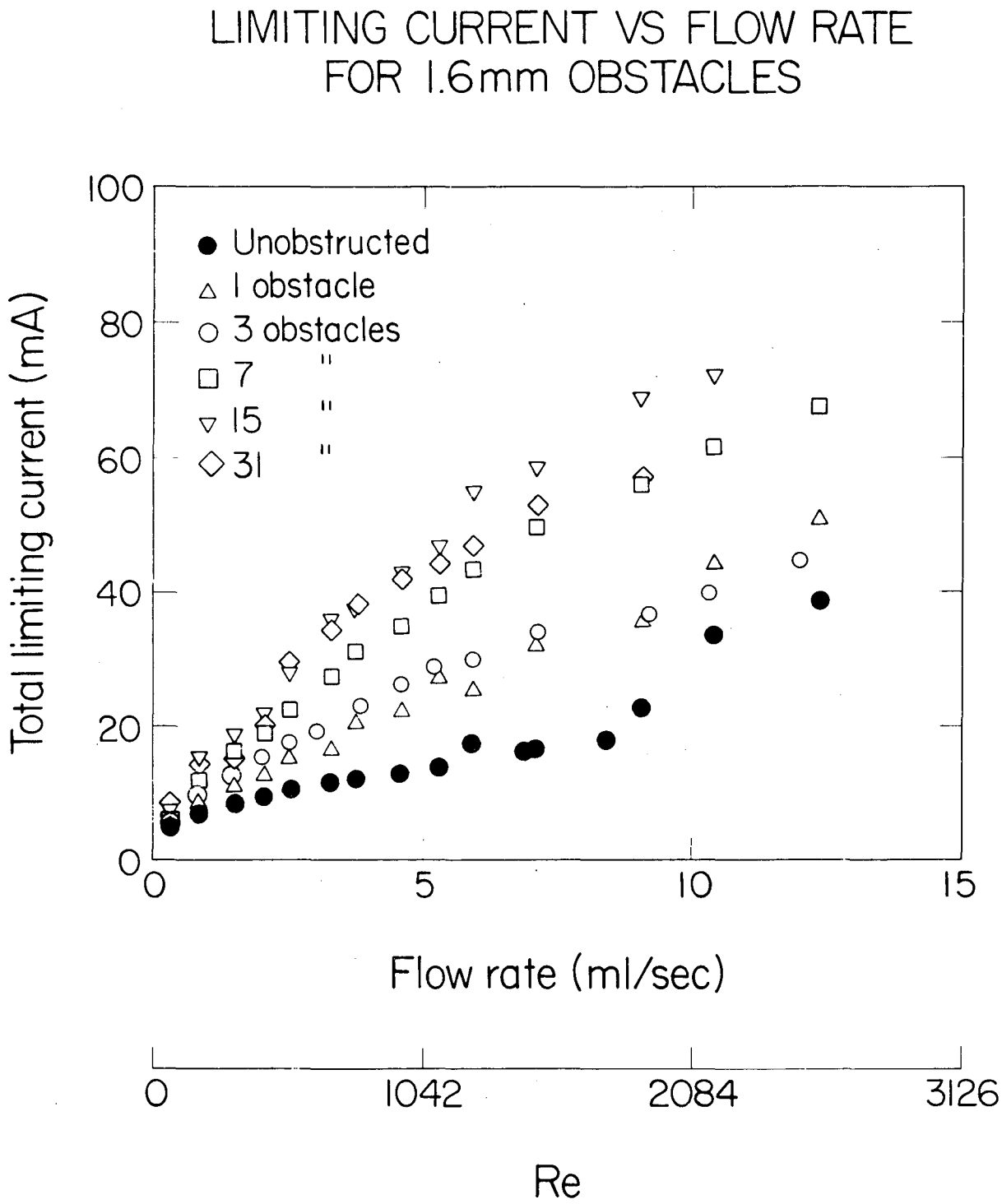

XBL 838-10936

Fig. 34. Limiting current as a function of flow rate for the Large obstacles (0.160 cm). Note that increasing the number of obstacles from 15 to 31 does not increase the limiting current.

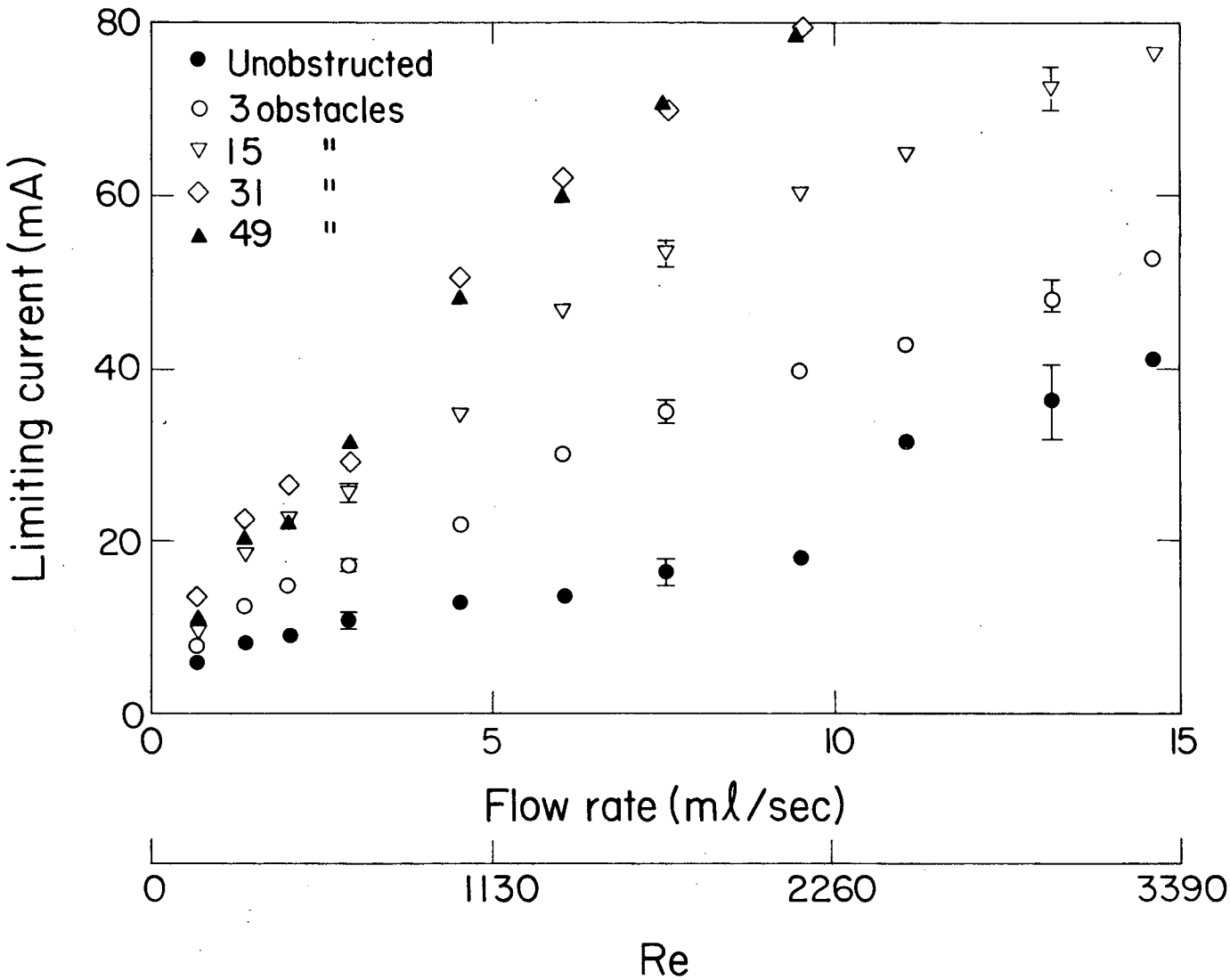

XBL 837-2818

Fig. 35. Limiting current as a function of flow rate for the Small obstacles (0.0762 cm).

obstacles produce slightly lower currents than 31 obstacles (Fig. 35). It is interesting to note that for a given number of obstacles (say 15) the enhancement of mass transfer is almost equal between the Large and Small obstacles. However, the Small obstacles enhance mass transfer to a slightly lesser degree.

The dependence of the experimentally obtained Sherwood number (Sh) on the Reynolds number (Re), the Schmidt number (Sc), and the equivalent duct diameter (D_e) divided by the electrode length (L) is shown in Fig. 36 for the unobstructed square duct. Also shown on Fig. 36 is the numerical solution by I. Rousar et al. [14], valid for the laminar flow regime and this duct geometry, given below:

$$Sh = 1.56 \left[Re\ Sc\ \frac{D_e}{L} \right]^{1/3}$$

The agreement is quite good in the laminar region. The mass transfer rates are shown to rapidly increase over the laminar trend at Reynolds numbers larger than 2100.

The excellent reproducibility of the results is shown in Fig. 37 for the Small obstacles. The results were obtained from experiments on four different days for each obstacle configuration (variation occurs with 10 percent). Data on this plot was taken on different days, with fresh new electrolyte solutions, newly prepared electrodes, and with new obstacles attached to the cathode.

The dimensionless mass transfer rates in terms of the Sherwood number are plotted as a function of (Re Sc D_e/L) and number of

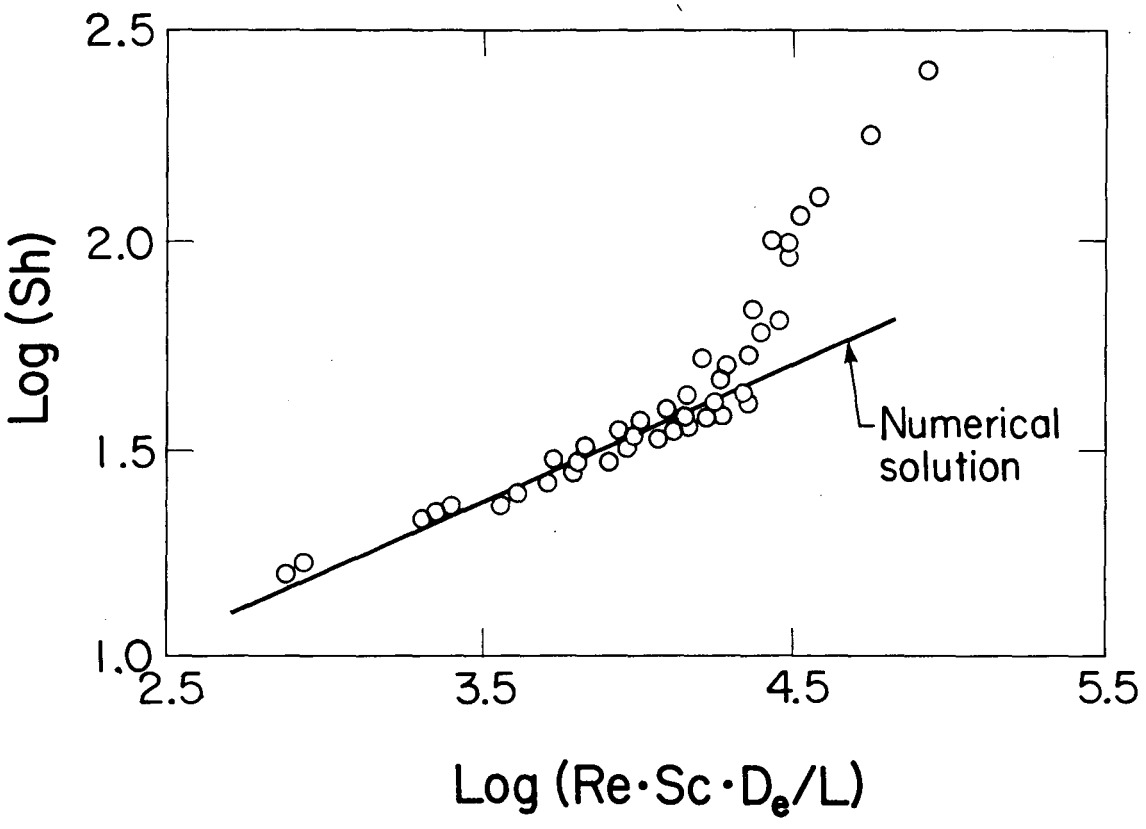

XBL 837-2765

Fig. 36. Dimensionless mass transfer rates in the unobstructed square duct. Numerical solution is by I. Rousar et al. [14].

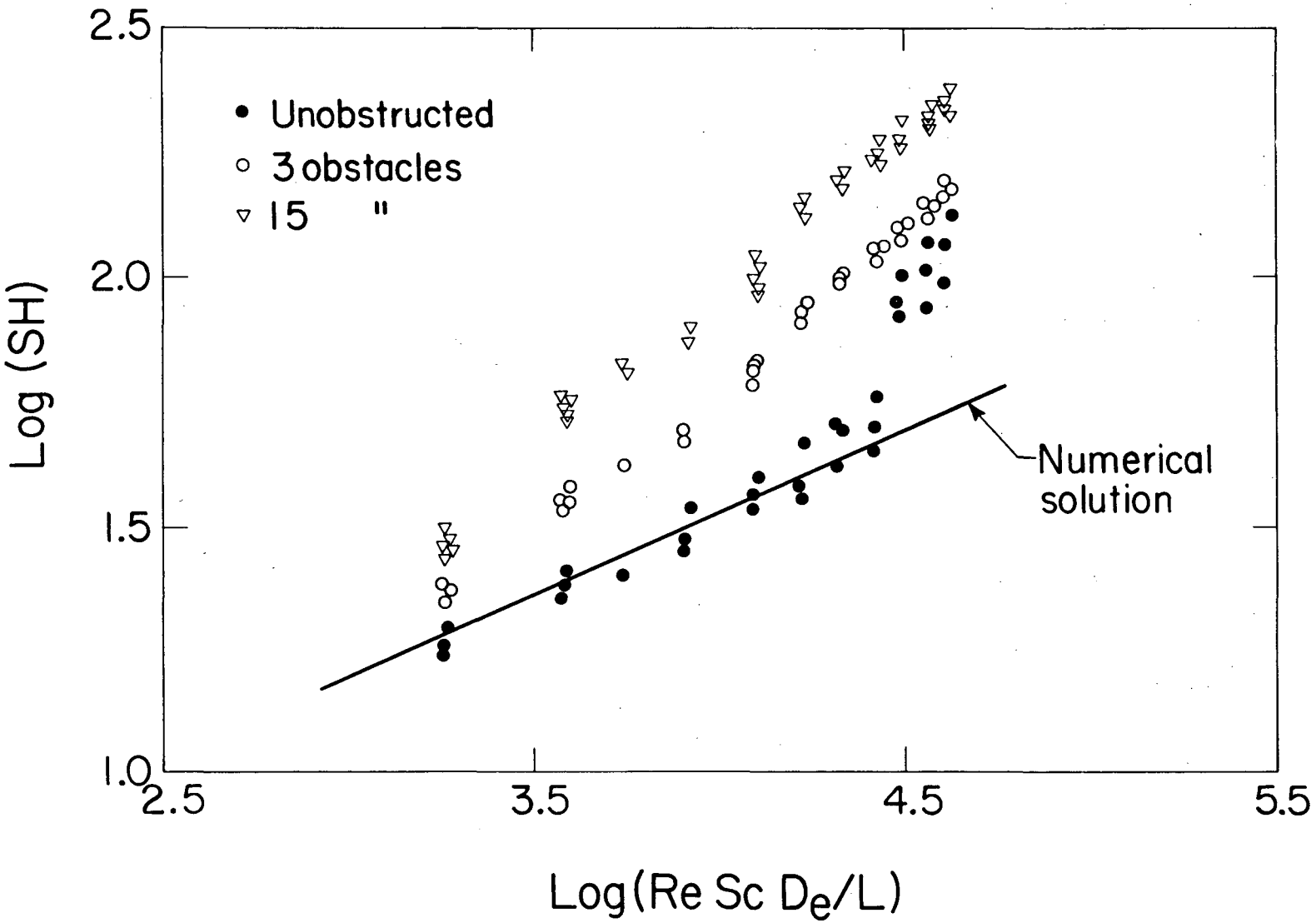

XBL 837-2822

Fig. 37. Reproducibility of the results. Numerical solution [14] for the unobstructed duct is provided. Results are for the Small obstacles (0.0762 cm).

obstacles in Fig. 38 (Large 0.16 cm obstacles) and Fig. 39 (Small 0.0762 cm obstacles). The unobstructed channel results are depicted as solid dots. Again the trend seen before is apparent. Closer spacing (more obstacles) yields a greater mass transfer enhancement until a maximum is reached. Beyond this, closer spacing decreases the enhancement. When comparing the two sizes, the same number of obstacles give nearly the same enhancement to mass transfer until the optimum spacing is reached for the Large obstacles. The largest enhancement for the Small occurs with 31 obstacles and for the Large with 15 obstacles. The 31 Small obstacles give greater enhancement than the 15 Large obstacles. When comparing the enhanced mass transfer rates to the rates in the unobstructed duct, it is concluded that the enhancement increases with increasing flow rate, until Reynolds numbers greater than 2100. With these higher flow rates "natural, unobstructed" turbulence occurs in the duct and the enhancement of the obstacles is decreased. A maximum enhancement due to the obstacles is observed just before "natural, unobstructed" turbulence is produced in the unobstructed channel.

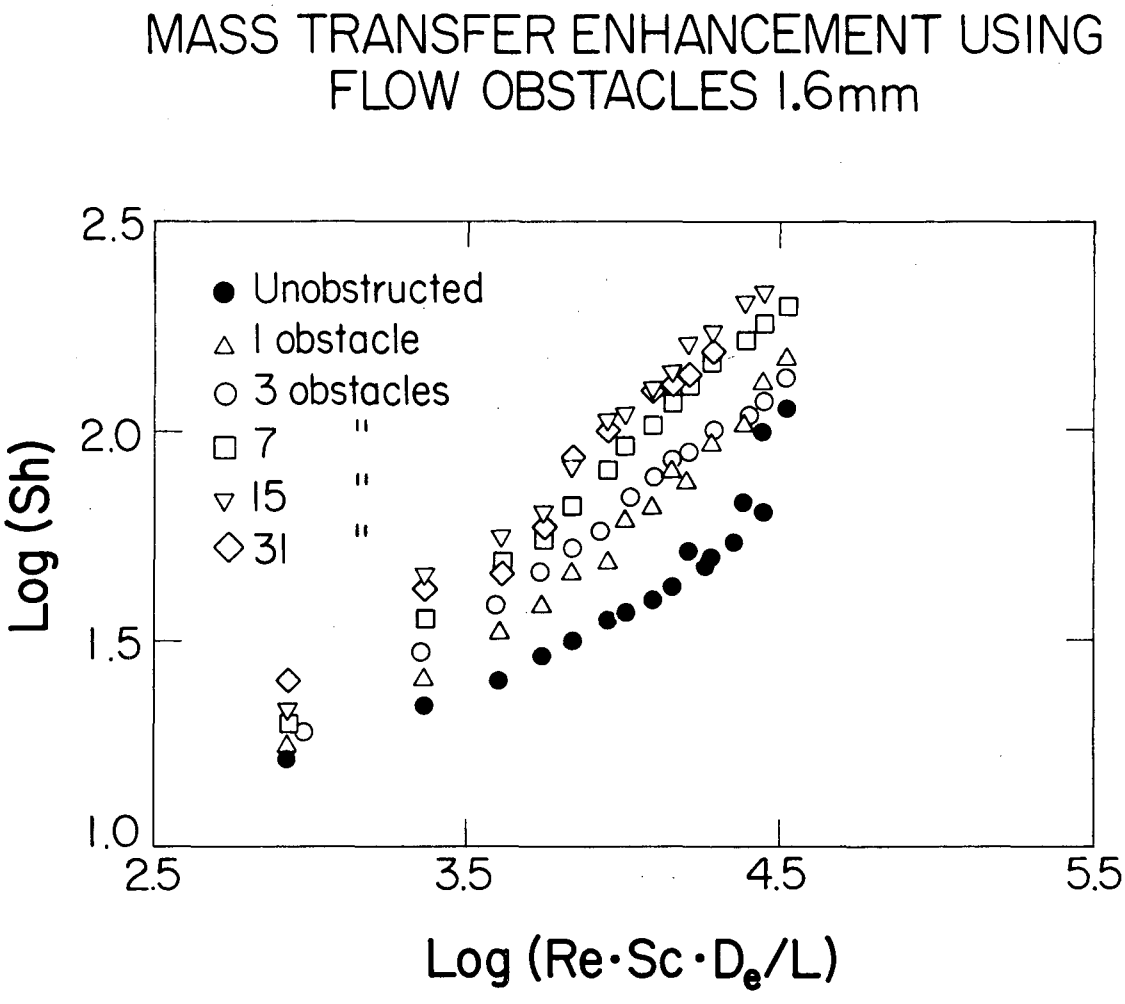

XBL 837-2776

Fig. 38. Dimensionless plot of mass transfer rates for the Large obstacles (0.160 cm). Note that increasing the number of obstacles from 15 to 31 does not increase the limiting current.

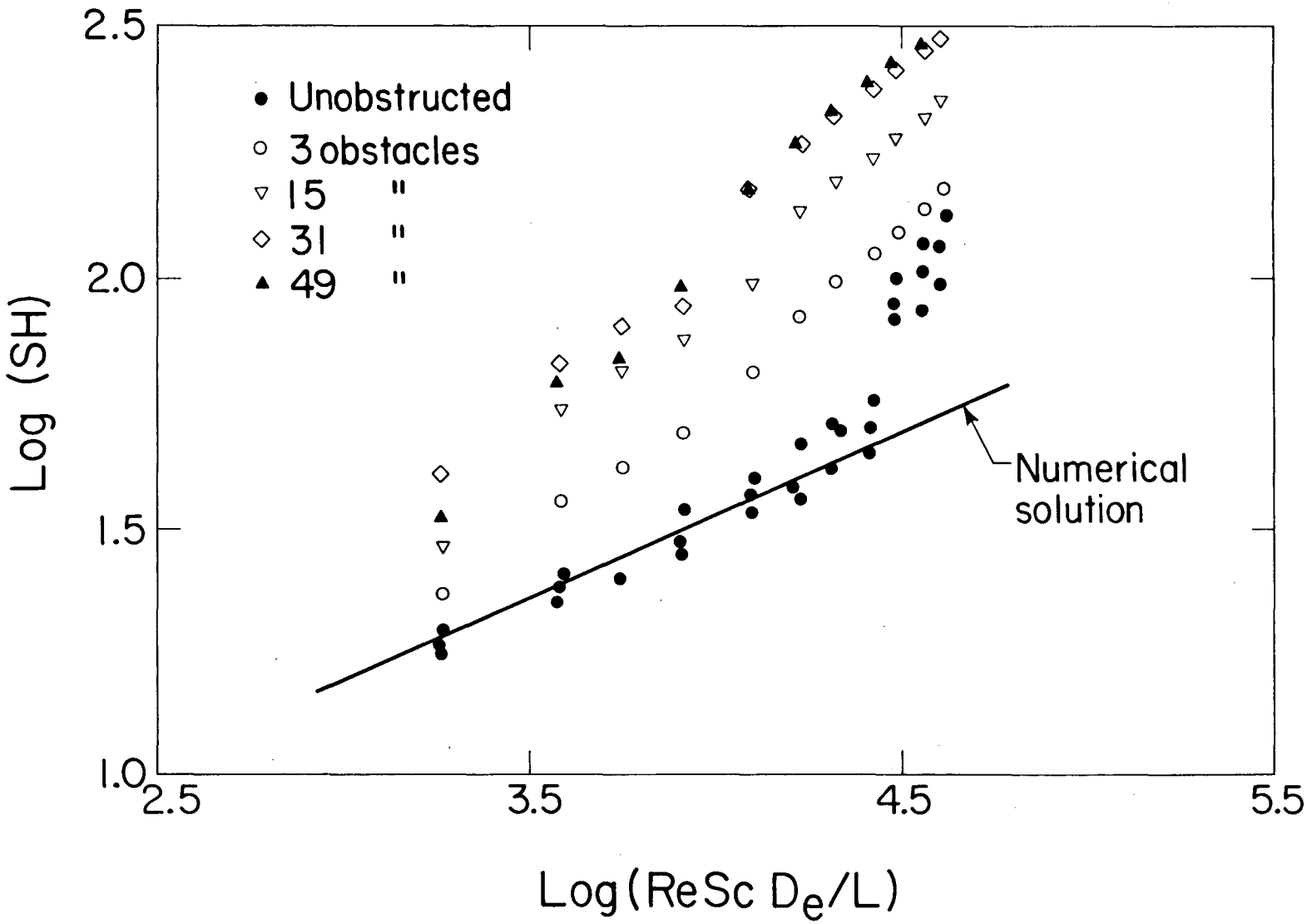

XBL 837-2824

Fig. 39. Dimensionless plot of mass transfer rates for the Small obstacles (0.0762 cm).

Pressure Drop Measurement

The results in the preceeding section have shown that obstacles substantially enhance the mass transfer rates. However, these obstacles also cause an increase in the resistance to fluid flow that can be determined through pressure drop measurements. To assess the overall benefit of the presence of obstacles, a comparison must be made between the pumping power requirement and the mass transfer enhancement effect. The methods used to measure the pressure drop over the length of the active electrodes are described in the Experimental Apparatus and the Experimental Technique sections. It was noted that transient pressure fluctuations could be recorded with the electronic transducer (DC to 1000 Hz). Figures 40 and 41 are plots obtained using the transducer with the unobstructed duct, and in the presence of 15 Small obstacles, respectively. The fluctuations shown by the limiting current values are also reflected in the pressure drop. However, the pressure fluctuations are lower. Large fluctuations are also evident around Re = 2100 in the unobstructed channel. Fluctuations start at lower flow rates in the presence of the obstacles. As in the case of the limiting current, there are virtually no fluctuations at low Reynolds numbers.

The reproducibility of the pressure drop data were even better than that of the limiting current data. This was probably due to the smaller amplitude of the fluctuations.

Figures 42 and 43 are plots of the pressure drop versus the flow rate as a function of the obstacle number for the Large and Small

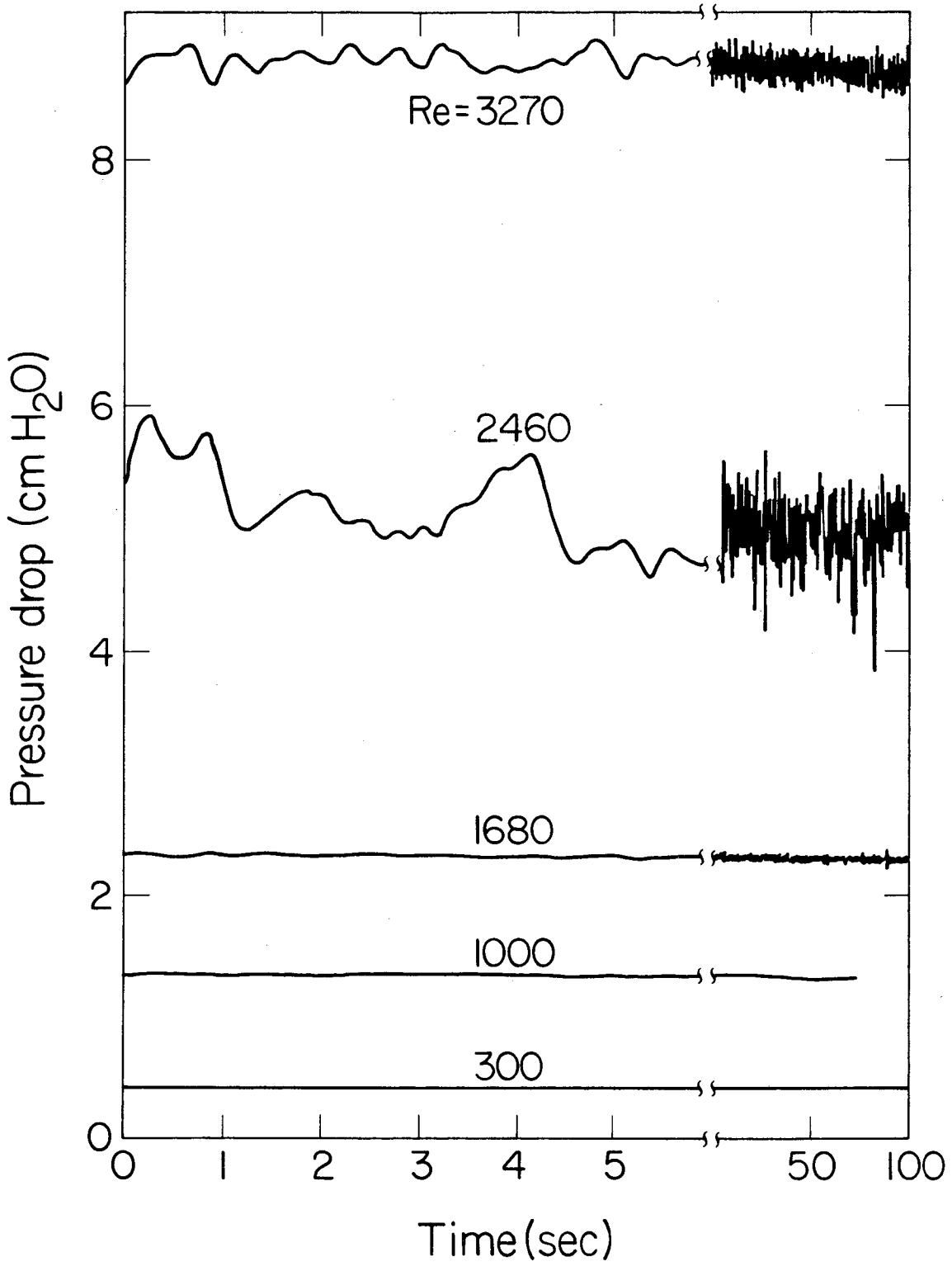

XBL 837-2763

Fig. 40. Fluctuations of the pressure drop in the unobstructed duct as the Reynolds number (Re) is increased. Note the effect of turbulence.

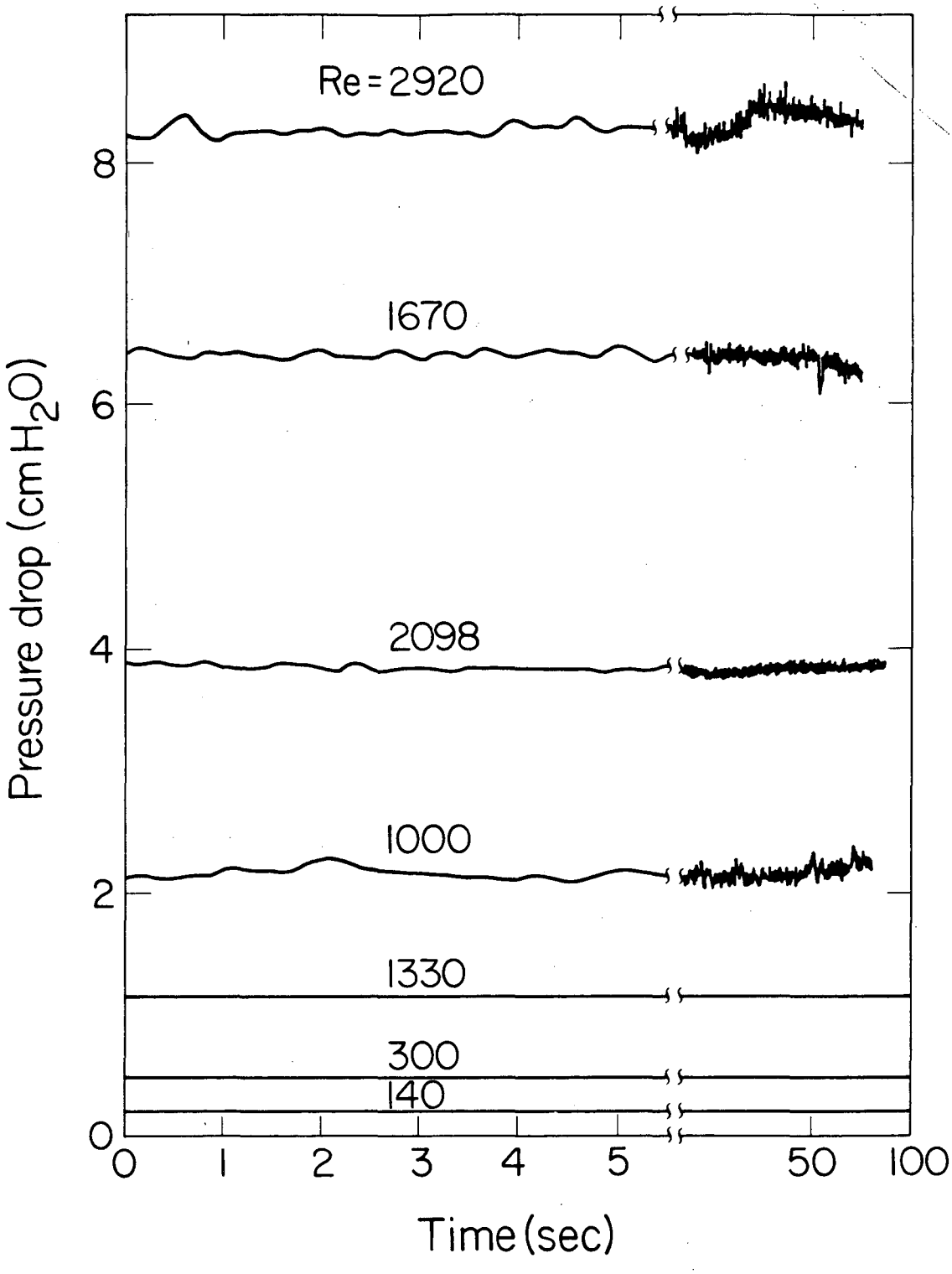

XBL 837-2761

Fig. 41. Fluctuations of the pressure drop in the presence of 15 Small obstacles (0.0762 cm).

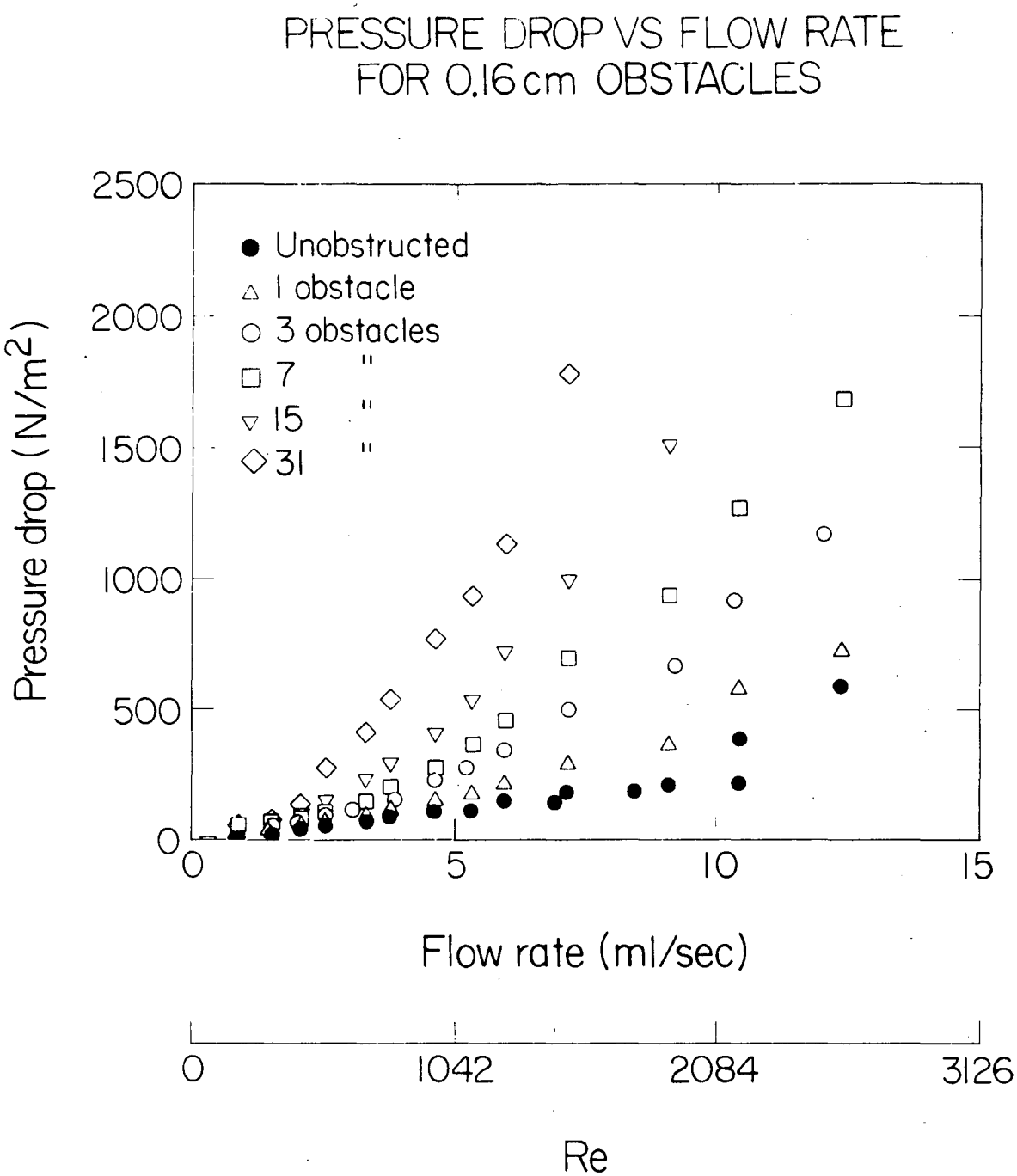

XBL 838-10937

Fig. 42. Pressure drop as a function of flow rate and number of Large obstacles (0.160 cm).

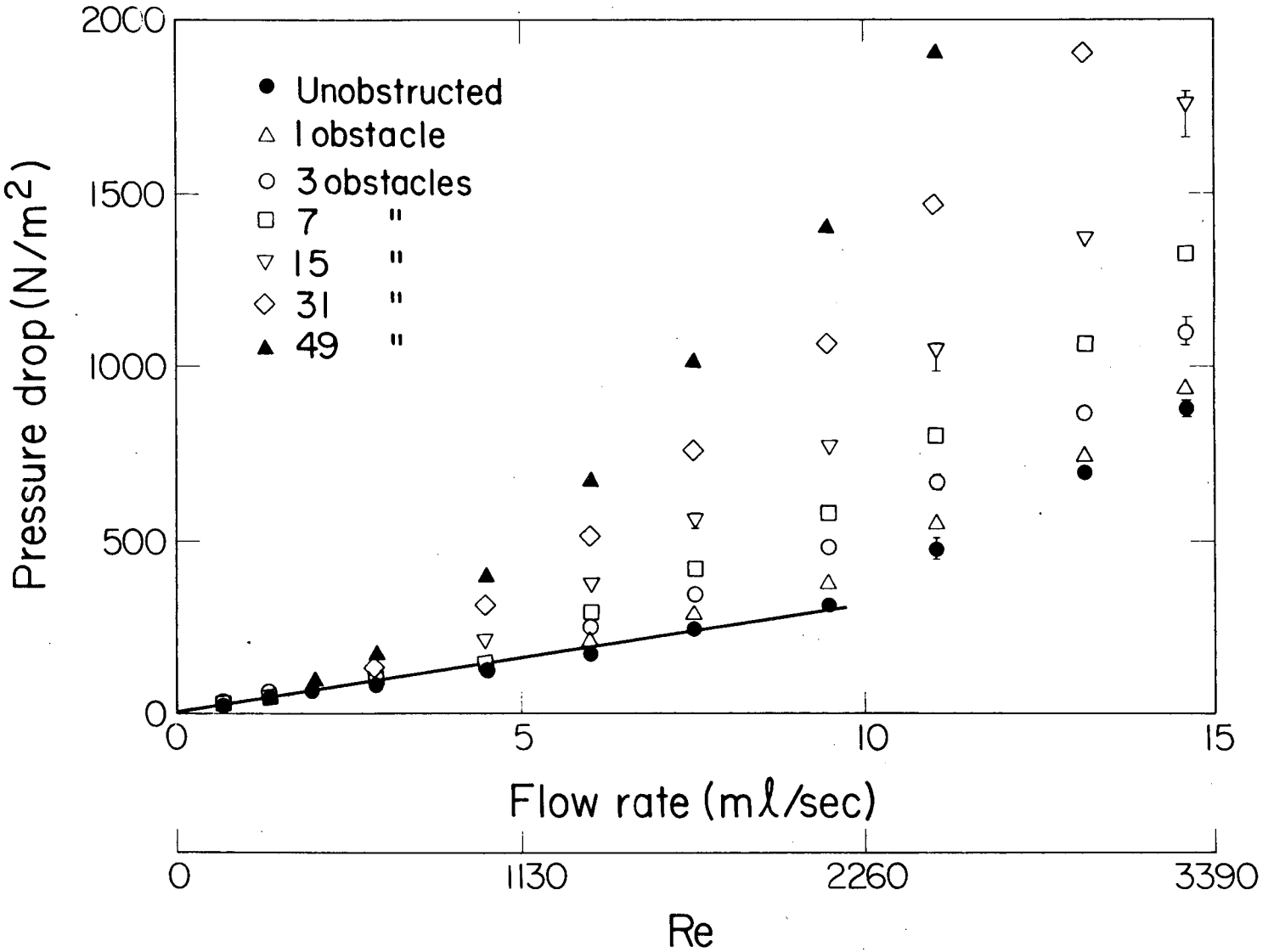

XBL 837-2820

Fig. 43. Pressure drop as a function of flow rate and number of Small obstacles (0.0762 cm). Note linear slope in the laminar regime for the unobstructed duct.

obstacles respectively. Results from the unobstructed duct are depicted by the solid dots. Increasing the number of obstacles always yielded an increase to the pressure drop caused by the flowing fluid. In the laminar regime, for an unobstructed square duct the dependence of pressure drop (ΔP) on flow rate (Q) is linear, given by the equation:

$$\Delta P = \left[\frac{28.45\ \mu L}{D_e^{\ 4}} \right] Q$$

Evaluation of the slope representing laminar flow yielded an equivalent hydraulic diameter (D_e) that differed by only 1.6 percent from the value measured with a micrometer. The obstacles show exponential behavior even at low Reynolds numbers. The Small obstacles produce substantially lower pressure drop than the Large ones. The ΔP is drastically increased by additional numbers of obstacles. This effect and the decrease in the mass transfer enhancement caused by the close spacing of the obstacles leads to the conclusion that an optimum spacing exists. This optimum spacing (number of obstacles) is dependent on the size of the obstacles and the Reynolds number. Furthermore, the optimum arrangement of the Smaller obstacles - 31 - produced a larger enhancement than the optimum arrangement of the Larger obstacles - 15.

Figures 44 and 45 are "Moody" plots [150] for the Large and Small obstacles respectively. These plots relate the dimensionless Fanning friction factor (f) to the Reynolds number. The definition of the friction factor is:

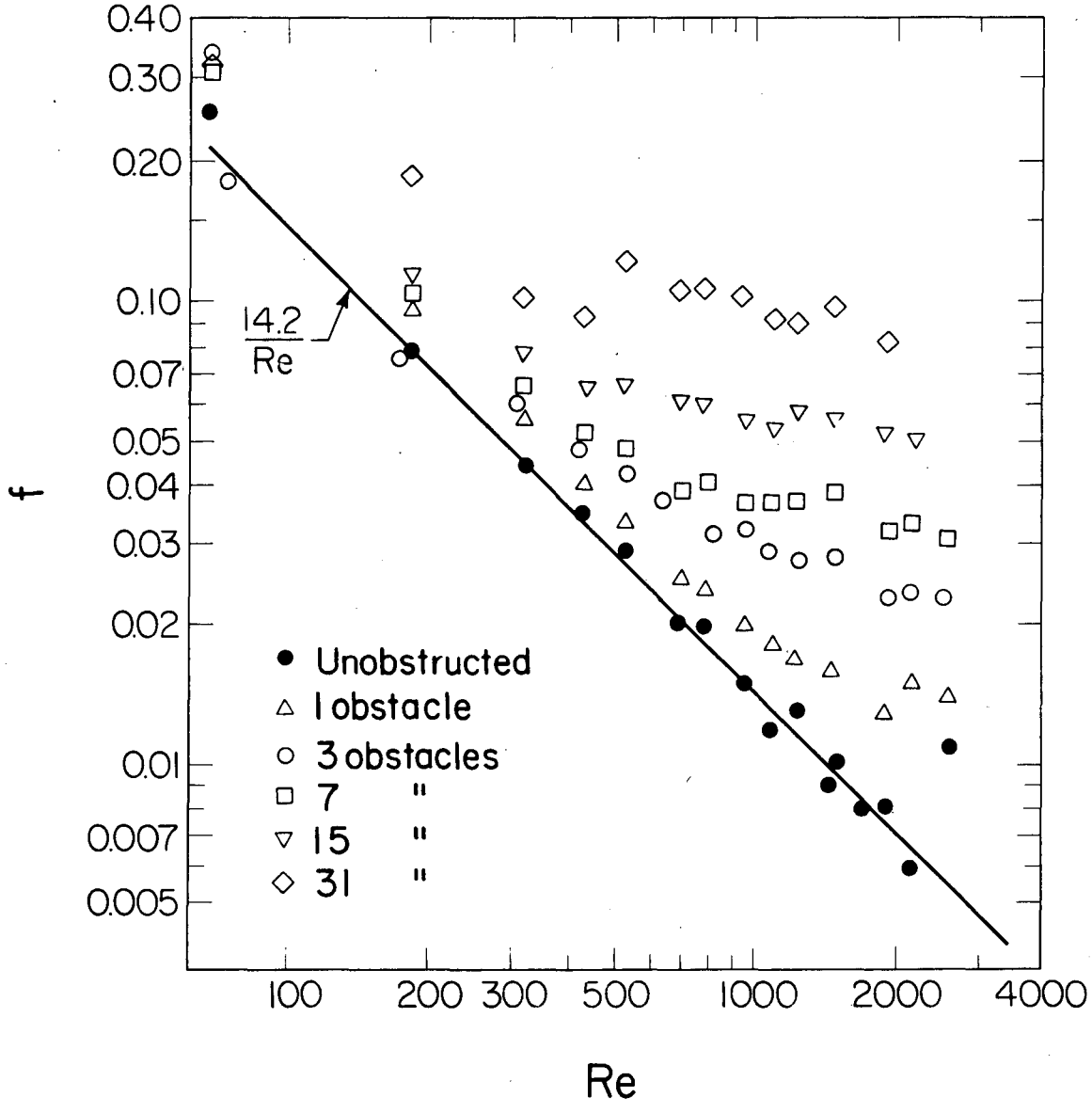

XBL 837-2821

Fig. 44. Friction factor (f) plot for the Large obstacles (0.160 cm). Black line depicts the analytic solution for the laminar flow regime in a square duct.

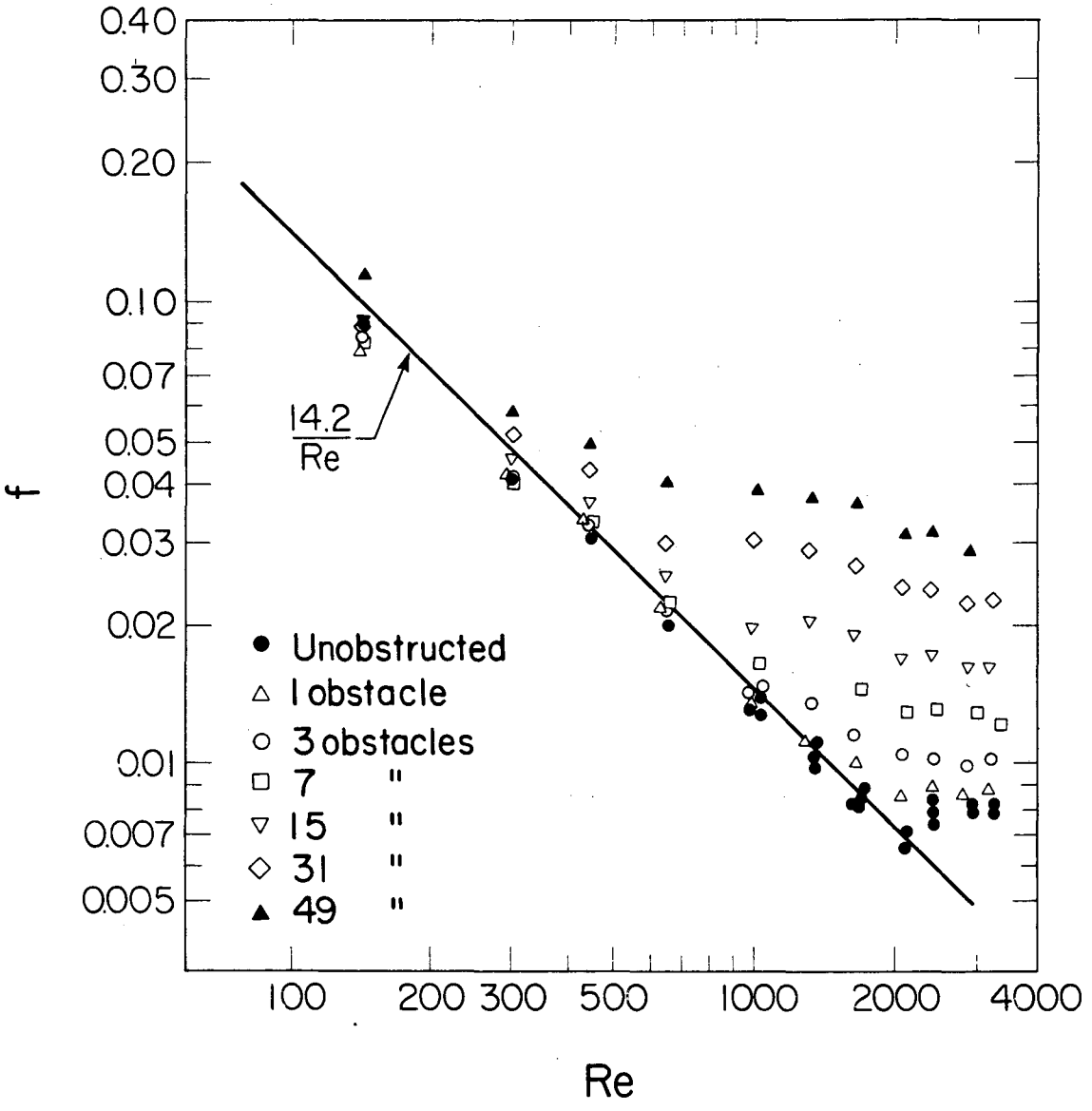

XBL 837-2825

Fig. 45. Friction factor (f) plot for the Small obstacles (0.0762 cm). Black line depicts the analytic solution for the unobstructed square duct in the laminar flow regime.

$$f = \frac{1}{4} \frac{D_e \left(\frac{\Delta P}{L}\right)}{\left(\frac{1}{2}\rho \quad V_b^2\right)}$$

Using the pressure drop equation for laminar flow in a square duct, the following relation is obtained:

$$f = \frac{14.2}{Re}$$

This dependence, which is drawn on the Moody diagrams, is valid for the laminar regime (Reynolds numbers below 2100). The unobstructed channel results (solid dots) are in excellent agreement with this line. As the flow mechanism changes from laminar to turbulent, the dependence of friction factor on Reynolds number changes proportionality from Re^{-1} (laminar) to $Re^{-1/4}$ (Blasius equation for turbulent flow). On a Moody diagram, turbulent flow behavior is represented by a nearly horizontal line with a slope of -1/4. The Moody diagrams show that the obstacles could be considered "turbulence promoters", because they produce the effect of turbulence on the friction factor at Reynolds numbers below 2100.

The "turbulence promoting" effect is produced at even lower Reynolds numbers as the obstacle size is increased or spacing decreased. These figures show that the Larger obstacles produce a much larger resistance to pumping and therefore cause much higher friction factors.

<u>ΔP versus I - Introduction to Obstacle Benefit</u>

The goal of this study was to observe the effect of flow obstacles on mass transfer rates and to determine the corresponding pumping

requirements. To begin evaluating the possible benefit of the obstacles, the data is plotted on Figs. 46 and 47 as pressure drop versus limiting current for the Large and Small obstacles respectively. Figures 48 and 49 expand the lower range of the figures before. In all the figures the unobstructed channel results, depicted by solid dots, show rapidly increasing behavior. To obtain a greater rate of mass transfer (higher limiting current), the flow rate can be increased or obstacles can be attached. Both of these enhancement methods require an increased power input to pump the electrolyte. In all cases the pressure drop in the presence of obstacles fall well below those for the unobstructed channel at the same limiting currents. This means, a desired mass transfer rate (limiting current) can be achieved with a significantly lower fluid pumping power input by adding obstacles.

It is very important to realize that the achieved current is obtained at a lower fluid flow rate when obstacles are added, and this produces an obstacle benefit that is even greater than the figures show, because, to calculate the required pumping power, the pressure drop in the duct must be multiplied by the flow rate (Eq. (38)). Comparing Figs. 46 with 47 and 48 with 49 show the Small obstacles are more beneficial than the Large ones because they cause lower pressure drops at all the limiting current values. Furthermore, because the obstructed channel eventually shows rapidly increasing behavior (exponential rise) similar to that for the unobstructed channel, there seems to be a point of maximum benefit with respect to system operation. An analysis yielding the quantitative advantage and benefit of these flow obstacles will be presented in the Discussion section.

Blank Page

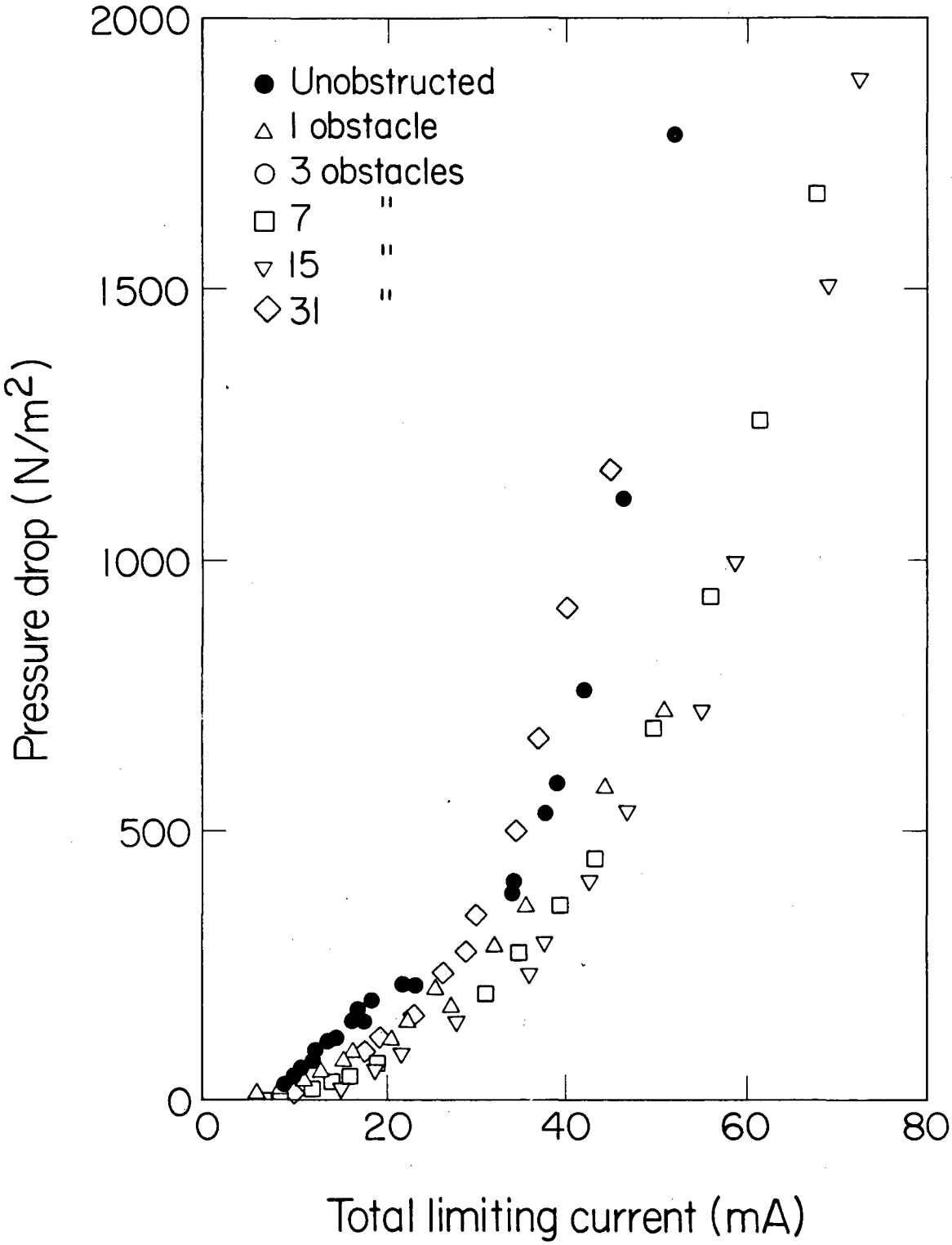

XBL 837-2795

Fig. 46. Pressure drop as a function of limiting current and number of Large obstacles (0.160 cm). Note that in the presence of obstacles the same limiting current is achieved by a respectively lower pressure drop than in the unobstructed duct.

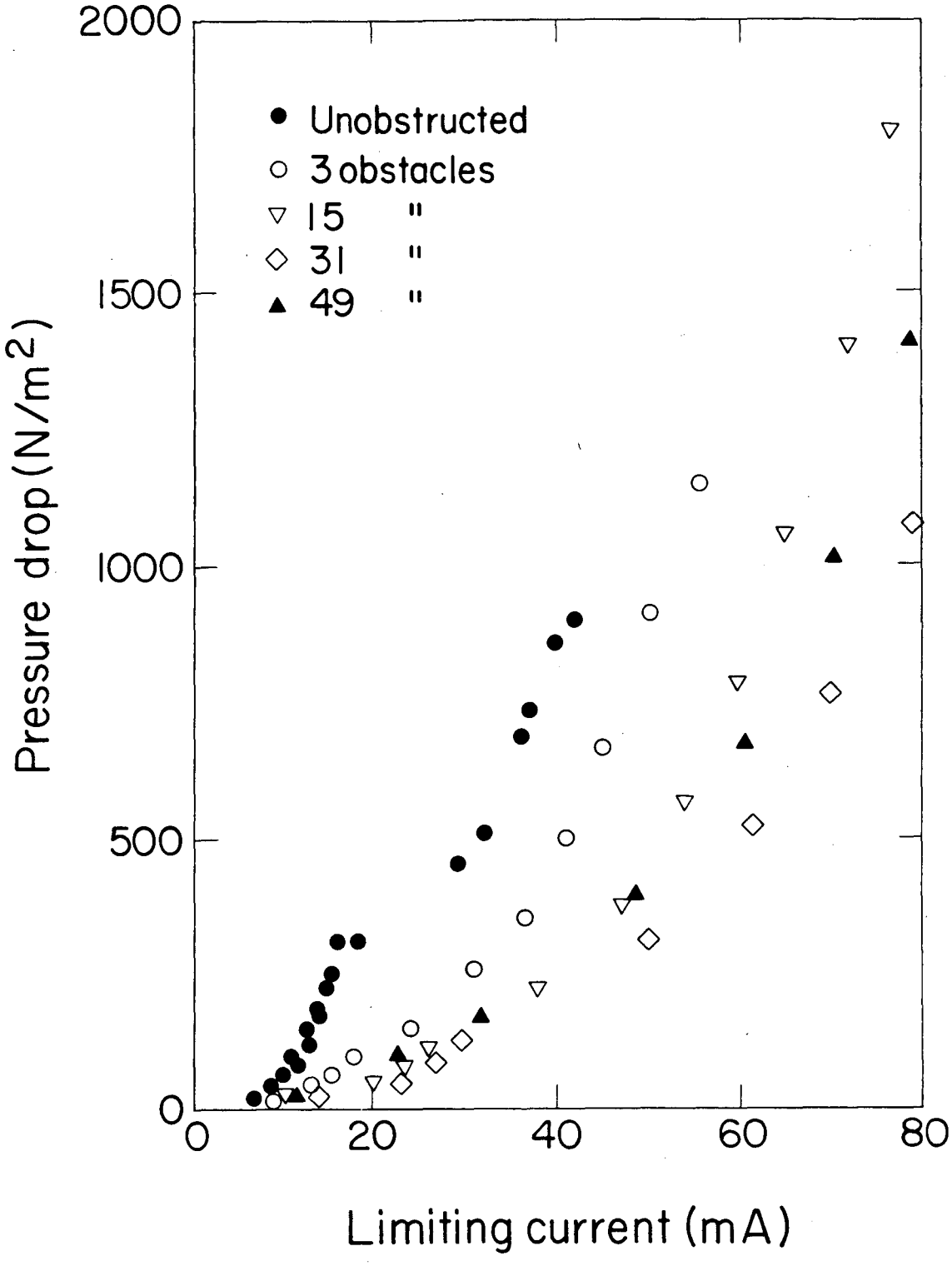

XBL 837-2823

Fig. 47. Pressure drop as a function of limiting current and number of Small obstacles (0.0762 cm). Note that in the presence of obstacles the same limiting current is achieved by a respectively lower pressure drop than in the unobstructed duct.

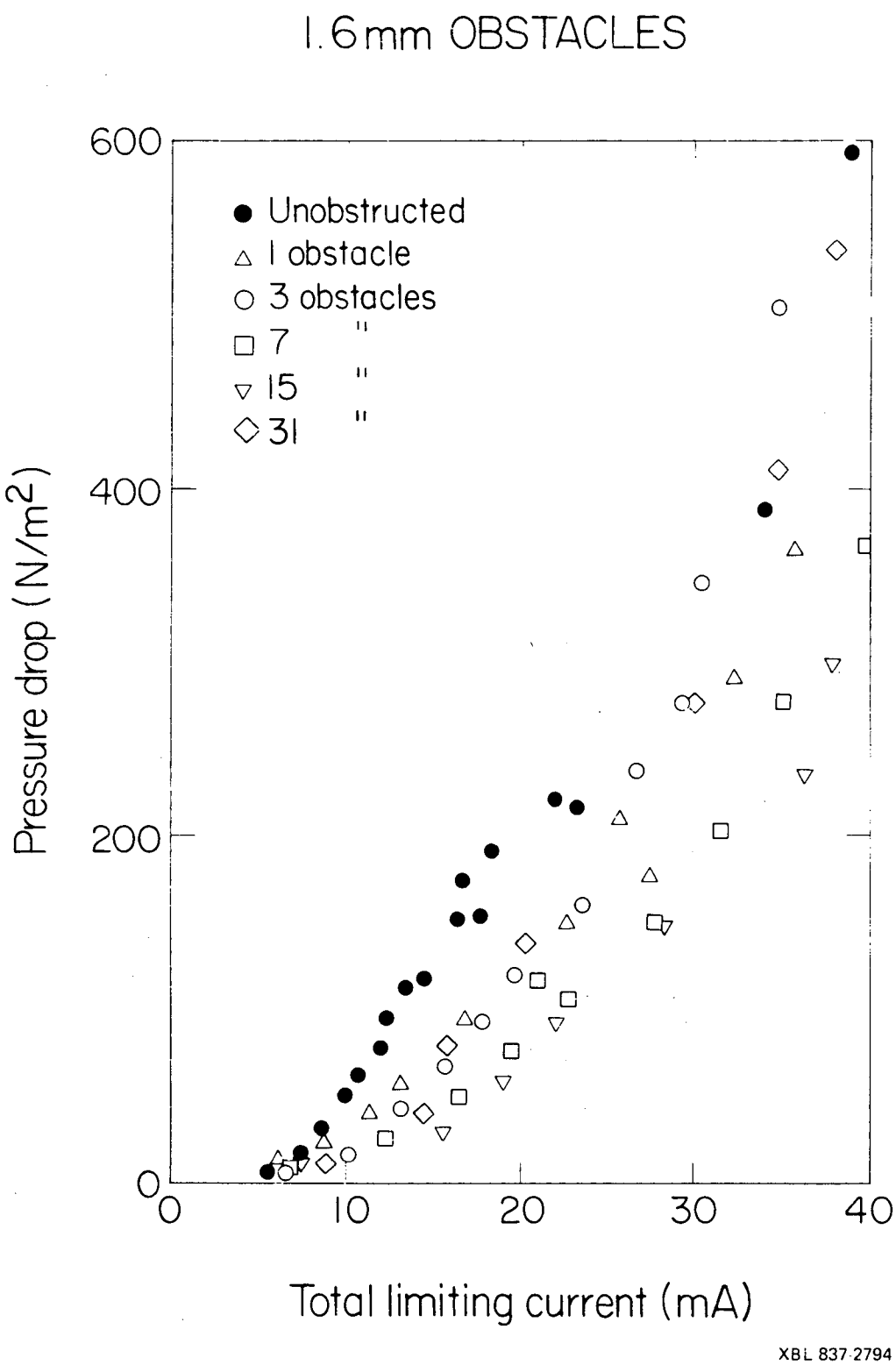

Fig. 48. Expanded view of lower range of Fig. 46 for the Large obstacles (0.160 cm).

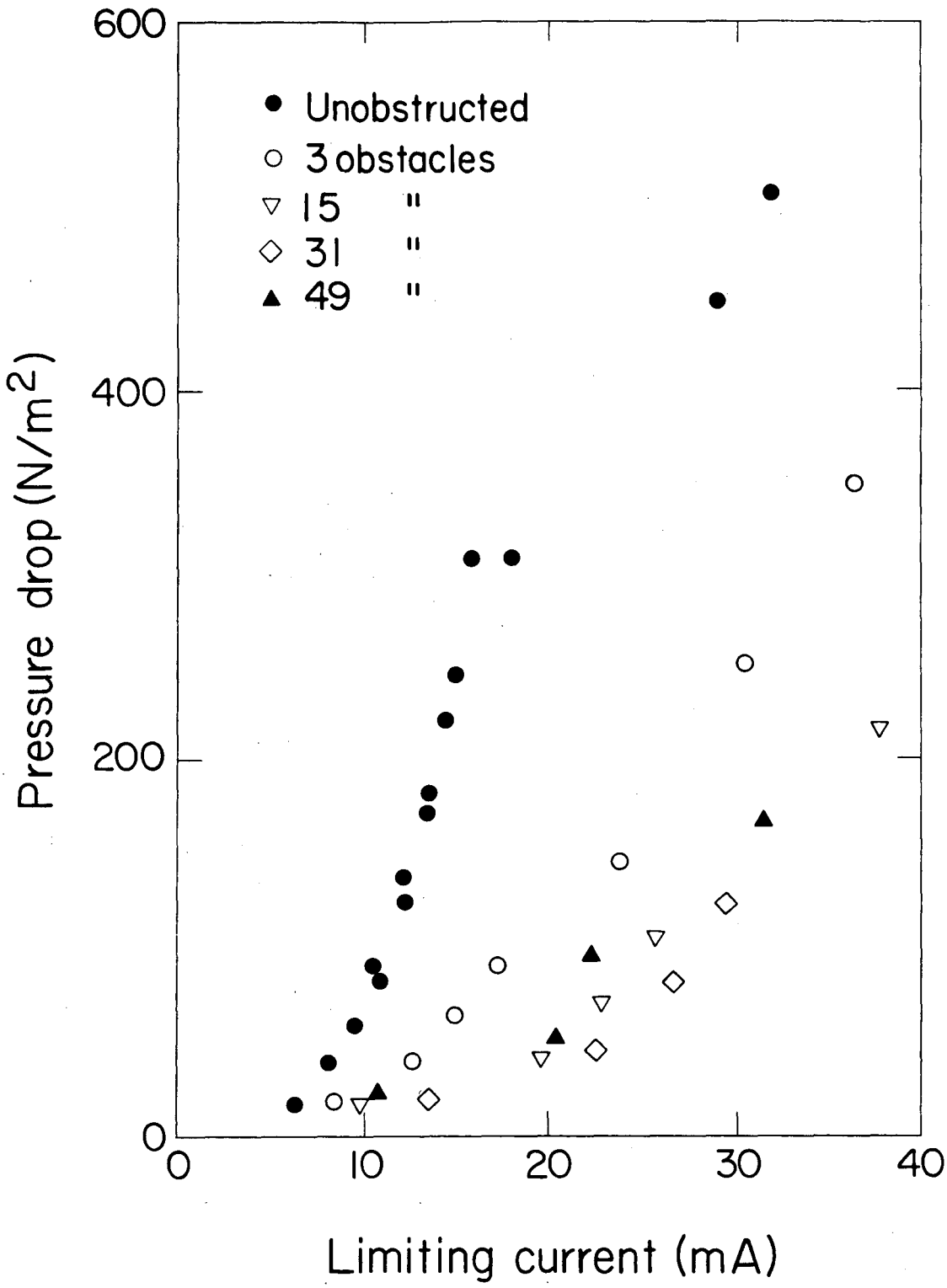

XBL 837-2819

Fig. 49. Expanded view of the lower range of Fig. 47 for the Small obstacles (0.0762 cm).

Flow Visualization

Flow patterns produced by the obstacles were observed and photographed. As described earlier; milk, gas bubbles, and Mearlmaid were used to visualize filament lines, streamlines and particle paths.

Results from the milk technique are shown on Fig. (50). This figure shows the flow patterns at three different Reynolds numbers (Re) around a single Large (0.16 cm) obstacle. The downstream recirculation zone is clearly visualized; its size is shown to grow as the flow rate (Reynolds number) increases. This recirculation zone has been observed and described by previous workers investigating flow downstream from a step [170-171].

The effect of increasing the Reynolds number (Re) on the flow pattern around the single large obstacle is also shown on Figs. 51 and 52. In these photographs, hydrogen bubbles were used to follow the streamlines. The downstream recirculation zone is observed to elongate in the flow direction. The elongation continues until turbulence is produced and the zone disappears (around Re = 868). Turbulence is shown in Fig. 52. Here the bubbles are observed to follow non-laminar paths and oscillate across the channel, implying eddy motion. These two photographs were taken with the camera looking down on the channel at a slight angle relative to horizontal instead of exactly perpendicular to it. This was done to show the three dimensional nature of the flow pattern the obstacles produced. The bottom electrode (anode) and plexiglas spacer are visible from this position. With the bubble experiments, three dimensional motion was observed downstream from the

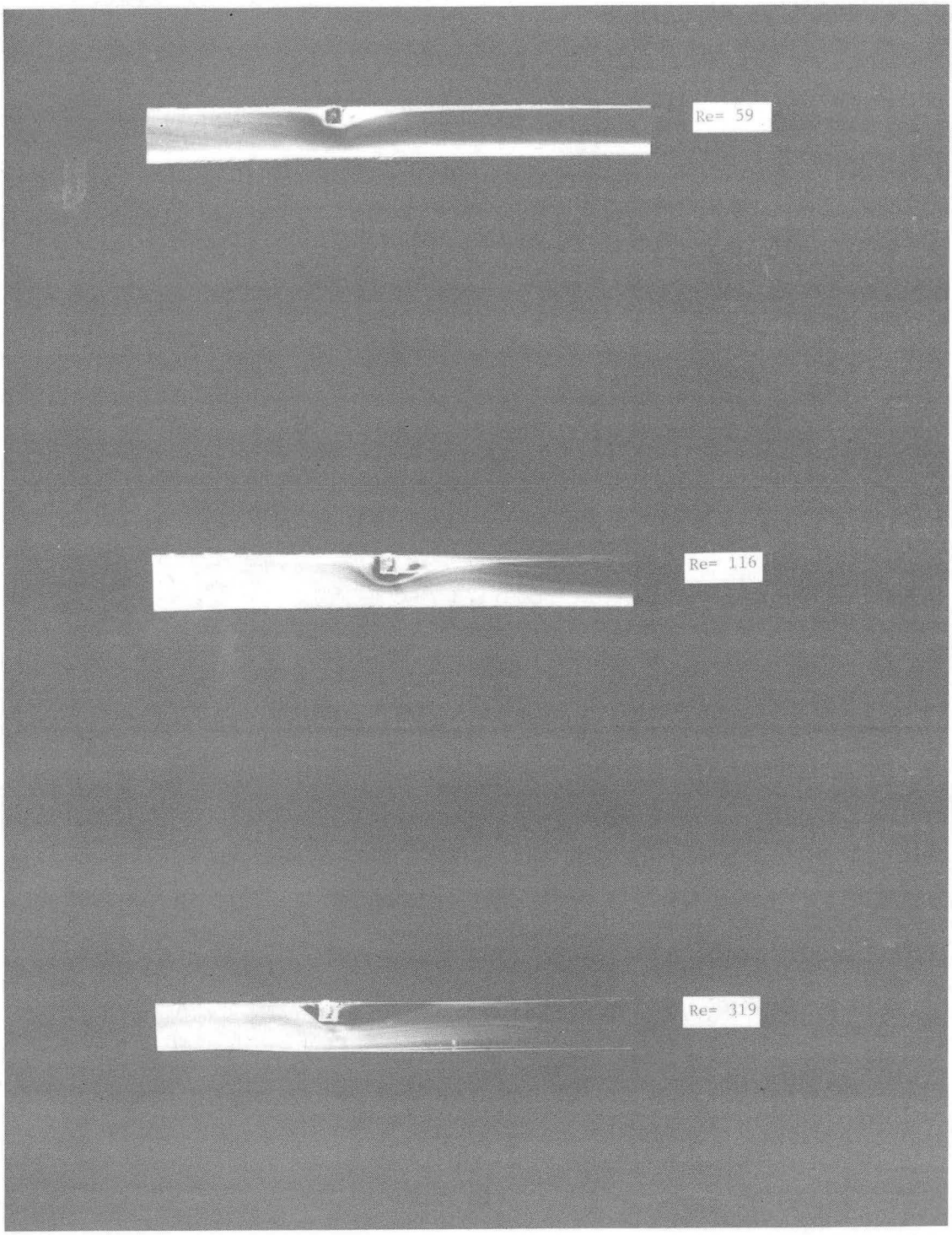

XBB 838-6896

Fig. 50. Flow visualization using milk injected into water around a single Large obstacle (0.160 cm).

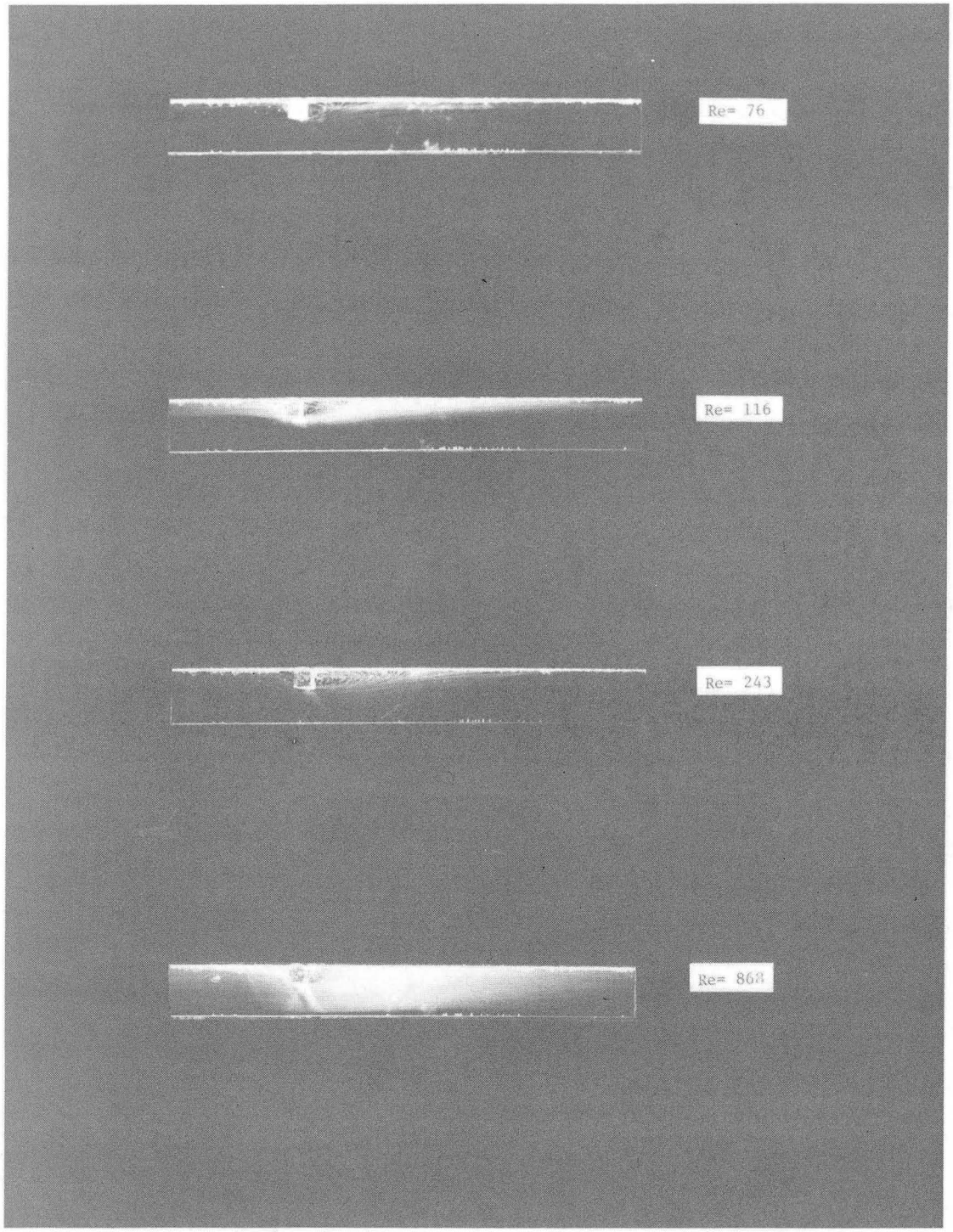

XBB 838-6892

Fig. 51. Flow visualization using hydrogen bubbles evolved from NaOH solution around a single Large obstacle (0.160 cm).

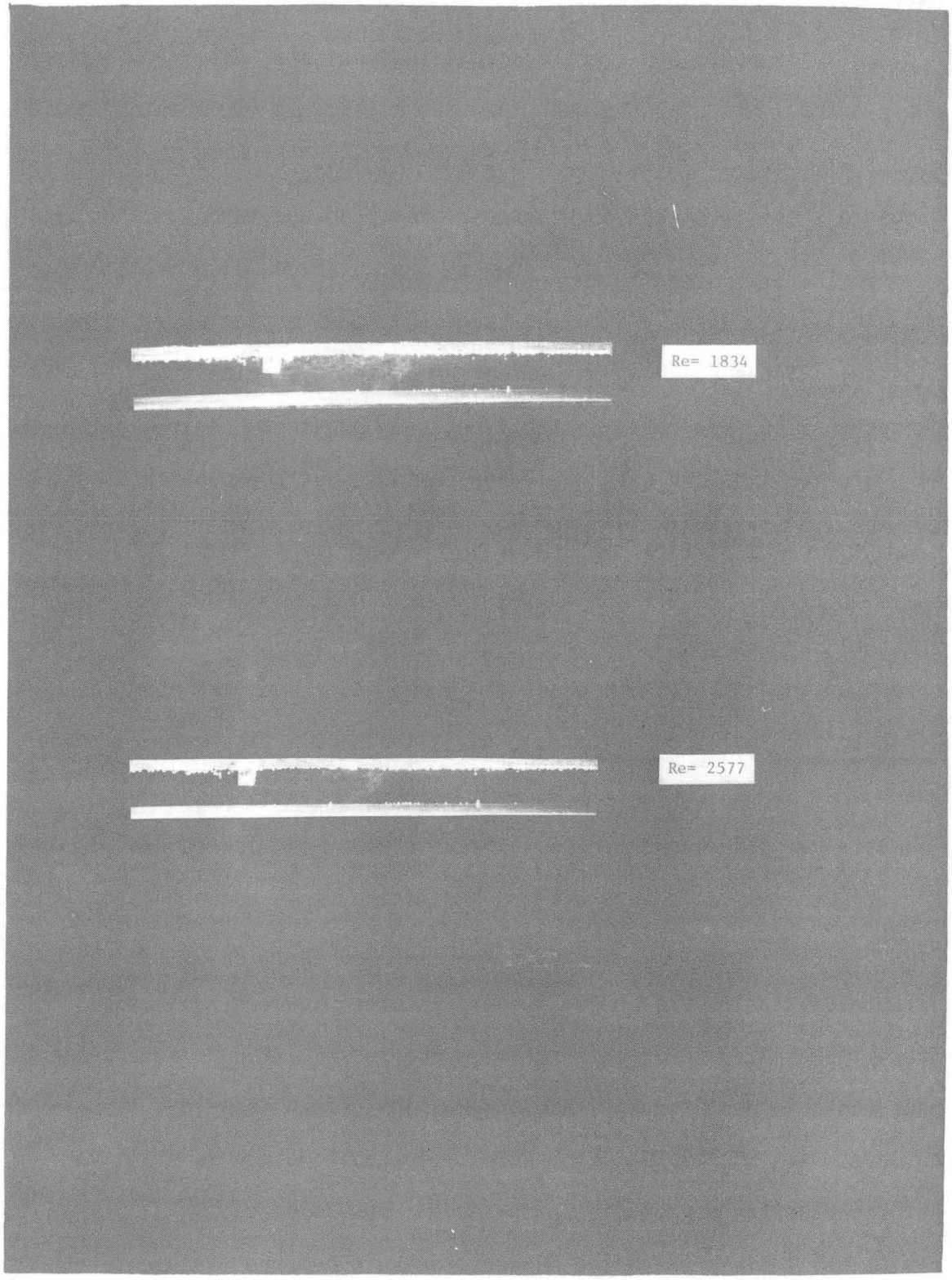

XBB 838-6897

Fig. 52. Flow visualization using hydrogen bubbles evolved from NaOH electrolyte around a single Large obstacle (0.160 cm). Note that the observer is tilted from horizontal and looking down into the duct.

obstacle. The photographs show the vertical swirling motion of the recirculation zone. However, recirculation was also observed in the cross-channel direction between the side walls. It is important to note that there is a limit to how large the recirculation zone elongates in the flow direction before it breaks up and turbulence occurs.

The effect of the obstacle spacing was observed using Mearlmaid as the visualizing agent. Both the Large and Small obstacles were investigated. Figure 53 shows the effect of obstacle spacing at a Reynolds number of 275. One observes the elongated downstream recirculation zone previously shown with the large obstacles by the bubble technique. An upstream effect can also be seen with the Mearlmaid. The elongated downstream recirculation zone does not interact with the next obstacle. However, with 31 large obstacles there is almost an interaction. The effect on the bulk flow is drastically reduced when going from the Large to the Small obstacles; and so is the size of the recirculation zone.

At a Reynolds number equal to 583, shown by the photographs in Fig. 54, the obstacle interactions and size effects are apparent. The larger obstacles create much more bulk turbulence. In the presence of 31 Large obstacles the motion is very chaotic; however, with the 31 Small there is no interaction between the recirculation zone and the next obstacle downstream. This interaction effect, however, is observed with the 49 Small obstacles. The bulk motion is still laminar with the farther spacings and smaller obstacles.

At still higher Reynolds numbers the bulk becomes turbulent with even the small obstacles. This is shown in Fig. 55. One sees the

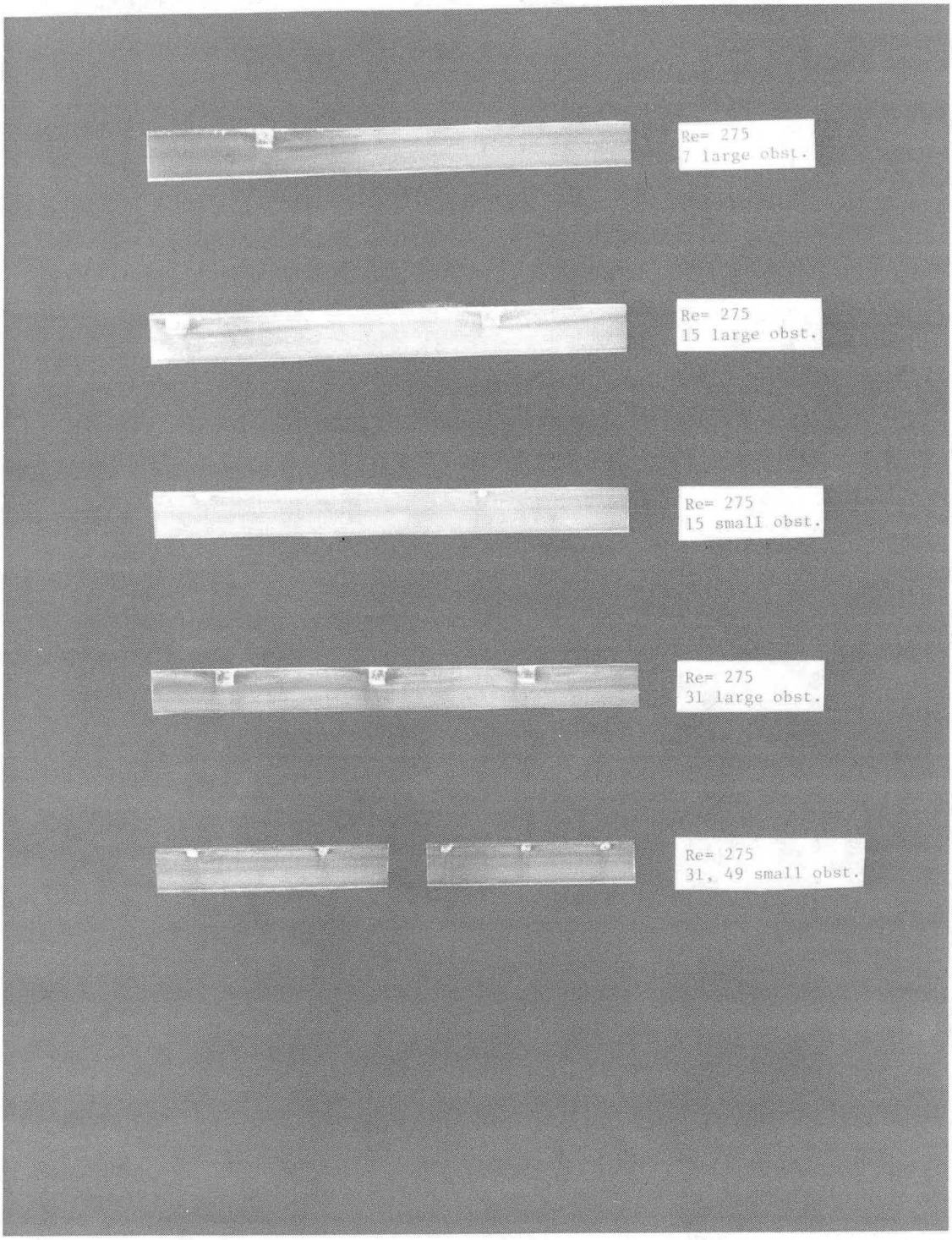

XBB 838-6895

Fig. 53. Flow visualization using a dilute Mearlmaid suspension in water. Effect of Large and Small obstacle spacing is illuminated at Re = 275.

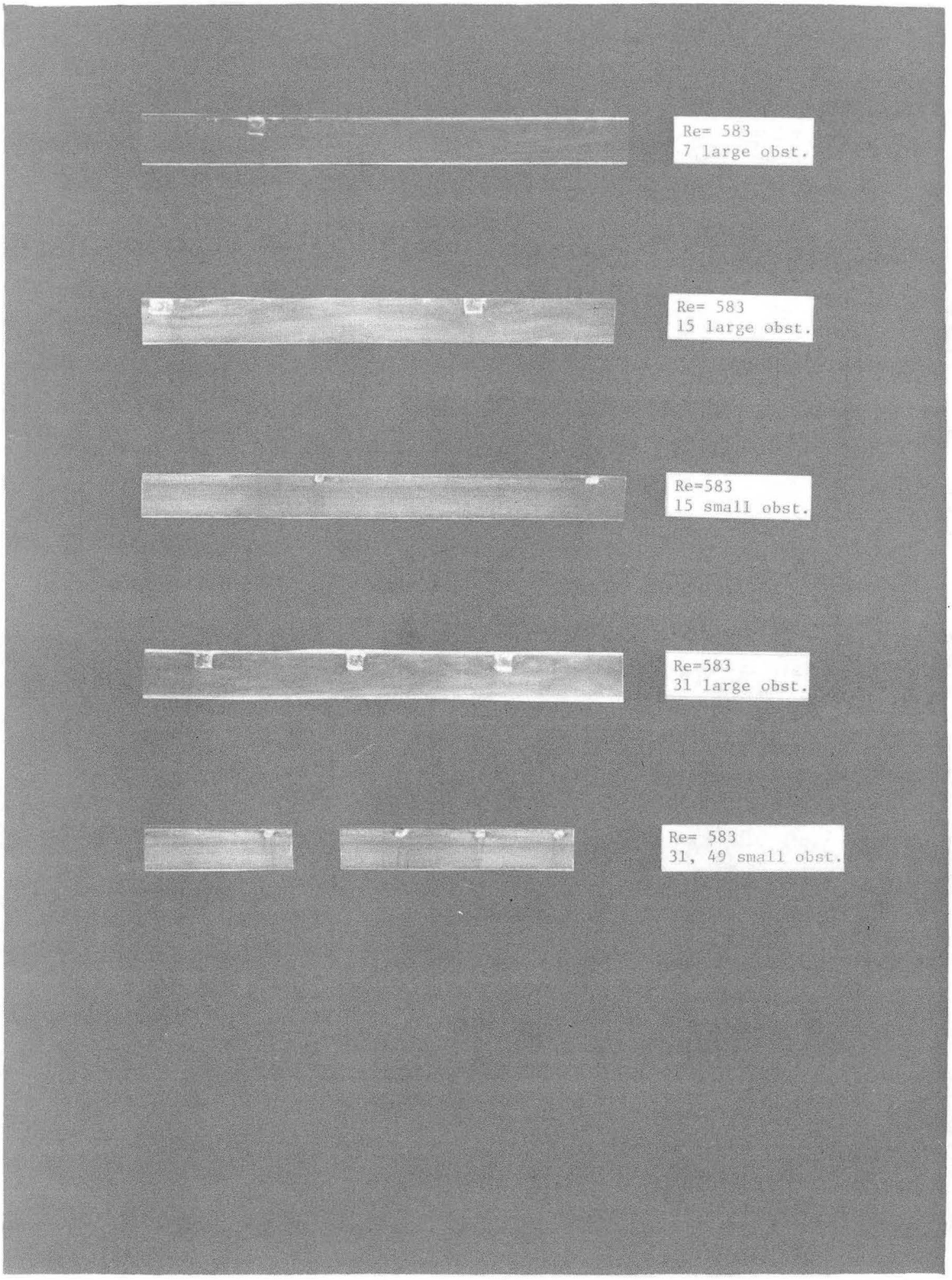

XBB 838-6894

Fig. 54. Flow visualization using a dilute Mearlmaid suspension in water. Effect of Large and Small obstacle spacing is illuminated at Re = 583.

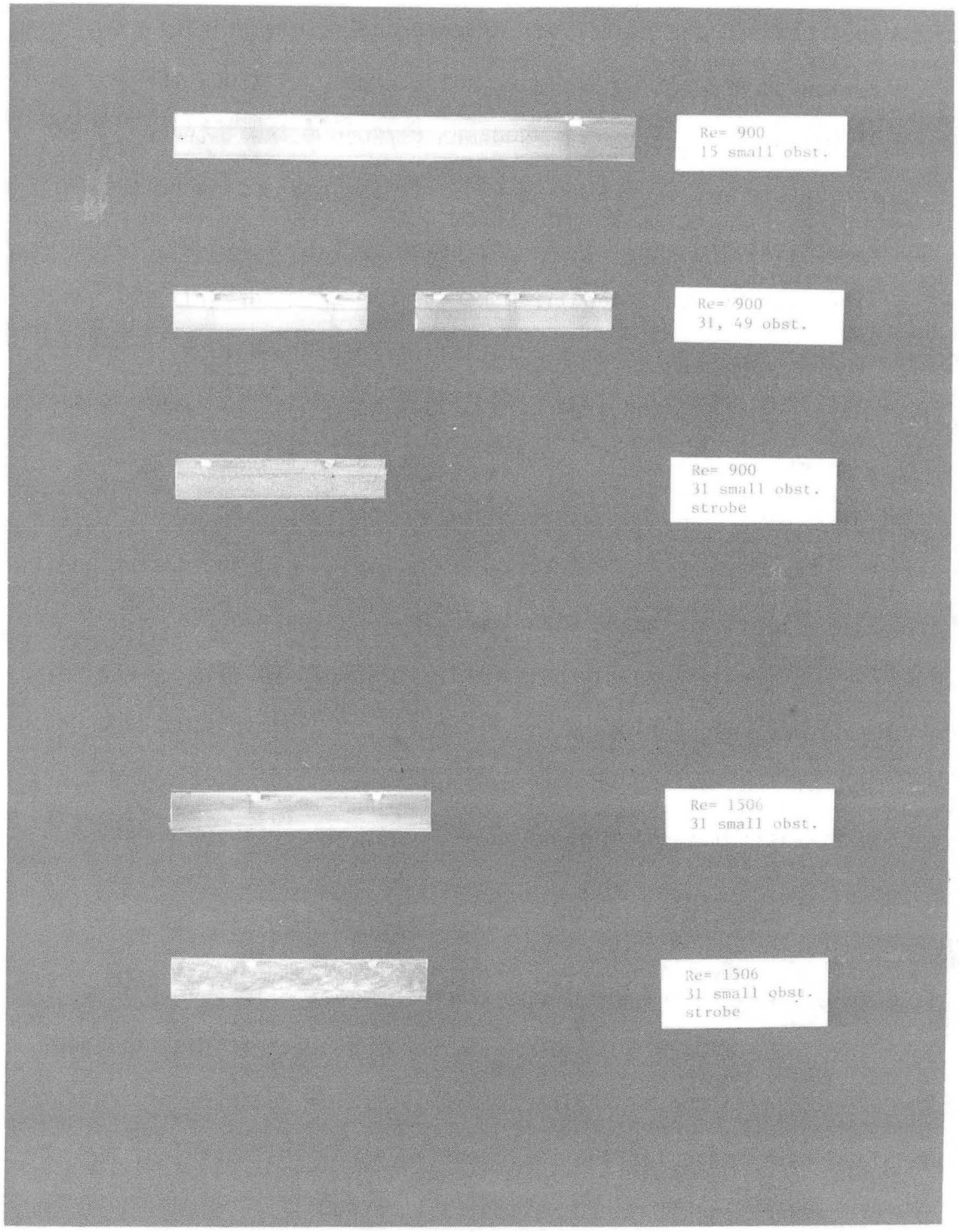

XBB 838-6893

Fig. 55. Flow visualization using a dilute Mearlmaid suspension in water. Effect of obstacle spacing at Re = 900 and 1506 for the Small obstacles is shown.

difference between the relatively ordered and stable bulk flow at Re = 900 and flow at Re = 1506. At a Reynolds number of 1506, the photograph, taken with a short time exposure (1/20,000. sec strobe), shows a chaotic nature not seen at Re = 900. It is interesting to see the localized effect the small obstacles have. Their effect on mixing is not in the bulk but in a localized region close to the wall. It is observed that the downstream recirculation zone grows with increasing flow rates. However, the ordered swirling motion of the zone is lost when it grows to such a size as to interact with the next obstacle.

It is interesting to realize that the spacings that gave the best mass transfer performance (15 Large or 31 Small) had recirculation zones that did not interact with the next downstream obstacle. If the zone grew to a length equal to the inter obstacle spacing before bulk turbulence occurred (31 Large, or 49 Small), performance was decreased from that of the maximum enhancement spacing, which allowed the zones to grow to their largest elongation without interacting the next obstacle.

Micro Obstacles

Only one experiment was performed with the smallest or "Micro" obstacles. These were 0.0254 cm high perpendicular to the flow and 0.0762 cm long in the flow direction (Fig. 18). Because very reproducible data existed for the Small obstacles at this spacing, for the sake of comparison, 15 Micro obstacles were equally spaced (3.175 cm apart) along the entire cathode length. They were attached in a manner similar to the method used for the other obstacle sizes. Unfortunately, the temperature of the electrolyte was higher for this run

(28.8°C) than that in the previous experiments. The measured viscosity and calculated ferricyanide diffusion coefficient were 0.906 cp and 7.83×10^{-6} cm^2/sec respectively; resulting in a Schmidt number of 1133 for the electrolyte used with the Micro obstacles.

Figure 56 shows limiting current curves produced by the 15 Micro (0.0254 cm) obstacles as the Reynolds number was increased.

The behavior is compared to the curves produced by the Small (0.0762 cm) obstacles shown on Fig. 28. The limiting current plateaus for the Micro obstacles are lower than those for the Small obstacles. The Micro obstacles yield curves similar to those obtained with an unobstructed channel (Fig. 26). However, mass transfer is still enhanced with these Micro obstacles. The interesting "spiked" behavior shown on Fig. 32 by the unobstructed channel at a Reynolds number of 2120 is seen on Fig. 56 for the 15 Micro obstacles at a Reynolds number of 1680. Besides these transition spikes, current fluctuations at Re = 2460 are also observed.

The current versus flow rate and pressure drop versus flow rate behavior of the 15 Micro obstacles is shown on Fig. 57. The dependence of the limiting current on the flow rate in the presence of the 15 Micro obstacles is very linear and produces mass transfer enhancement rates greater than those produced by 3 Small obstacles but lower than those produced by 15 Small obstacles (Fig. 35). The pressure drop behavior was close to that of an unobstructed channel operating in the laminar regime. Above Re = 2260 the 15 Micro obstacles yielded larger pressure drops than the unobstructed channel.

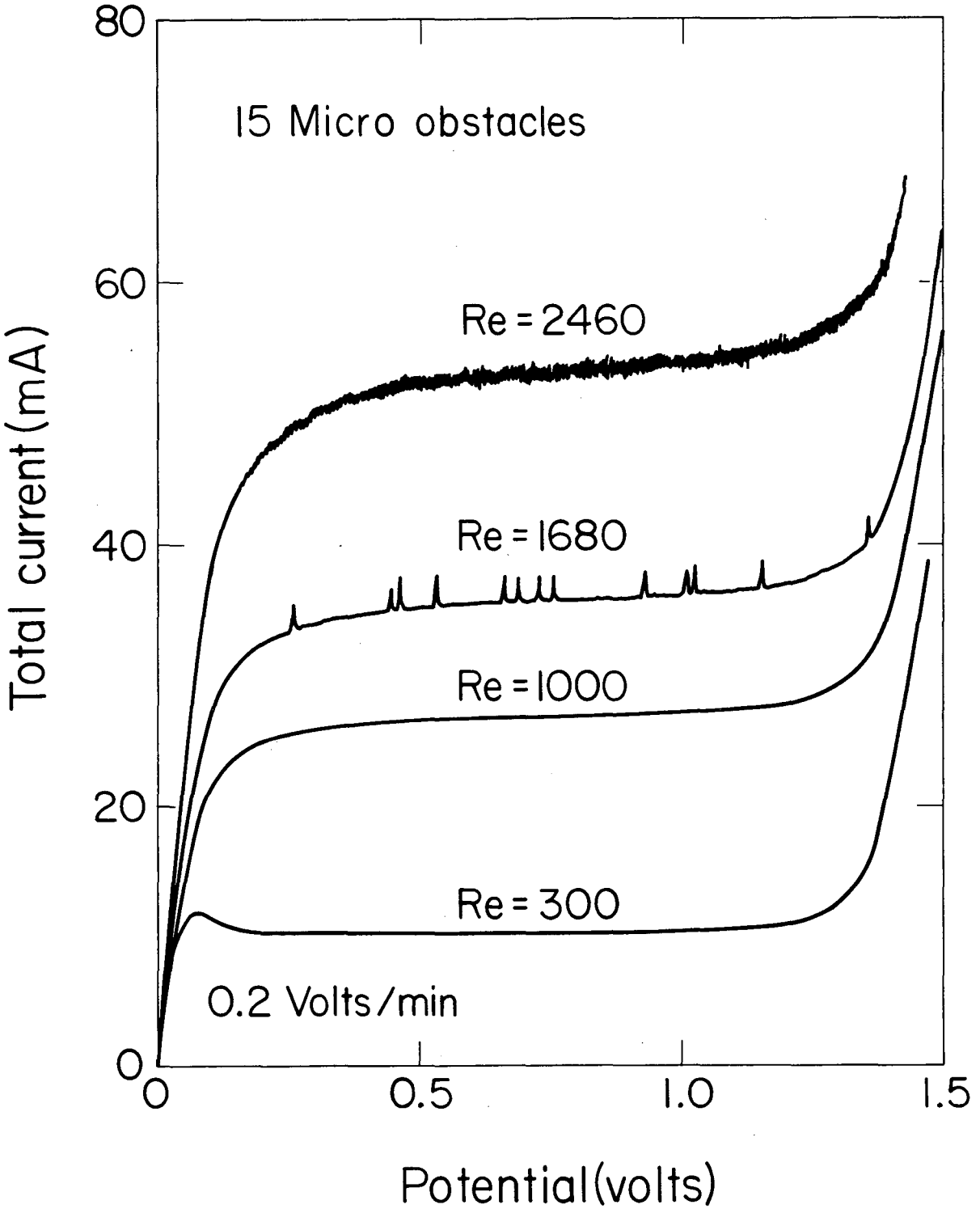

XBL 838-3059

Fig. 56. Limiting current curves for 15 Micro obstacles (0.0254 cm) at different Reynolds numbers (Re). Note spikes at Re = 1680.

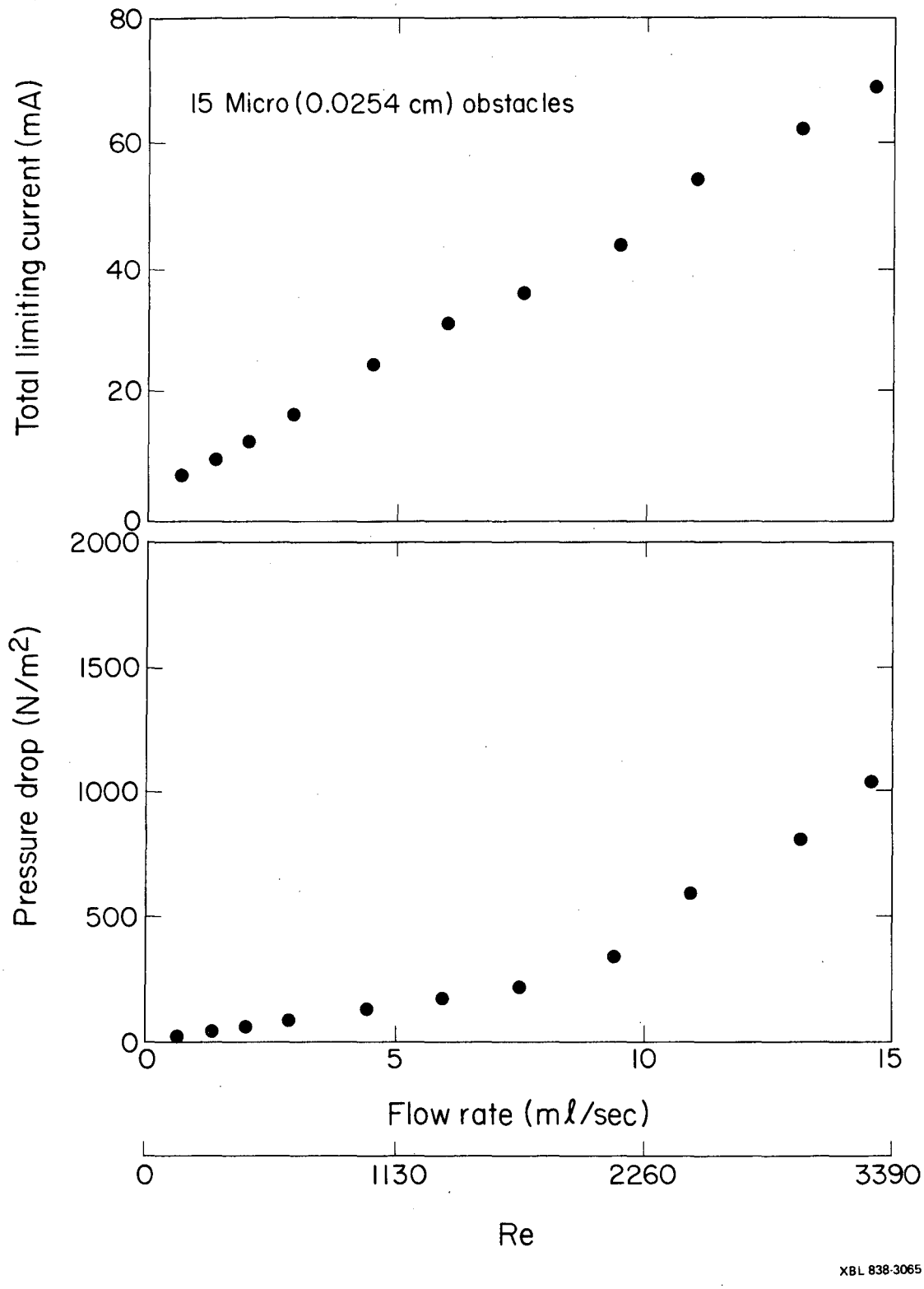

Fig. 57. Limiting current and pressure drop plotted vs. flow rate for 15 Micro obstacles (0.0254 cm) attached to the cathode.

The dimensionless mass transfer rates of the 15 Micro obstacles are plotted on Fig. 58 (the temperature effect is considered in the calculations). The results are quite interesting. At very low Reynolds numbers (below 300) the mass transfer rates are about equal to those of an unobstructed duct. In the middle range, enhancement to transfer occurs and it continues to increase until the enhancement rates equal to those produced by the 15 Small obstacles (Re = 3600) are obtained.

A plot of pressure drop versus limiting current is shown in Fig. 59. Comparison with a similar plot for the Small obstacles (Fig. 47), shows the beneficial effect of Micro obstacles over the unobstructed channel. The results for the 15 Micro are very similar to the results for the 15 Small obstacles. However, the Small obstacles are more beneficial than the Micro at lower limiting currents (below 27 mA). It is important to remember that the Micro results were obtained with an electrolyte that was much warmer (28.8°C) than the electrolyte used for the Small results (24.0°C). The former case had a viscosity that was reduced by 10 and a diffusivity that was 11 percent greater than the latter case. This temperature difference must be taken into consideration when comparing these results.

Though the 15 Micro obstacles do not produce as much mass transfer enhancement as the 15 Small obstacles, they produce considerably less resistance to flow; which therefore allows them to be nearly equivalent to the 15 Small obstacles in overall benefit. Because they can probably be placed closer together than the larger sized obstacles,

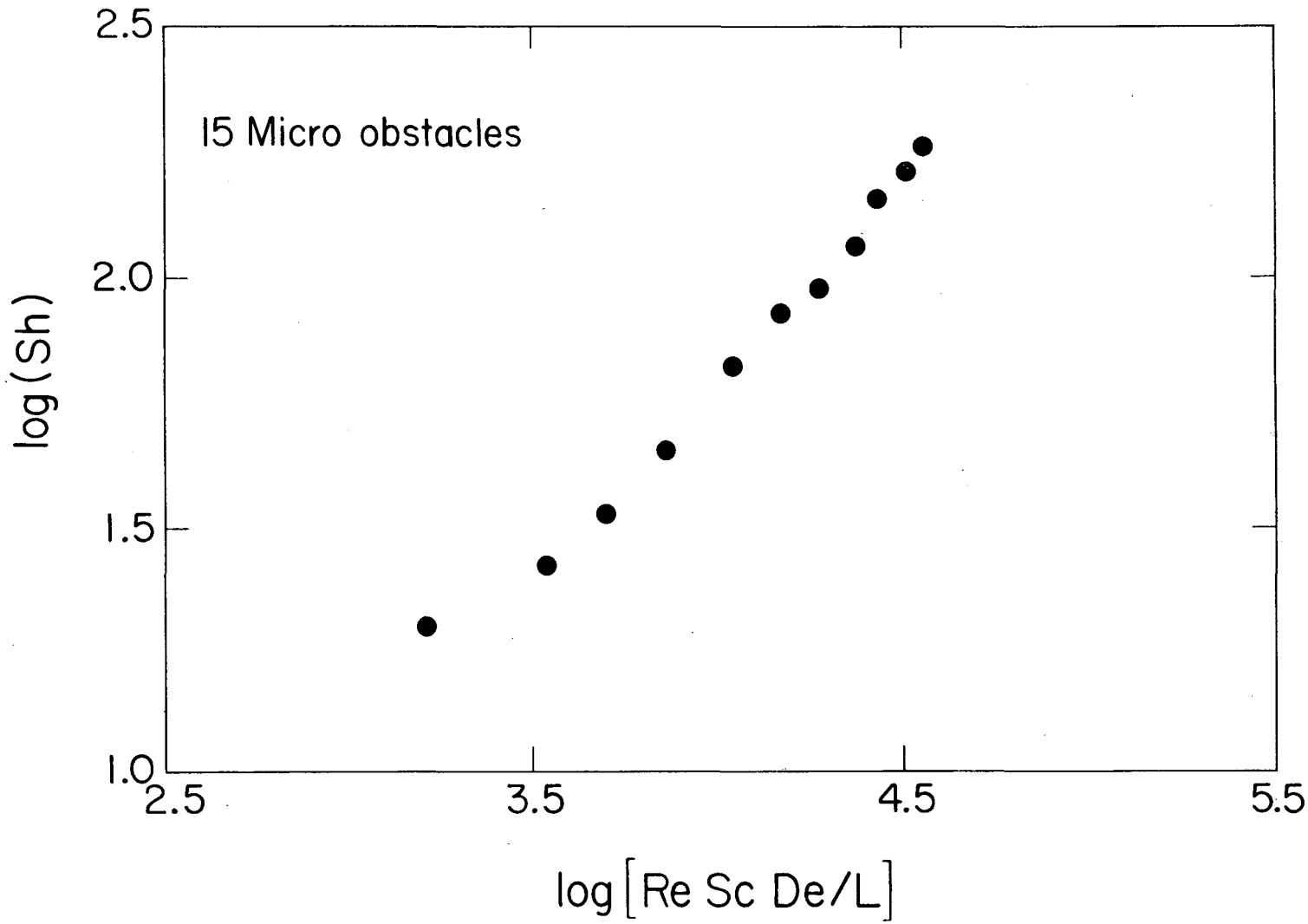

XBL 838-3063

Fig. 58. Dimensionless plot of mass transfer rates for 15 attached Micro obstacles (0.0254 cm).

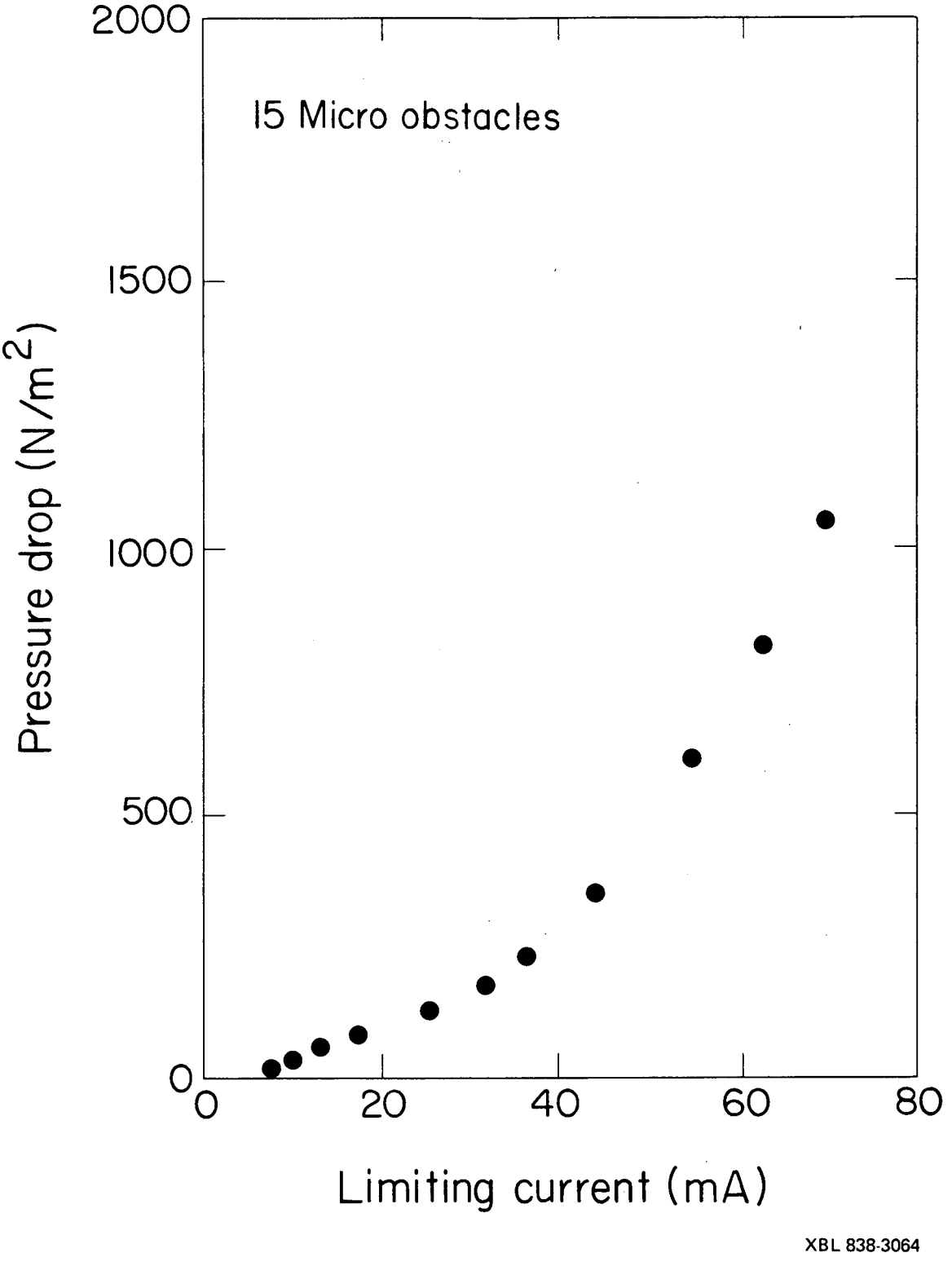

Fig. 59. Pressure drop versus limiting current in the presence of 15 Micro obstacles (0.0254 cm).

these "Micro" obstacles might yield more benefit, in terms of pumping power requirement, over the "Small" obstacles.

QUANTITATIVE DISCUSSION OF OBSTACLE BENEFIT

It has been shown that obstacles attached to the surface of the cathode in an electrochemical square duct reactor yield enhanced mass transfer rates and increased pressure drops. The higher limiting currents (mass transfer rates) obtained with the obstacles were also shown to produce less pressure drop than if these currents were produced only by increasing the electrolyte flow rate. This benefit is shown in figures 46 through 49. Comparison of these figures show that the Smaller (.0762 cm) obstacles are more beneficial than the Larger (0.16 cm) ones. This is because both sizes increase mass transfer by approximately the same factor; however, the Smaller obstacles present drastically less resistance to flow. It is also observed that closer spacing of the obstacles provides increased mass transfer enhancement and overall benefit until a maximum is reached. Beyond this, the addition of more obstacles decreases the enhancement.

Previous studies with large turbulence promoters in a channel observed a limiting situation when $\Delta l/h = 4$ [68]. In this investigation the optimum spacing was found to be a function of obstacle size. The optimum spacing for the Smaller obstacles is smaller and therefore allows more obstacles to be attached to the surface. It is shown that the flow recirculates downstream from the obstacle producing efficient mixing very close to the electrode surface. As flow rate is increased this recirculation zone grew to a maximum length that depends on the obstacle size and spacing. Closer obstacle spacing or larger obstacles produces turbulent flow behavior at lower flow rates. Furthermore, the optimum spacing is achieved when the point of recirculation

zone reattachment does not interact with the next downstream obstacle. Using semi-cylindrical obstacles, Focke [89] observed the maximum elongation of the recirculation zone in the laminar regime to equal 15 times the obstacle height. For the obstacles in this study, fifteen times the obstacle height would equal 2.4 cm and 1.14 cm respectively for the Large and Small obstacles. Actual optimum spacing was observed to be between 1.58-3.175 cm for the Large obstacles and between 1.02-1.58 cm for the Small ones. These results provide further evidence that the size of the recirculation zone determines the optimum obstacle configuration.

An optimum obstacle height must exist because eventually the surface, with increasingly smaller obstacles, would behave as a smooth surface. Unfortunately, the limited scope of the experiments with the Micro (0.0254 cm) size does not allow definitive conclusions to be reached concerning the optimum obstacle height.

At a specific flow rate, the addition of obstacles produces an increase to the limiting current and the pressure drop over that of the unobstructed duct. This effect is shown by the plots on Fig. 60 for the Large obstacles and by Fig. 61 for the Small ones. On these plots, the current or pressure drop produced is normalized by the values obtained for the unobstructed duct operating at the <u>same</u> flow rate. (The unobstructed duct gives ratios of 1.0.) At low Reynolds numbers (around 100) the current is increased in the presence of obstacles without significantly increasing the pressure drop over the pressure drop in the unobstructed system operating at the same flow

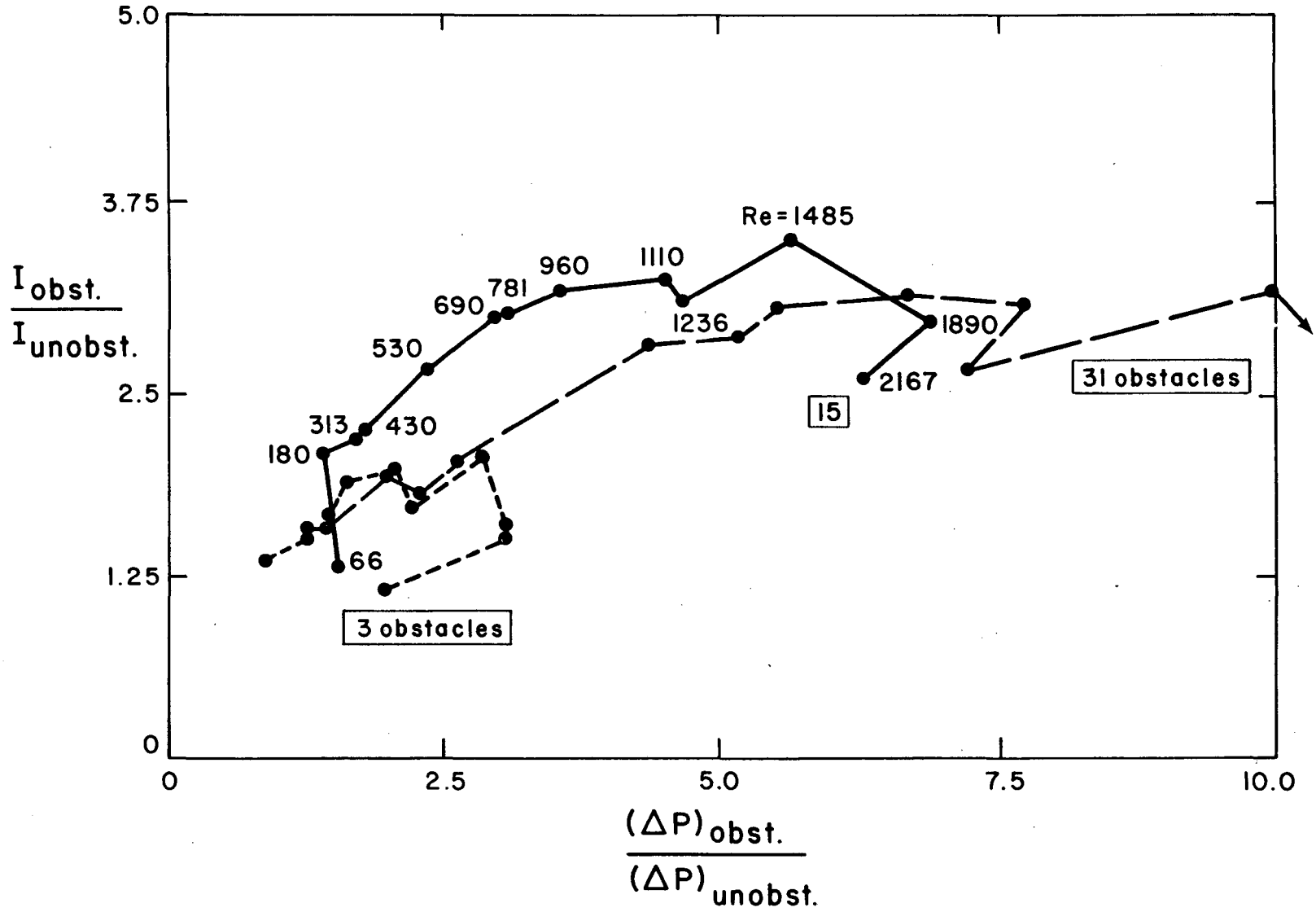

XBL 838-511

Fig. 60. Normalized plot of limiting current (I) vs. pressure drop (ΔP). Each point is evaluated at the indicated Reynolds number (Re). Notice drop-off around Re = 2100. Results for Large obstacles (0.160 cm).

Fig. 61. Normalized plot of limiting current (I) versus pressure drop (ΔP) in the presence of Small obstacles (0.0762 cm). Each point is evaluated at the indicated Reynolds number (Re). Notice the dramatic drop off at Re approximately equal to 2100.

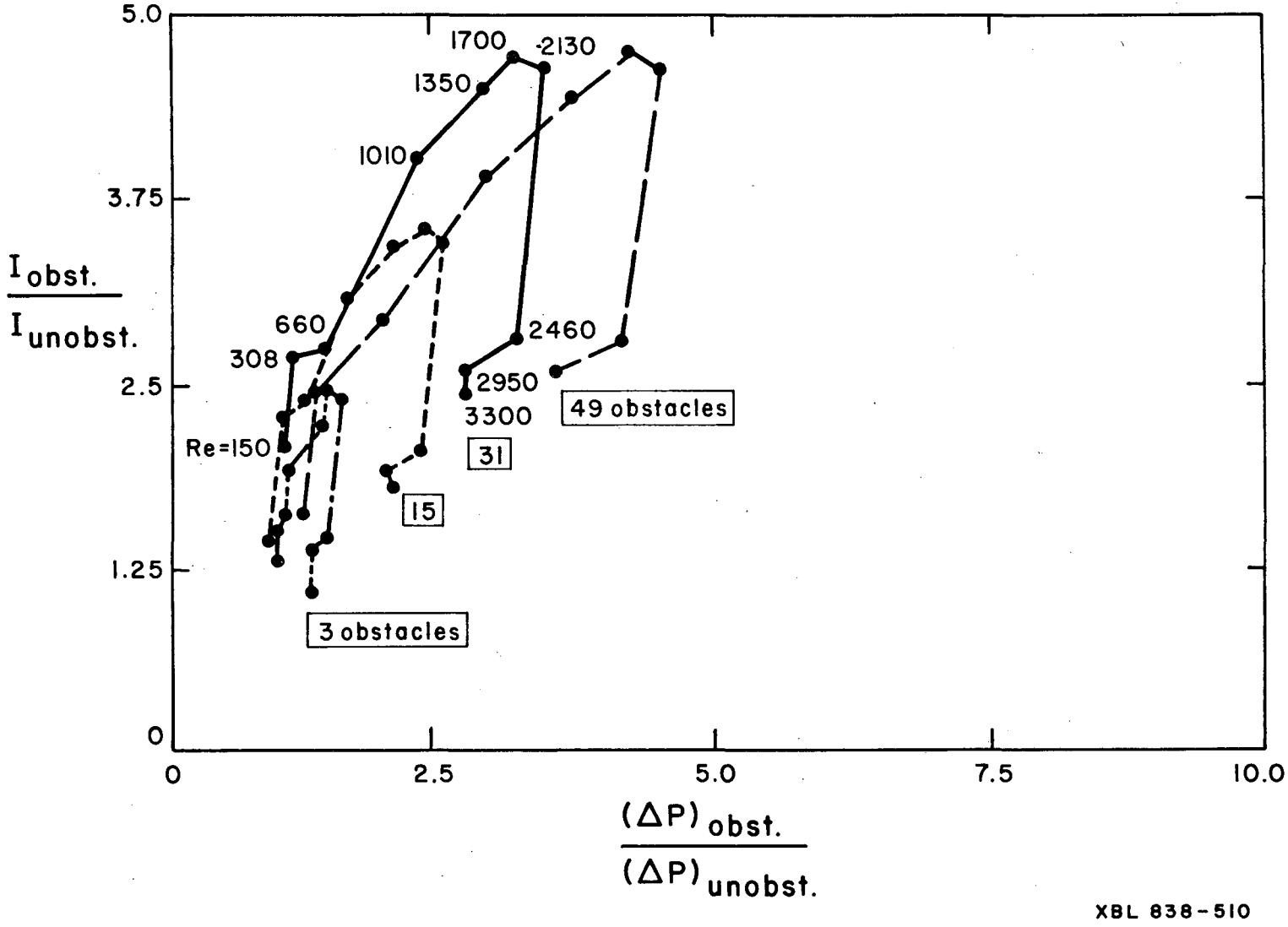

XBL 838-510

Fig. 61.

rate. A greater increase in the current over the pressure drop is observed with the addition of more Small obstacles. The optimum with respect to number of obstacles is clearly seen; a mass transfer rate enhancement of almost 5 fold over that of the unobstructed duct is obtained with 31 Small obstacles. The maximum enhancement of the Small obstacles is observed at a flow rate just below the onset of turbulence in the unobstructed duct. The drop-off in the enhancement ratio is very sharp as Reynolds numbers of 2100 are exceeded. The Larger (0.16 cm) obstacles do not produce a benefit as great as the Smaller (0.0762 cm) obstacles. For the Larger obstacles the decline in the enhancement occurs at a lower Reynolds number.

For this investigation the limiting current or mass transfer rate is an output variable, and the input variables include the number of obstacles, obstacle size, and pumping power. In a system such as this, a plot of the inputs will yield lines of constant output. For this electrochemical reactor, lines of constant limiting current are obtained when the number of obstacles attached is plotted against the pumping power required to obtain the current. These "isocurrent" curves are shown in Fig. 62 for the Small (0.0762 cm) obstacles. The curves show that an increased output (current) can be obtained by an increase in one or both of the inputs (obstacles and pumping power).

Figure 63 displays how the output (current) varies with changes in the pressure drop and obstacles. The points on this curve were calculated by evaluating the pressure drop, with obstacles, needed to obtain a specific current as compared to the pressure drop needed to

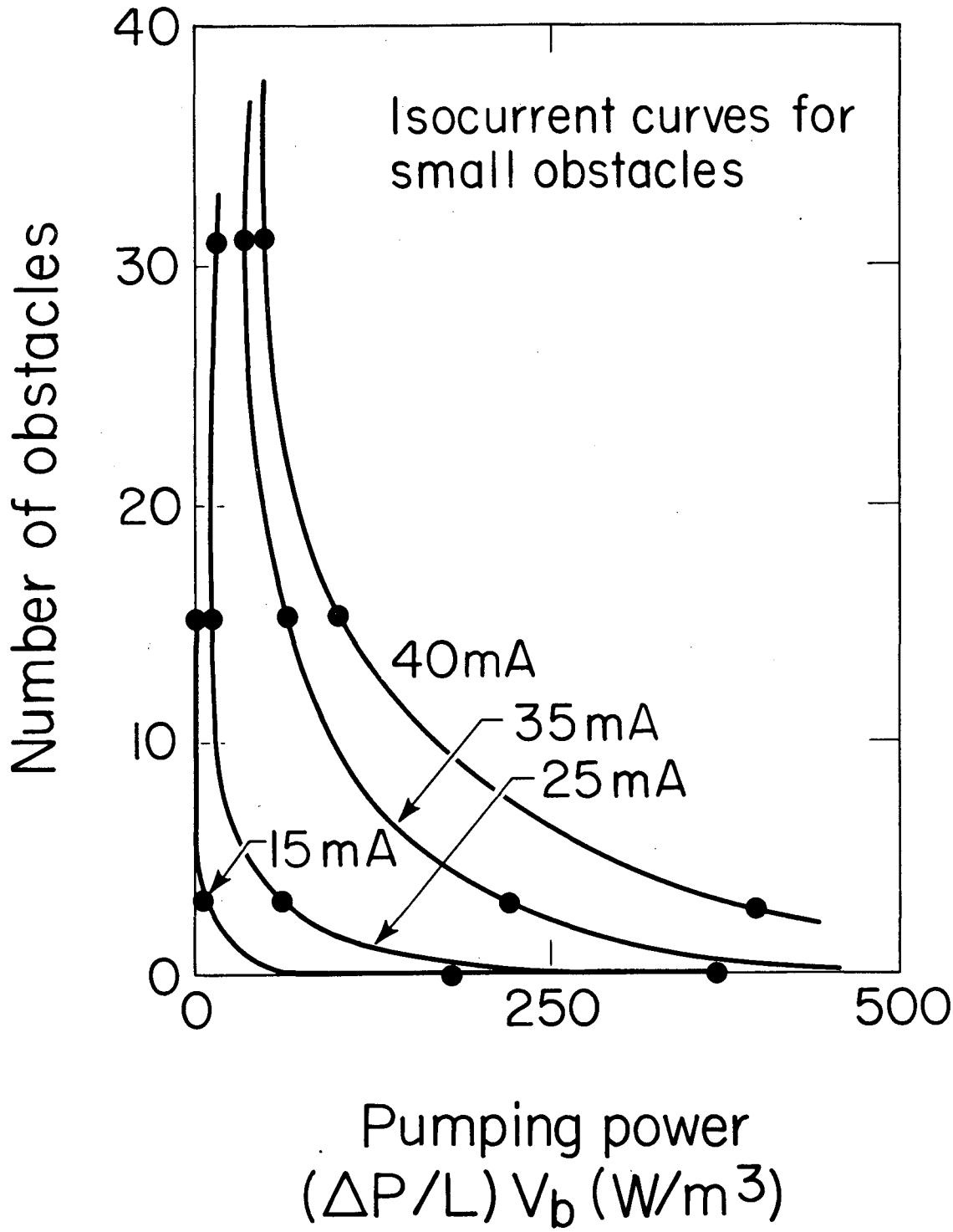

XBL 838-3060

Fig. 62. Lines of constant limiting current as a function of number of Small obstacles and pumping power.

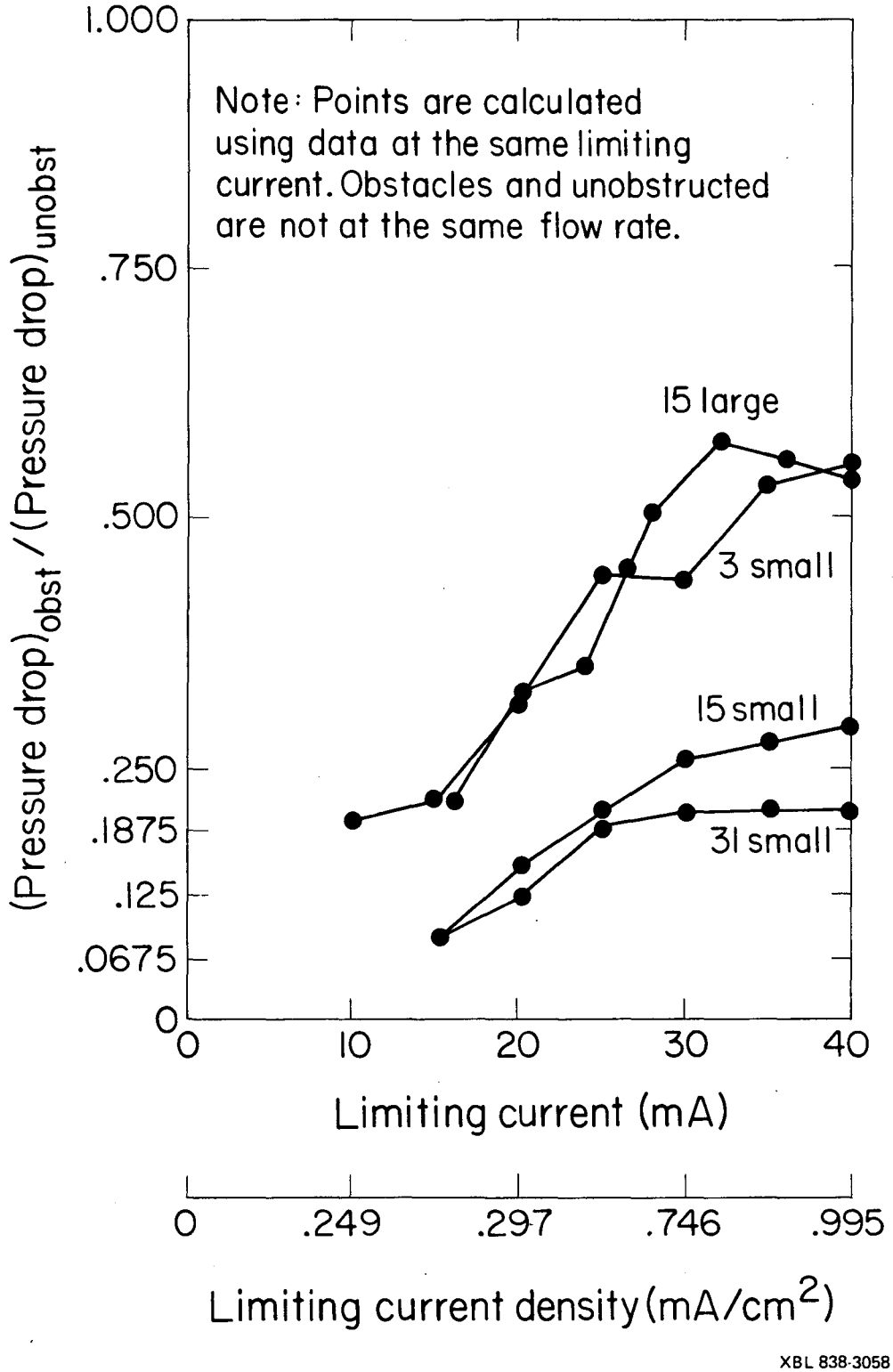

Fig. 63. Normalized pressure drop as a function of number of obstacles and of limiting current. Note the unobstructed duct corresponds to a horizontal line at 1.0.

obtain the same current without obstacles. The flow rate will not be the same for the two pressure drops, because obstacles produce higher currents at lower flow rates (Fig. 34 or 35). The curves show the advantage of the obstacles. The unobstructed duct would produce a horizontal line at (ΔP obs/ΔP unobs) = 1.0. The Small (0.0762 cm) obstacles provide a greater advantage over the Large (0.16 cm) obstacles. The benefit of the obstacles decreases at higher currents (transfer rates).

As mentioned earlier, it is the pumping power $(\Delta P/L)V_b$ and not the pressure drop (ΔP) which determines the additional fluid flow power input required to obtain higher limiting currents. A plot of pumping power input versus the limiting current (I_L) and limiting current density (i_L) is shown on Fig. 64 for the unobstructed channel and for the Small obstacles. The unobstructed channel requires a large input of pumping power. The power requirement increases drastically, especially when higher currents must be achieved. For the unobstructed duct, the flow rate must be greatly increased to obtain a higher current. When the turbulent flow regime is reached, the pressure drop incurred by the electrolyte is greatly increased over that of the laminar regime. These combined effects produce large increases in the required pumping power for the unobstructed duct because the turbulent flow regime must be reached in order to obtain total currents over approximately 20 mA (shown in Fig. 35). The tremendous advantage of the 31 Small obstacles is demonstrated in Fig. 64. The required pumping power input is greatly reduced compared to operation

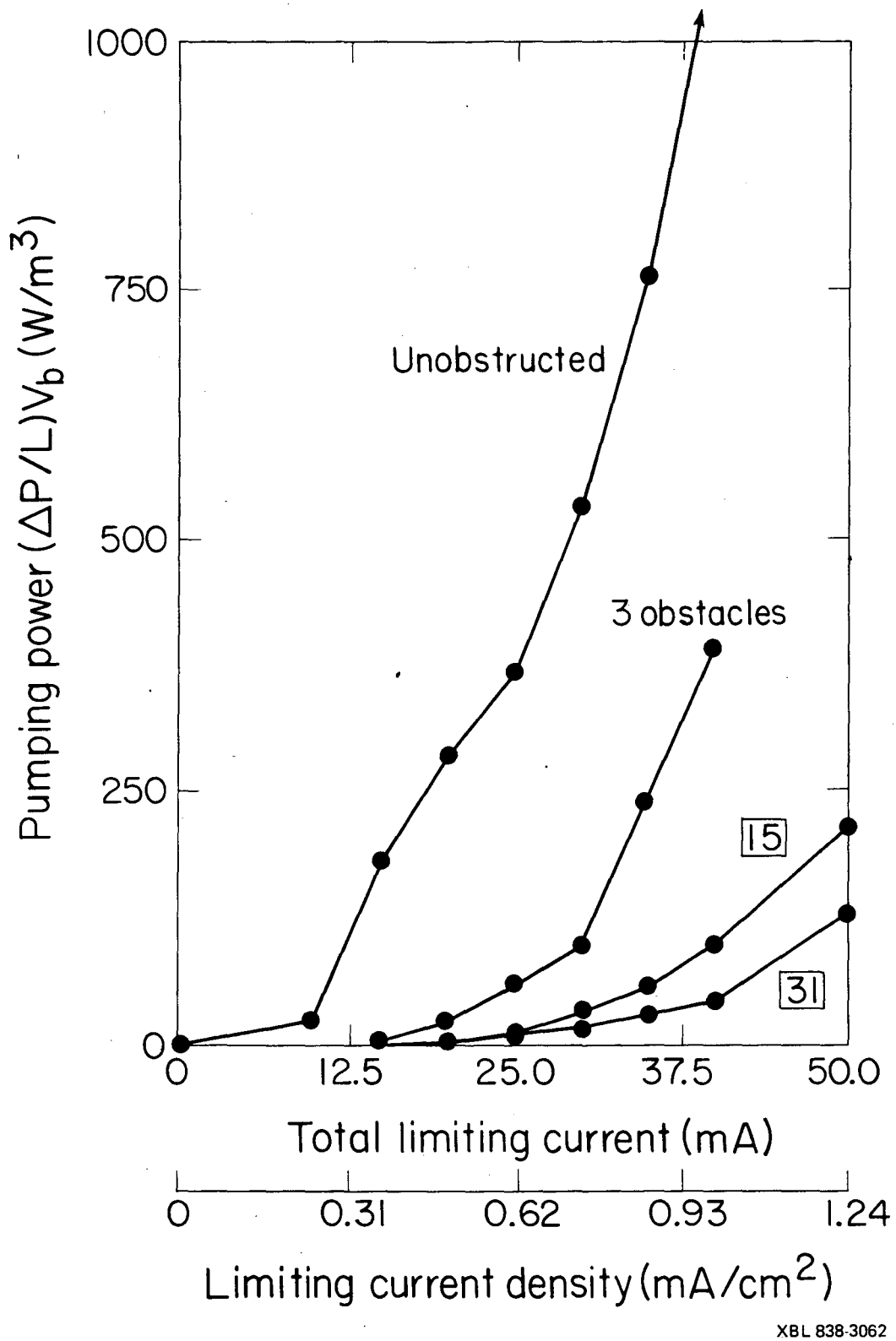

Fig. 64. Required pumping power as a function of limiting current in the presence of Small obstacles (0.0762 cm). Note that obstacles achieve a given limiting current at significantly lower flow rates.

at the same current with the unobstructed duct. To obtain a 25 mA current a 27 fold reduction in the pumping power requirement occurs with the attachment of 31 Small obstacles. (At 40 mA it is a 23 fold reduction.)

The specific advantage of the obstacles over the unobstructed channel is again shown in Fig. 65. In this plot the pumping power input is non-dimensionalized by the pumping power required for the unobstructed system to obtain the same current output. These power inputs will be at different flow rates. The unobstructed duct's performance would be represented by a horizontal line at 1.0. The benefit of the obstacles decreases at higher operating currents. This is due to the eventual formation of bulk turbulence in all systems as the flow rate is further increased. The required pumping power for the system containing 31 Small obstacles is approximately 2 to 5 percent that of the unobstructed duct. By utilizing obstacles, 20 to 70 times <u>less</u> pumping power is required to obtain a given mass transfer rate compared to obtaining the same mass transfer rate by increasing the fluid flow rate in an unobstructed system (Fig. 66). The benefit of the obstacles is a result of efficient mixing near the wall which produces mass transfer enhancement at lower flow rates and allows the bulk fluid to remain in the laminar regime.

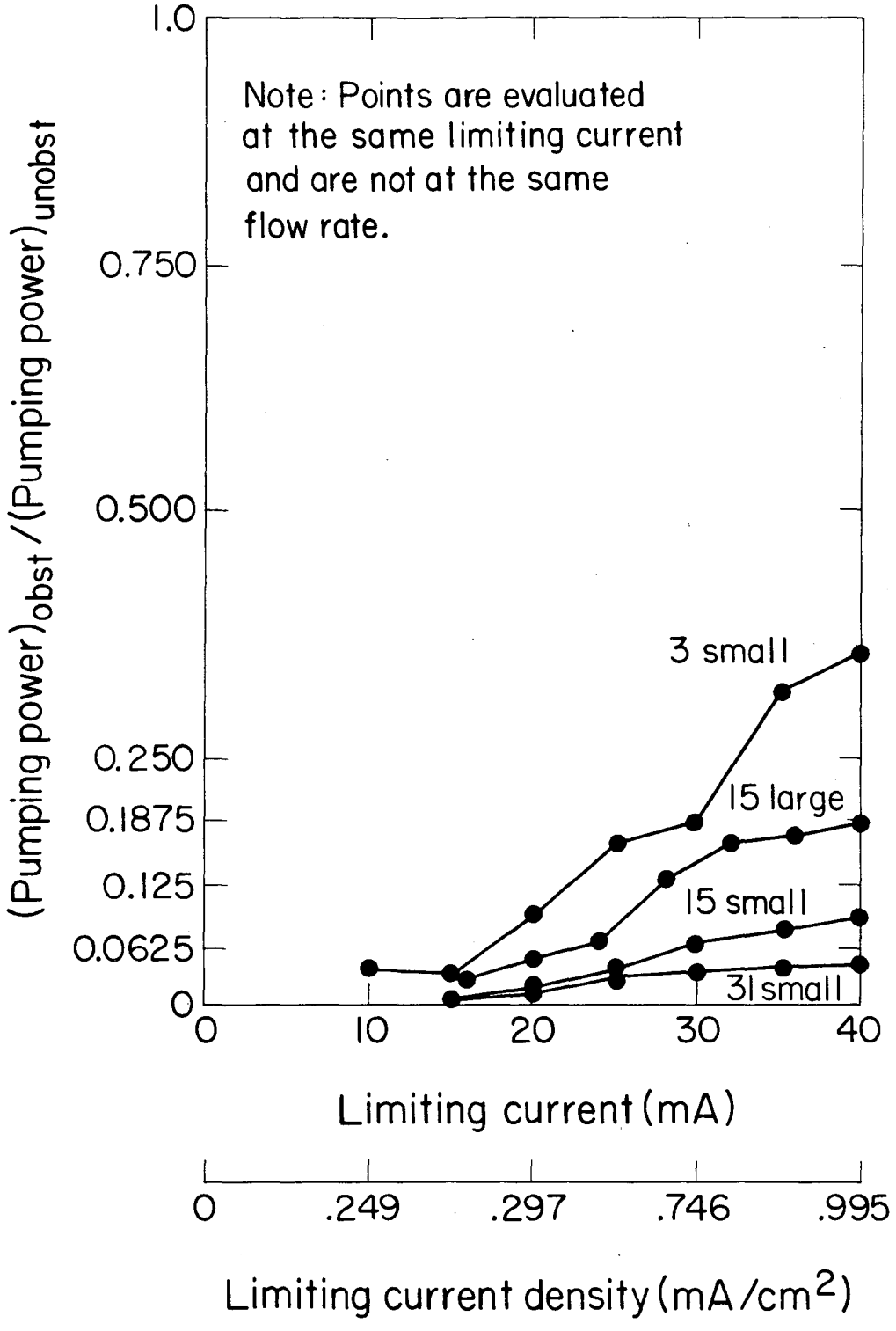

XBL 838-3057

Fig. 65. Normalized pumping power as a function of limiting current and number of obstacles. The unobstructed duct corresponds to a horizontal line at 1.0. To achieve the same limiting current in the presence of 31 Small obstacles the required power for pumping is only 2 to 5 percent of that required without obstacles.

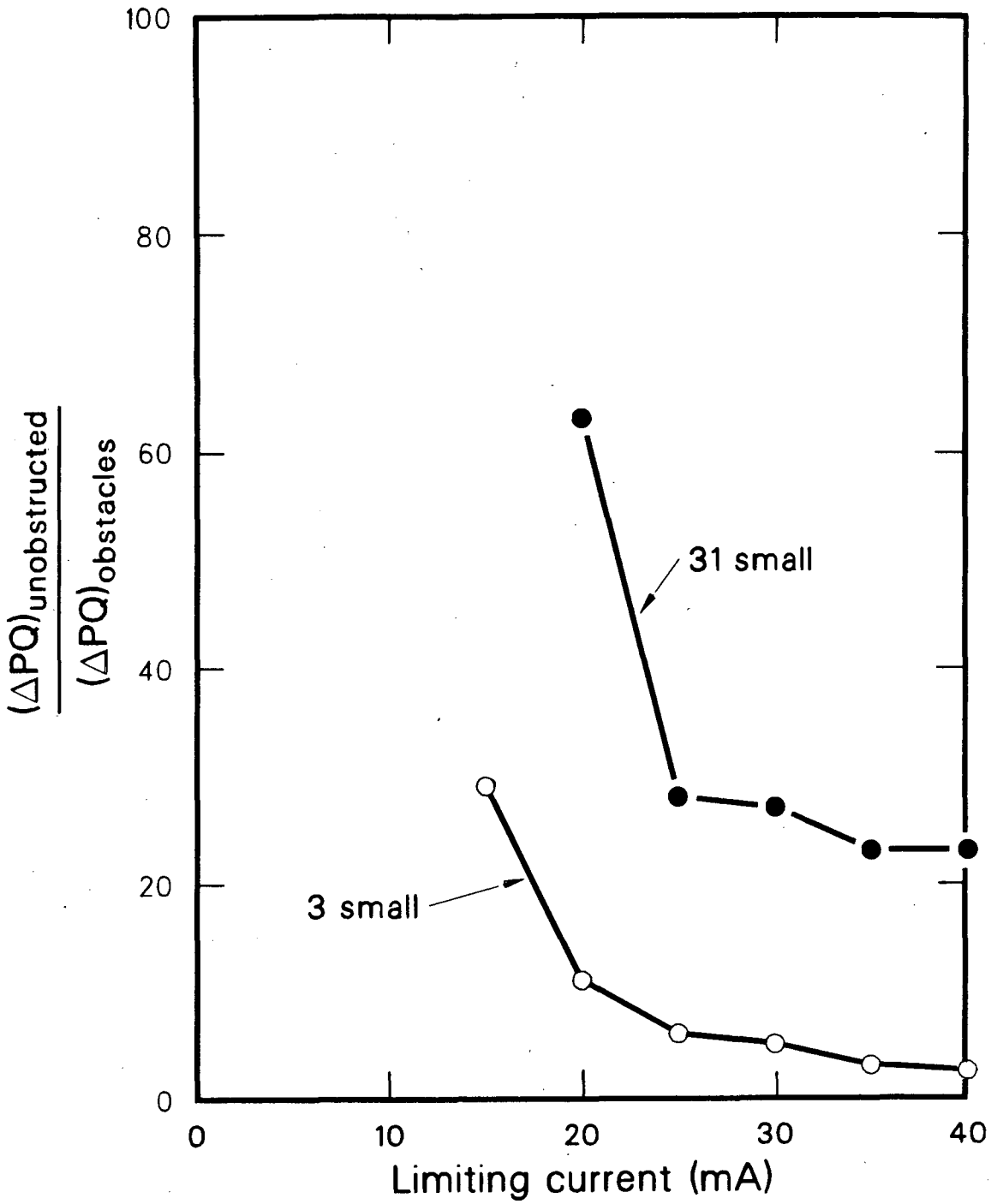

XCG 838-7229

Fig. 66. Normalized pumping power as a function of limiting current and number of Small obstacles (0.0762 cm). The unobstructed system corresponds to a horizontal line at 1.0. The large reduction of the required pumping power by the 31 Small obstacles is shown (20 to 70 times less).

CONCLUSIONS AND SUMMARY OF FINDINGS

In this study a square duct (0.46 cm equivalent diameter) flow cell was used to investigate the benefits with respect to mass transfer enhancement of small (0.160, 0.0762, and 0.0254 cm high) obstacles. The obstacles were attached to the cathode which was built into the duct wall. Flow visualization studies along with pressure drop and limiting current measurements led to the following conclusions:

1) The obstacles provide efficient mixing close to the electrode surface and allow laminar flow in the bulk.
2) At a given flow rate, the presence of obstacles increases both the mass transfer rate and the pressure drop in the duct.
3) Reducing the spacing between the obstacles produces increased mass transfer enhancement and pressure drop; however, too close a spacing results in loss of effectiveness.
4) The optimum spacing is smaller for smaller obstacles and approximately 15 times the obstacle height.
5) Obstacles product a downstream recirculation zone the size of which depends on flow rate and obstacle height.
6) The recirculation zone extends further in the flow direction with increasing flow velocity and reaches a limiting size corresponding to the optimum spacing.
7) Compared to the unobstructed system, the obstacles provide a considerable reduction in the pumping power required to achieve a given rate of mass transfer.
8) The advantage of the flow obstacles is greatly decreased when bulk turbulence is produced.

ACKNOWLEDGMENTS

I would like to thank my advisors, Dr. Charles W. Tobias and Dr. Rolf H. Muller, for their support during the course of this investigation.

I am also grateful to Dr. Lawrence Talbot for reviewing this thesis and providing valuable suggestions.

Other individuals have helped this project either directly or indirectly and these include the following: Panos Andricacos, Glen Baum, Sandy Stewart, Cathy Sterling, Jim Severns, Peter Bray, Weyland Wong, Don Bowman, Hank Brentel, Lee Johnson, Herb Riebe, Joe Farmer, John Holthuis, John Jacobsen, Karrie Hanson, and the entire LBL photo lab staff.

Finally, a special thanks goes to Mark Verbrugge for his countless helpful literary suggestions, Leda Schulak for, among other things, the visualization layouts, and to Connie Silva for typing and preparing this manuscript.

This work was supported by the Director, Office of Energy Research, Office of Basic Energy Sciences, Materials Sciences Division of the U.S. Department of Energy under Contract No. DE-AC03-76SF00098.

APPENDIX A

LIMITING CURRENT CURVE TRANSIENT "MAXIMA"

As described earlier, the work of P.C. Andricacos and H. Y. Cheh [162] on cyclic voltametry has led to a quantitative description of the limiting current curve transient "maxima." By assuming a constant average Nernst diffusion layer thickness δ_{avg} over the reacting electrode and that reactant is transported by diffusion only, the following relation holds:

$$\sigma = \frac{nF\bar{V}\,\delta_{avg}^2}{RT\,D_i}$$

no hump $\sigma < 3$
hump $\sigma > 3$

The value 3 is determined by assuming infinitly fast surface reaction kinetics--which is approximately valid for the ferricyanide ion reduction reaction. If finite kinetics are controlling, the value of σ where the "maxima" is observed will change [165-166]. By obtaining limiting current curves at different sweep rates ($\bar{V}$), plots similar to Fig. A1 can be produced. By identifying the sweep rate at which the "maxima" first appears, the diffusion layer thickness and mass transfer rate can be obtained from the equation below:

$$\delta_{avg} = \frac{3\,RT\,D_i}{nF\,\bar{V}}$$

since $\delta_N = \delta_{avg}$ (linear approximation of constant diffusion layer thickness)

$$i_L = \frac{nF\ D_i\ (C_{bulk})}{\delta_{avg}}$$

This result shows that, within the assumptions, the average diffusion layer thickness can be obtained without directly measuring the limiting current or without exact knowledge of the electrode active area.

For a Reynolds number of 305 the curves on Fig. A1 show that the "maxima" first appears at a sweep rate between 3 and 4 mV/sec. Using 3.5 mV/sec in the above equation, an average diffusion layer thickness (δ_{avg}) of 0.0134 cm was calculated. Remarkably, the diffusion layer thickness calculated from direct measurement of the limiting current (using 24.2 cm^2 active area) was 0.0132 cm. Figures A2 and A3 are provided to show the effect of increasing the flow rate on the technique. All three figures were obtained with 3 Small (0.0762 cm) obstacles attached on the cathode. The current fluctuations are seen with the slower sweep rates at Reynolds number equal to 1700. In this investigation the limiting currents were not obtained by this technique. However, it provided an important check (or measurement) of the electrode active area.

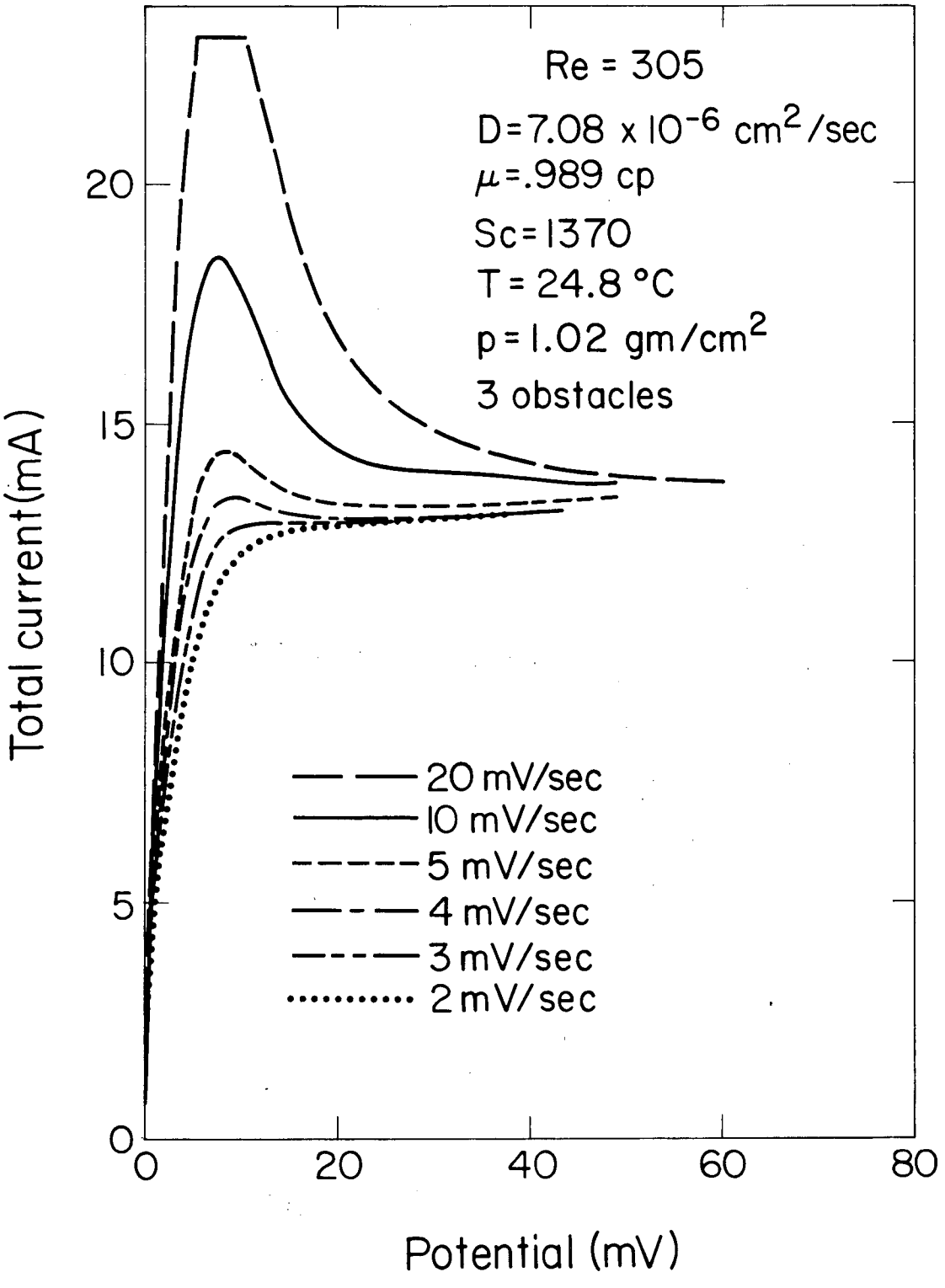

XBL 837-2883

Fig. A1. Effect of varying sweep rate on limiting current curve maxima. In the presence of three Small obstacles at Re = 305.

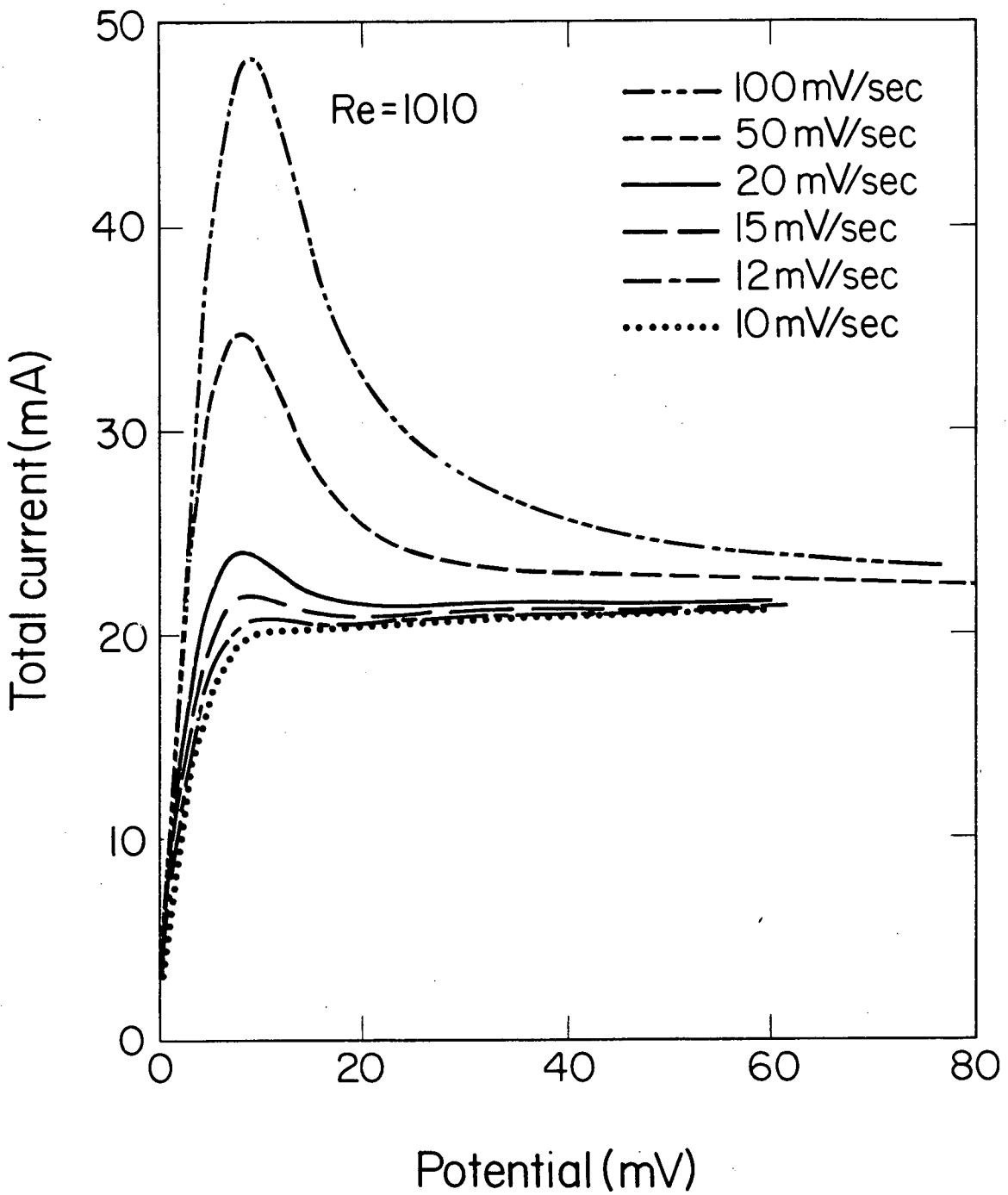

XBL 837-2882

Fig. A2. Effect of sweep rate on limiting current curve maxima in the presence of three Small obstacles. Re = 1010.

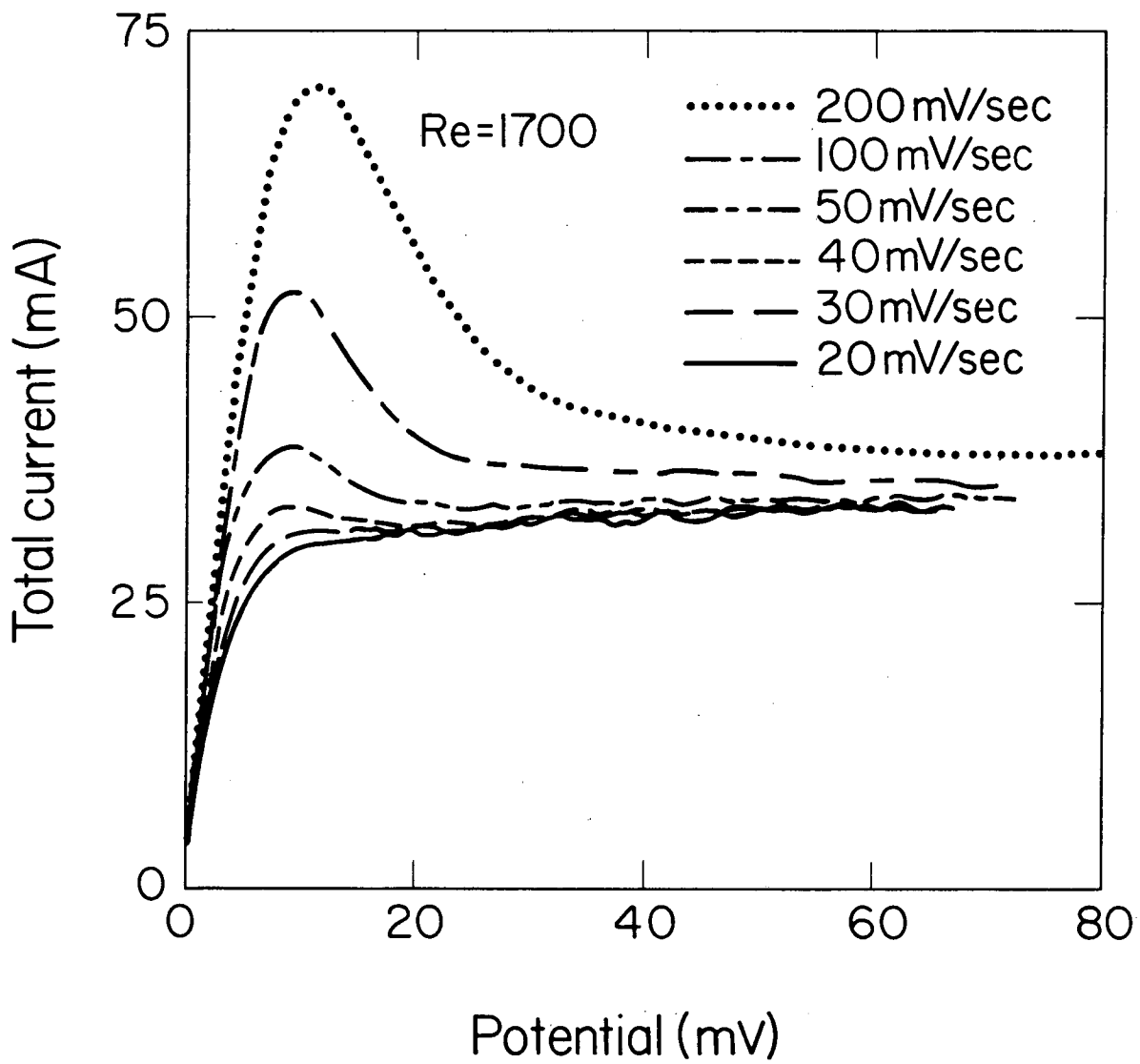

XBL 837-10730

Fig. A3. Effect of sweep rate on limiting current curve maxima in the presence of three Small obstacles at Re = 1700.

APPENDIX B

TITRATION TECHNIQUES

Ferricyanide [172]

1) Use 50 ml of soln.
2) Add 20 ml of 10 percent KI (by wt).
3) Add 25 ml of 2 N H_2SO_4 containing 2g $ZnSO_4$. (The $ZnSO_4$ is suspended and the soln is then poured - turns milky brown.)
4) 1 ml 0.1 N sodium thiosulphate = 0.03292 g K_3 $Fe(CN)_6$.

Ferrocyanide [173] (Must have ferricyanide ion present)

1) Use 25 ml of soln.
2) Add 1-3 drops 1 percent diphenylamine in conc. H_2SO_4 (turns slightly milky).
3) Add 10-20 ml of 4 N H_2SO_4.
4) Titrate with 0.05 M $ZnSO_4$ (turns green then blue green at endpoint).
5) Note: endpoint comes 0.9 percent too soon so increase by 0.009 times.
6) 1 ml 0.05 M $ZnSO_4$ = .014078g $K_4Fe(CN)_6$.

Sodium Hydroxide

1) Use HCl and phenolthalein indicator.

APPENDIX C

COMPARISON WITH INTERFEROMETRIC RESULTS

Comparison of the results from this study with the interferometric measurements performed by Hanson [2] is not easy. Hanson produced plots of the ninety-nine percent boundary layer thickness (δ_{99}) around obstacles with the same dimensions as the Small obstacles (0.0762 cm) used in this study. Assuming a parabolic concentration profile, the ninety-nine percent boundary layer thickness (δ_{99}) is approximately double the linear Nernst boundary layer thickness (δ_N) (Fig. 4) [2].

Hanson observed δ_{99} during copper deposition from a 0.05 M copper sulfate solution (Sc = 2000.) without supporting electrolyte (migration/transference number significant) at Re = 756 and a current density below limiting current.

In contrast to Hanson's work, in this study limiting currents were measured for the reduction of ferricyanide in a solution with excess supporting electrolyte (negligible migration).

Hanson's results showed that the obstacles produce a characteristic boundary layer thickness that repeated with multiple obstacle spacing. Using this result, plots of δ_{99} over the electrode length at Re = 756 were drawn for the specific spacings used in this study (unobstructed, 3, and 15 obstacles). Integrating the area under these curves yields the approximate average ninety-nine percent boundary layer thicknesses based on interferometric observations.

The limiting current measurements obtained in this study were used to calculate average Nernst boundary layer thicknesses (δ_N). The

operating conditions used by Hanson (Sc = 2000., Re = 756) yield $\log(ReScD_e/L)$ equal to 4.13. At this value Sherwood numbers were extrapolated from Fig. 39 for the unobstructed, 3, and 15 obstacle spacings (37.3, 72.3, and 113.4 respectively). Using Eq. (17) and Eq. (40), at limiting current the following relation is obtained:

$$\delta_N = \frac{D_e}{Sh}$$

The above expression is used to calculate an average Nernst diffusion layer thickness from the limiting current measurements.

Values of twice the average Nernst diffusion layer thickness ($2\delta_N$) calculated from the limiting current measurements obtained in this study and values of the approximate average ninety-nine percent diffusion layer thickness (δ_{99}) obtained through transformations of Hanson's results are summarized in the following table:

Number of Obstacles	$2\delta_N$ (cm)	δ_{99} (cm)	$\frac{2\delta_N - \delta_{99}}{2\,\delta_N} \times 100$ (percent)
Unobstructed	0.0246	0.02177	11.5
3	0.00636	0.01137	78.7
15	0.00405	0.00625	54.3

Agreement is good considering the substantial differences between the techniques.

It is important to realize that the current distribution to the electrode is not the same at limiting current (this study) as it is when oprating below limiting current (Hanson).

REFERENCES

1. Frank R. McLarnon, "Interferometry of Electrochemical Mass Transfer Boundary Layers," Ph.D. thesis, UCB, 1975.
2. Karrie J. Hanson, "Interferometric Study of Mass Transfer Enhancement by Turbulence Promoters," M.S. thesis, UCB, LBL No. 9038, April 1979.
3. Kirk W. Beach, "Optical Methods for the Study of Convective Mass Transfer Boundary Layers on Extended Electrodes," Ph.D. thesis, UCB (1971).
4. J. Happel and H. Brenner, Low Reynolds Number Hydrodynamics; Prentice Hall, Englewood Cliffs, NJ (1965), p. 39.
5. Frank M. White, Viscous Fluid Flow, McGraw-Hill, NY (1974) p. 123.
6. H. F. P. Purday, Streamline Flow, Constable and Company LTD, London(1949) p. 14.
7. R. S. Schechter, The Variational Method in Engineering, McGraw-Hill Book Co., NY (1967) p. 91.
8. R. B. Bird, W. E. Stewart, E. N. Lightfoot, T. W. Chapman; AIChE Continuing Education Series No. 4, Lectures in Transport Phenomena; AIChE, NY (1969), p. 124.
9. John Newman, Electrochemical Systems, Prentice-Hall, Inc., Englewood Cliffs, NJ (1973).
10. W. R. Parrish and J. Newman; J. Electrochem. Soc., 117, 43-48 (Jan. 1970).
11. C. W. Tobias and R. G. Hickman, Zeitschrift fur Physikalische Chemie (Leipzig), 229, 145-166 (1963).

12. Acosta, AIChE meeting Atlantic City 1976.

13. V. Landau and C. Tobias, Extended Abstract No. 266, Electrochem. Soc. spring meeting, Washington, D.C. May 1976.

14. I. Rousar, J. Hostomsky, V. Cezner, J. of Electrochem. Soc., 118, 881 (June 1971).

15. D. F. Dipprey and R. H. Sabersky, Int. J. Heat Mass Transfer, 6, 329-353 (1963).

16. W. F. Cope, Proc. Inst. Mech. Engrs., 145, 99-105 (1941).

17. J. W. Smith and N. Epstein, J. AIChE, 3, 242-248 (1957).

18. W. Nunner, VDI-Forschungsheft 455, Series B, 22, 5-39 (1956); A.E.R.E. Lib./Trans. 786 (1958).

19. G. Grass, Atomkernenergie, 3, 328-331 (1958); A.E.C. Translation No. 3641.

20. W. R. Gambill, R. D. Bundy, and R. W. Wammbrough, Oak Ridge Nat. Lab., No. 2901 (March 1960).

21. J. Nikuradse, VDI-Forschungsheft 361, Series B, 4 (1933); NACA TM 1292 (1950).

22. W. A. Sutherland, Int. J. Heat Mass Transfer, 10, 1589-1599 (1967).

23. W. B. Hall, J. Mech. Engng. Sci., 4, No. 3, 287-291 (1962).

24. V. Walker and A. C. Rapier, Jl. Brit. Nucl. Energy Soc., 2, No. 2, 268-275 (1963).

25. D. Wilkie, Proceedings of the Third International Heat Transfer Conference, Vol 1, 1-19. AIChE (1966).

26. N. Sheriff and P. Gumley, Int. J. Heat Mass Transfer, 9, 1297-1320 (1966).

27. J. Gargard and G. Paumard, France, CEA-R 2464 (1964).

28. E. W. Sams, US NACA, RM E52D17 (1952).

29. E. W. Sams, US AEC TID 7529 Pt. 1, Book 2, 390-415 (1965).

30. F. J. Edwards and N. Sheriff, Inter. Developments in Heat Transfer, Pt. II, 415-425, ASME (1961).

31. R. L. Webb, E. R. G. Eckert and R. J. Goldstein, Int. J. Heat Mass Transfer, 15, 180 (1972).

32. R. E. Hicks and W. G. B. Mandersloot, Chem. Engng. Sci., 23, 1202-1210 (1968).

33. J. T. McConnachie and G. Thodos, AIChE J., 9, 61 (1963).

34. D. G. Thomas, AIChE J., 11, 848 (1965).

35. J. Marriott, Chem. Engineering, 78:8, 127, April 5, 1971.

36. J. C. Han, L. R. Glicksman, and W. M. Rohsenow, Inter. J. Heat Mass Transfer, 21, 1143-1156 (1978).

37. E. D. Brouillette, T. L. Mefflin, and J. E. Myers, ASME paper 57-A-47 (Dec. 1957).

38. R. Koch, English translation, AEC-Tr-3875 (1960).

39. J. Molloy, UKAEAAERE-R5415 (1967).

40. E. K. Kalinin, G. A. Dreistler and S. A. Yarkho, Augmentation of Convective Heat and Mass Transfer, edited by A. E. Bergles and R. L. Webb, ASME, NY (1970).

41. R. L. Webb, E. R. G. Eckert and R. J. Goldstein, Int. J. Heat Mass Transfer, 14, 601-617 (1971).

42. M. D. Dalle Donne, and L. Meyer, Int. J. Heat Mass Transfer, 20, 582-620 (1977).

43. J. A. C. Humphrey and J. H. Whitlaw, Turbulent Shear Flows 2, in Second Int. Symp. on Turb. Sheat Flows, Imperial College London, July 2-4 1979, pp. 174-188.

44. S. E. Faas and D. M. McEligot, 5th Annual Summary Report, Contract No. N00014-75-C-0694, report No. 1248-7, Office of Naval Research (Jan. 15, 1980).

45. A. Solan, Y. Winograd, and U. Katz, Desalination, 9, 89-95 (1971).

46. A. A. Sonin and R. F. Probstein, Desalination, 5, 293, (1968).

47. D. Pnueli and G. Grossman, Desalination, 7, 297 (1970).

48. H. Gregor, P. Bruins, and M. Rothenberg, Ind. Eng. Chem. Process Design Develop, 4, 3-6, (1965).

49. Y. Winograd, A. Solan and M. Toren, Desalination, 13, 171-186, (1973).

50. G. Belfort and G. A. Guter, Desalination, 10, 221-262 (1972).

51. E. Schalch and N. Ibl, Electrochimica Acta, 20, 435-440 (1975).

52. D. Landolt, R. H. Muller, and C. W. Tobias; J. of Electrochem. Soc., 116, 1384 (1969).

53. F. B. Leitz, L. Marincic, P. Johnson, and J. Liston, "Effect of Turbulence Promoters on Local Mass Transfer, 3rd Report," Ionics Technical Report, Waltham, Mass. (1974).

54. F. B. Leitz, L. Marincic, J. of Applied Electrochemistry, 7, 473-484 (1977).

55. P. M. Robertson, F. Schwager, N. Ibl, J. Electroanal. Chem., 65, 883-900 (1975).

56. P. M. Robertson, N. Ibl, J. of Applied Electrochemistry, 7, 323-330 (1977).

57. F. Schwager, ETH dissertation.

58. A. K. P. Chu, M. Fleschmann and G. J. Hills, J. Appl. Electrochem., 4, 323 (1974).

59. D. Bennion and J. Newman, J. Appl. Electrochem., 2, 113 (1972).

60. A. T. Kuhn and R. W. Houghton, J. Appl. Electrochem., 4, 69 (1974).

61. G. B. Adams, R. P. Hollandsworth and D. N. Bennion, J. Electrochem. Soc., 122, 1043 (1975).

62. S. Germain and F. Goodridge, Electrochim. Acta., 21, 545 (1976).

63. J. M. Williams, U.S. Pat. 3,859,195 (Jan 1975).

64. P. M. Robertson, P. Berg and H. Reimann, J. Electrochem. Soc., 130, No. 3, 591 (1983).

65. A. A. Sonin and M. S. Isaacson, Ind. Eng. Chem., Process Des. Develop., 13, No. 3, 241 (1974).

66. N. W. Rosenberg and C. E. Tirrell, Ind. Eng. Chem., 49, 780 (1957).

67. A. Kitamoto and Y. Takashima, Desalination, 9, 51 (1971).

68. M. S. Isaacson and A. A. Sonin, Ind. Eng. Chem. Process Des. Dev., 15, No. 2, 313 (1976).

69. A. Storck and F. Coeuret, Electrochimica Acta, 22, 1155-1160 (1977).

70. A. Storck and F. Coeuret, Ind. Eng. Chem. Process Des. Dev., 17, No. 1, 99 (1978).

71. J. J. S. Shen and R. F. Probstein, Ind. Eng. Chem. Process Des. Dev., 18, No. 3, 547-554 (1979).

72. D. G. Thomas and J. S. Watson, Ind. Eng. Chem. Process Des. Dev., 7, 897 (1968).

73. P. Dejmek, B. Funeteg, B. Hallstrom, L. Wirge, Food Sci, 39, 1014, (1974).

74. E. W. Pitera and S. Middleman, Ind. Eng. Chem., Process Des. Dev., 12, 52 (1973).

75. A. L. Copas and S. Middleman, Ind. Eng. Chem. Process Des. Dev., 3, 143, (1974).

76. A. E. Bergles, Handbook of Heat Transfer, Section 10, W. M. Sohsenow and J. P. Hartnett, Ed., McGraw-Hill, New York, NY (1973).

77. E. V. Seymore, Trans. Inst. Chem. Eng., 41, 159 (1963).

78. F. Schwager, P. M. Robertson, N. Ibl, Electrochimica Acta, 25, 1655-1665 (1980).

79. E. Ruckenstein, Chem. Eng. Sci., 7, 265 (1958).

80. A. Storck and D. Hutin, The Canadian J. of Chem. Eng., 58, 92 (Feb. 1980).

81. I. Moscicka, I. Westwal, Bull. Polish Acad. Sci., 8, 837 (1972).

82. H. Miyashita, K. Murokawa, and N. Sugata; Kagaku Kogaku Ronbunshu, 2, 200 (1976).

83. E. M. Sparrow and J. W. Ramsey, Int. J. Heat and Mass Transfer, 21, 1369 (1978).

84. A. Storck and D. Hutin, Electrochimica Acta, 26, 117-125, (1981).

85. A. Storck and D. Hutin, Electrochimica Acta., 26, 127-137 (1981).

86. In Seok Kang and Ho Nam Chang, Int. J. Heat Mass Trans., 25, No. 8, 1167-1181 (1982).

87. G. Carlsson, B. Sandegren, D. Simonsson, and M. Rihousky, J. Electrochem. Soc., 130, No. 2, 342-346 (1983).

88. Swedish National Development Co., specifications sheet and direct observations (1983).

89. W. W. Focke, Electrochimica Acta, 28, 1137-1146 (1983).

90. D. J. Roha, M.S. thesis, UCB, LBL-12737, June 1981.

91. R. C. Blackmore, Brit. Pat., 1, 070, 968.

92. M. Kawaski, S. Mizumoto, Kinzoku Hyomen Gijutsu, 21, No. 3, 119-125 (1970).

93. K. Butter, W. Wittich, Ger. Offen. Pat., 1, 807, 481.

94. G. A. Zarb, Proc. Congr. Int. Union Electrodeposition Surface Finish, 8th, 171-179 (1972).

95. H. F. Bok, E. St. Onge, U.S. Pat., 3,824,137.

96. W. Reidel, Technik, 31, No. 5, 306-307 (1976).

97. A. A. Sonin, J. Electrochem. Soc., 130, No. 7, 1501-1505 (July 1983).

98. R. A. Spaulding, Agresta, Dolan, Chambers, Matrille, Teno, U.S. Pat. No. 3,276,978.

99. W. H. Safranek, The Properties of Electrodeposited Metals and Alloys, American Elsevier, 1974.

100. W. H. Safranek, C. H. Layer, Trans. of Instit. Metal Finishing, 53, 121-125 (1975).

101. J. Jacob, D. Maestri, Proc. Congr. Int. Union Electrodeposition Surface Finish, 8th, 136-141 (1972).

102. Der-Tau Chin, Plating and Surface Finishing, 57-58 (Sept. 1977).

103. Marculla, A. J., Ger. Offen. Pat., 2,228,811.

104. M. Patat, Surfaces, 9, No. 58, 41-43 (1970).

105. M. P. Ellis, R. J. Gavasso, U.S. Pat., 3,616,289.

106. M. P. Ellis, R. J. Gavasso, U.S. Pat., 3,751,346.

107. J. D. Watts, U.S. Pat., 3,959,089.

108. S. Eisner, Plating, 993-996 (Oct. 1971).

109. S. Eisner, N. E. Wisdom, Plating, 1099-1101 (Nov. 1971).

110. S. Eisner, U.S. Pat., 3,619,384.

111. A. M. Al-Taweel, M. I. Ismail, M. Z. El-Abd, Chemie Ing. Technik., 46, No. 20, 861 (1974).

112. M. I. Ismail, A. M. Al-Taweel, M. Z. El-Abd, J. Appl Electrochemistry, 9, 347-350 (1974).

113. A. M. Al-Taweel, M. I. Ismail, J. Appl. Electrochemistry, 6, 559-564 (1976).

114. Robert Walker, Hydrometallurgy, 4, 209-215 (1979).

115. J. Enchev, M. Gramatikov, N. Makhailov, Metalurgiya (Sofia), 29, No. 8, (1974).

116. S. Mohanta, T. Z. Fahidy, Can. J. Chem. Eng., 50, 248-253 (April 1972).

117. R. Sunderman, T. Z. Fahidy, J. Appl. Electrochemistry, 6, 89-92 (1976).

118. J. W. Evans, Y. Zundelevich, E. D. Tarapore, D. Sharma, Lawrence Berkeley Lab. Report, No. 8519.

119. A. B. Bobrov, A. V. Buzhinskaya, L. A. Sergeev, V. I. Trovimov, V. B. Bobrov, A. I. Migina, T. F. Perelygina, Can. Pat., 960, 997.

120. W. W. Harvey, M. R. Randlett, K. I. Bangerskis, J. Metals, 32-41 (July 1978).

121. N. Ibl, R. Kind, E. Adam, Anales de Quimica, 71, 1008-1016 (1975).

122. C. J. Reed, U.S. Pat., 712, 153.

123. P. LeGoff, F. Vergnes, F. Coeuret, J. Bordet., Ind. Eng. Chem., 61, No. 10, 8-17 (1969).

124. D. C. Carbin, D. R. Gabe, Electrochimica Acta, 19, 645-652 (1974).

125. D. C. Carbin, D. R. Gabe, J. Appl. Electrochemistry, 5, 129-135 (1975).

126. R. Thangappan, S. Nachippan, S. Sampth, Ind. Eng. Chem. Prod. Res. Develop., 9, No. 4, 563-567 (1970).

127. M. E. Giles, J. G. Waller, U.S. Pat., 3,617,449.

128. S. Eisner, N. E. Wisdom, Plating, 1183-1186 (Dec. 1971).

129. S. Eisner, U.S. Pat. No. 3,699,017.

130. J. Postlethwaite, D. N. Holdner, Can. J. Chem. Eng., 53, 31-35 (Feb. 1975).

131. J. Postlethwaite, D. N. Holdner, Can. J. Chem. Eng., 54, 255-258 (Aug. 1976).

132. G. C. Pini, P. L. DeAnna, Electrochimica Acta, 22, 1423-1425 (1977) .

133. H. J. Bixler, G. C. Rappe, U.S. Pat. No. 3,541,006.

134. Avtar Singh Ahuja, J. Appl. Phys., 46, No. 8, 3408-3425 (1975).

135. Avtar Singh Ahuja, J. Appl. Phys., 47, No. 2, 775-777 (1976).

136. H. Zeilmaker, E. Barendredt, Abstract, 31st Meeting of the I.S.E., Venice, Italy, 22-26 September 1980.

137. A. Storck, J. F. Brodberger, D. Hutin, G. Valentin, J. Applied Electrochem., 11, 727-733 (1981).

138. G. H. Sedahmed and L. W. Shemilt, J. of Applied Electrochemistry, 11, 537-542 (1981).

139. B. K. Sadananda Rao and G. Venkataraman, Electrochimica Acta, 26, No. 5, 653-655 (1981).

140. D. J. Pickelt and C. J. Wilson, Electrochimica Acta, 27, No. 5, 591-594 (1982).

141. K. W. Pratt Jr., D. L. Johnson, Electrochimica Acta., 27, No. 8, 1013-1021 (1982).

142. G. H. Sedahmed, A. M. Asfour, M. M. Nassr, and O. A. Fadal, J. of Applied Electrochem., 12, 7-11 (1982).

143. S. Endaie, M. Fleischmann, and R. E. W. Jansson, J. Applied Electrochem., 12, 59-67 (1982).

144. T. N. Andersen, C. H. Pitt, and L. S. Livingston, J. of Applied Electrochem., 13, 429-438 (1983).

145. H. K. Kuiken, F. E. P. Mikkers, and P. E. Wierenga, J. Electrochem. Soc., 130, No. 3, 554 (March 1983).

146. V. Strimming, G. V. Arbach, and P. Bindra, Extended Abstracts No. 838, 163rd Meeting Electrochem. Soc., Vol. 83-1, p. 1245, San Francisco, CA (Spring 1983).

147. A. J. C. P. M. Boeffard, "Ionic Mass Transport by Free Convection in a Redox System," M.S. thesis, UCB, UCRL-16624 (1966).

148. S. C. Gordon, J. S. Newman, C. W. Tobins, Berichte der Bunsengesellschaft fur Physikalische Chemie, 70, No. 4, 414-420, (1966).

149. Glasstone, Introduction to Electrochemistry, Van Nostrand, NY, 60 (1942).

150. Bird, Stewart, Lightfoot, Transport Phenomena; Wiley, NY (1960).

151. U. Landau, "Plating New Prospects for an Old Art," in Electrochemistry in Industry: New Directions, ed. by U. Landau, E. Yeager, D. Kortan (NY: Plenum Press, 1982) p. 215.

152. Nernst, Z. Physik, Chem., 47, 52 (1904).

153. R. G. Hickman, "The Effect of Buoyancy Forces on Forced Convection Ionic Mass Transfer at Horizontal Planar Electrodes," Ph.D. thesis, UCB, Dec. 1, 1963.

154. C. W. Tobias and R. B. Hickman, "Ionic Mass Transport by Combined Free and Forced Convection," Zeitschrift fur Physikalische Chemie (Leipzig), 229, 145-166 (1965).

155. U. Landau, "Distribution of Mass Transfer Rates Along Parallel Plane Electrodes in Forced Convection," Ph.D. thesis, UCB, LRL-2702, Jan. 1976.

156. C. S. Lin, E. D. Denton, H. S. Gaskill and G. C. Putnam, Industrial and Engineering Chem., 43, 2136 (1951).

157. M. Eisenberg, "Studies on the Role of Ionic Diffusion and Mass Transfer in Electrode Processes," M.S. thesis, UCB (1951).

158. M. Eisenberg, C. W. Tobias, and C. R. Wilke, J. of the Electrochem. Soc., 101, No. 6, 306-319 (June 1954).

159. R. E. Acosta, "Transport Processes in High Rate Electrolysis," UCB, Ph.D. thesis (May 1974).

160. J. R. Selman, "Measurement and Interpretation of Limiting Currents," Ph.D. thesis, UCB, UCRB-20557 (June 1971).

161. J. R. Selman and C. W. Tobias; J. Electroanal. Chem. 65, 67-85 (1975).

162. P. C. Andricacos and H. Y. Chen; J. Electrochem. Soc., 127, 2385 (1980).

163. An Album of Fluid Motion, The Parabolic Press, P.O. Box 3032, Stanford, CA.

164. Wolfgang Merzkirch, Flow Visualization, Academic Press (1974).

165. P. C. Andricacos and H. Y. Cheh; J. Electroanal. Chem., 124, 95-101 (1981).

166. G. C. Quintana, P. C. Andricacos, and H. Y. Cheh; J. Electroanal. Chem., 144, 77-85 (1983).

167. M. Fleischmann and R. E. W. Jansson, Electrochimica Acta., 27, No. 8, 1023-1028 (1982).

168. Ibid., pp. 1029-1034.

169. R. S. Prengle and R. R. Rothfus, Ind. Eng. Chem., 47, 379-386, 1955.

170. R. E. Chilcott, Int. J. Heat Mass Transfer, 10, 783-797 (1967).

171. R. J. Goldstein, V. L. Eriksen, R. M. Olson, E. R. G. Eckert, J. of Basic Engineering, 92, 732 (1970).

172. F. Sutton, A Systematic Handbook of Volumetric Analysis, 13th ed., Butterworths Scientific Pub., London, 335 (1955).

173. I. M. Kolthoff and V. A. Stenger, Volumetric Analysis, 2, 2nd ed., Interscience Pub., New York, 305 (1947).

174. Kolthoff and Furman, Volumetric Analysis, 1, John Wiley and Sons Inc., New York, 231 (1928).

175. H. W. Emmons, J. of the Aeronautical Sci., 18, 490-498 (1951).

176. B. Cantwell, D. Coles and P. Dimotakis, J. Fluid Mech., 87, 641-672 (1978).

This report was done with support from the Department of Energy. Any conclusions or opinions expressed in this report represent solely those of the author(s) and not necessarily those of The Regents of the University of California, the Lawrence Berkeley Laboratory or the Department of Energy.

Reference to a company or product name does not imply approval or recommendation of the product by the University of California or the U.S. Department of Energy to the exclusion of others that may be suitable.

TECHNICAL INFORMATION DEPARTMENT
LAWRENCE BERKELEY LABORATORY
UNIVERSITY OF CALIFORNIA
BERKELEY, CALIFORNIA 94720